



CONSTRUCTING AND ASSESSING FIRE CLIMATES FOR AUSTRALIA

Technical Report

Abstract

This report constructs fire climates for Australia from high quality climate data, identifying specific regimes that change abruptly in response to warmer and drier conditions. Fire risk increased abruptly in the late 1990s and early 2000s leading to hotter and more frequent fires. These acute changes in risk are not predicted by the current generation of climate models. This is a global phenomenon related to large-scale shifts in the climate system.

Roger N Jones and James H Ricketts
roger.jones@vu.edu.au

This report was catalysed by the Black Summer fires in 2019–20, prompted by the recognition that the magnitude of current fire risk and its relationship with climate change was largely unrecognised in the formal scientific literature. The aim was to create a method for the rapid assessment of changes in fire climate, so that regime shifts could be attributed and compared with projections. It contributes to a long-term research program exploring how rapid shifts in climate are produced by gradual forcing and how the resulting risks can be better understood and managed. It has contributed to the independent review of progress being made with Victoria’s bushfire risk modelling system and risk-based decision-making framework (Risk 2.0) undertaken for the Department of Environment, Land, Water and Planning (Victoria) (DELWP) who have accepted its findings in principle.

Acknowledgments

Chris Lucas of the Bureau of Meteorology provided the original FFDI data for Victoria, and with Sarah Harris has made the updated data for Australia available. High quality climate data for Australia was sourced from the Bureau of Meteorology climate tracker. Acacia Pepler of the Bureau of Meteorology provided subtropical ridge data. The HadISDH is a global gridded monthly mean surface humidity dataset, quality controlled and homogenised/bias adjusted monthly mean anomalies (relative to a 1991–2020 base period) produced by the UK Met Office Hadley Centre. Data details and links are listed in the Appendix.

© Victoria University 2021

ISBN 978-1-86272-844-8

Citation: Jones, Roger N. and Ricketts, James H. (2021) Constructing and Assessing Fire Climates for Australia. Technical Report. Institute of Sustainable Industries and Liveable Cities (ISILC), Victoria University Melbourne.

Contents

1. Introduction.....	1
2. Constructing the model.....	3
Baseline data	3
The model.....	4
Model results.....	5
Extending the model to other regions	8
3. Assessing Fire Climate Regimes for Australia	13
Current understanding of fire climates and climate regimes.....	13
Assessing climate fire regimes.....	13
The extended climatology	14
Extending to other regions.....	16
Studies of changes in FFDI.....	21
4. Comparing recent regime change with projected future change	26
Comparisons with future projections.....	26
Comparing baselines, regimes and projections.....	26
Comparisons with regional studies	30
National	33
Summary.....	33
5. Attributing recent fire climate regime changes in Australia. Part I Dynamics	35
Introduction.....	35
Exploring individual contributions to regime change.....	35
Maximum temperature	35
Wind speed.....	36
Relative humidity.....	37
The subtropical ridge and FFDI.....	38
Linear inverse analysis.....	40
Dynamic influences on FFDI	43
6. Attributing recent fire climate regime changes in Australia. Part II Thermodynamics.....	45
Introduction to thermodynamic forcing.....	45
Thermodynamic drivers of fire climates.....	46
Timeline of historical regime changes.....	46
Thermodynamic processes influencing moisture transport.....	47
Is tropical expansion regime-like?.....	50
Thermodynamic drivers of regime change.....	52
7. Summary.....	54
Conclusions.....	56
Appendix 1. Model and data sources.....	57
References.....	58

Abbreviations

C3pm	3 pm cloud
CCIA2015	Climate Change in Australia (2015)
days Hi+	Days of high fire danger and above
days Sev+	Days of severe fire danger and above
days VHi+	Days of very high fire danger and above
DF	Drought factor, used in FFDI (Equation 1)
Ep	Potential evaporation
ENSO	El Niño–Southern Oscillation
FFDI	Forest Fire Danger Index
Σ FFDI	Annual sum of FFDI
M Σ FFDI	Fire year median Σ FFDI
MaxFFDI	Maximum annual daily value of FFDI
MFFDI	Median daily FFDI
97FFDI	Annual mean 97 th percentile daily FFDI
HadISDH	UK Meteorological Office Hadley Centre Integrated Surface Database Humidity
HQD	High quality data
IPO	Interdecadal Pacific Oscillation
KBDI	Keetch-Byron Drought Index
LH2019	The Lucas and Harris (2019) data set for FFDI and inputs for Australia
P	Precipitation
PDO	Pacific Decadal Oscillation
RCP4.5	Representative Concentration Pathway 4.5 – greenhouse gas forcing profile
RCP8.5	Representative Concentration Pathway 8.5 – greenhouse gas forcing profile
RH	3 pm relative humidity, when used in Equation 1, relative humidity elsewhere
STRI	Subtropical ridge intensity (sea level pressure hPa), 145–150 °E
STRP	Subtropical ridge position (latitude), 145–150 °E
Tav	Average temperature
Tmax	Maximum temperature
TmaxFS	Fire season maximum temperature
90Tmax	Areal coverage of 90 th percentile of Tmax
Tmin	Minimum temperature
V	3 pm wind speed, when used in Equation 1, wind speed elsewhere
VicHQD57–19	Victoria high quality data FFDI model 1957–2019 fire years
VicLH	Four Victorian station average from the LH2019 data set
VicSD72–10	Baseline FFDI for Victoria, station data 1972–2010 fire years
VP	Vapour pressure

1. Introduction

Over the past two decades Australia has experienced wildfires of increased frequency and severity due to climate change. The 2019–20 fire season, the black summer, was the worst on record for area burned and property loss (Abram et al., 2021; Hughes et al., 2020). Two outstanding issues in understanding the current level of fire risk are, how much of that risk is due to human-induced climate change, and how much of an increase do we need to plan for?

Both aspects are difficult to quantify. Fire risk indices require high-quality input data that is often unavailable. Existing data is of limited quality, spatial coverage and continuity. The risk of wildfire also depends on land surface and cover conditions. The fire response to increasingly severe fire weather is also highly nonlinear. Bradstock (2010) described four fire switches that dial up fire risk: biomass production, biomass readiness to burn, fire weather and ignition sources. Climate influences all of these, the third most directly. All four are needed for a comprehensive assessment of fire risk at a given location (Bradstock, 2010). The typical fire risk at a place taking account of these characteristics, make up the generally accepted definition of a fire regime (Krebs et al., 2010).

This report focuses on understanding and quantifying the external climatic conditions that contribute to fire risk of a region; i.e., the climate entering a region before considering its land use and land cover, level of fuel, dryness and topography. The incoming regional climate is conditioned by processes on the wider land and ocean surface but is largely independent of local conditions. This also applies to incoming rainfall and moisture availability, which make up the hydroclimate. There is a finer level of detail where local conditions modify the incoming climate, but these can be considered as local feedbacks.

Our starting definition is that a fire climate (pyroclimate) is a description of the statistics of fire weather external to a region that affects the propensity for wildfire to occur. This does not include the likelihood of ignition, which requires another layer of information. The pyroclimate is situated towards the hot and dry end of the hydroclimate where there is sufficient rainfall to accumulate biomass as fuel and sufficient heat for its growth, but not at the very dry extreme which is too arid. The basic partitioning between latent and sensible heat used to estimate runoff (e.g., Jones et al., 2006; Zhang et al., 2008) can therefore apply to fire, allowing relatively simple relationships to be constructed from mean climatological data.

This work is part of a larger project that aims to change the understanding of climate from being the statistics of weather to a physical system that exhibits complex system behaviour physically distinct to the behaviour of weather (Jones, 2012; Jones & Ricketts, 2017, 2019; Jones & Ricketts, 2021a, 2021b; Jones et al., 2013; Ricketts, 2019). The most recent results describe climate as a self-regulating system containing emergent structures and patterns that dissipate heat from the equator to the poles while maintaining energy balance between the hemispheres. These emergent climatic features include permanent structures, such as the Hadley and Walker Cells, quasi-permanent circulation such as deep ocean circulation, seasonal patterns, and oscillating patterns, such as the El Niño–Southern Oscillation (ENSO) and Pacific Decadal Oscillation (PDO) (Jones & Ricketts, 2021a, 2021b). Self-regulation is needed to maintain energy balance within a highly asymmetric system where the land-ocean mix in both hemispheres is very different producing a highly complex arrangement of forcing and feedbacks.

The basic unit of climate within this self-regulating system is the climate regime. This is a steady-state pattern kept stable by positive and negative feedbacks acting within a specific envelope of available potential energy (Jones & Ricketts, 2019; Jones & Ricketts, 2021a, 2021b). Steady-state conditions are maintained by the coupled shallow ocean–atmosphere. Globally, this process is governed by a heat engine in the tropical Pacific linked to the broader climate network through teleconnections (Jones & Ricketts, 2019; Jones & Ricketts, 2021b). A climate regime will remain stable unless internal and external forcing creates a critical imbalance

of heat available for dissipation, triggering a shift to a new stable state, either positive or negative. Forced by increasing greenhouse gases, from the mid-20th century to now climate, has been periodically switching new, warmer regimes that have the capacity to dissipate excess heat collecting in the tropical oceans (Jones & Ricketts, 2021b).

A major aim of this work is to explore to what extent fire climates form stable-state regimes that can shift, rapidly changing fire risk as a result. A regime shift in fire climate has already been shown for Victoria (Jones et al., 2013) so the aim is to expand this nationally. If a climate regime shift alters the balance between dry and moist atmospheric heat (sensible and latent heat), the outcome can be a shift in fire climate regime. This would be independent of fuel condition, ignition risks from people, and assets at risk but may, in turn, affect those. Having a robust and reliable estimate of the fire climate of a region will contribute to a better understanding as to how climate influences the four fire switches of a standard fire regime.

This project uses McArthur's Forest Fire Danger Index (FFDI, Luke & McArthur, 1978; McArthur, 1967; Noble et al., 1980) as the basis for developing and fire climate regimes. One aim is to determine whether FFDI can be used to estimate physically-realistic changes in fire risk in the way that rainfall and evaporation can be used to estimate potential changes in water supply (Jones et al., 2006), creating the capacity for rapid-assessment without the need to rely on resource-intensive modelling.

This report presents a proof-of-concept model for assessing fire risk indices from readily obtainable climatic variables that aims to:

- Build on daily records of fire danger indices to provide extended historical records for analysis
- Provide the capacity for the rapid assessment of evolving fire climates
- Test fire danger indices and related climate variables for regime-like behaviour
- Understand the relationship between current fire climate regimes and their recent past and contrast that with projected future change
- Better understand the role of anthropogenic forcing on pyroclimatic regimes.

The four measures used are the annual sum of FFDI (Σ FFDI) and days above high (days Hi+), very high (days VHi+) and severe fire danger (days Sev+). Not having to explicitly consider fuel condition or load, or the likelihood of ignition provides the advantage of being able to consider external changes solely due to climate as an input into strategic planning. This can then contribute to the more complex decision-making processes needed to manage fire risk in toto.

The development of methods to define fire climates is therefore not intended as a substitute for the application of higher-resolution data for research and operations. The aim is to develop a framework for a better understanding of pyroclimatology in a changing climate and to quantify the external climate signal influencing fire risk. In particular, if regime shifts in fire risk become an accepted part of the science and its application, current analytical methods will need to be revised, especially those centred on trend analysis and its use in detection and attribution.

Chapter 2 describes how the model is constructed from baseline data, using FFDI data from Victoria that has been homogenised, extending that to other regions of Australia. Chapter 3 builds fire climate regimes from that data, analysing shifts in those regimes. Chapter 4 compares regimes with past and future projections of climate risk. Chapter 5 undertakes attribution within a dynamic framework, including error and sensitivity analysis, while Chapter 6 moves to the thermodynamic realm, looking at how changing fire risk relates to tropical expansion and global climate change. Chapter 7 provides a summary and conclusions.

2. Constructing the model

This chapter constructs baseline fire climates for selected Australian states and regions starting with records of homogenized McArthur Forest Fire Danger Index (FFDI) from Victoria.

Baseline data

The baseline data used to construct the fire climate consists of daily FFDI data from nine stations for Victoria 1972–73 to 2009–10 from the Bureau of Meteorology (Mt Gambier in South Australia was included as the westernmost point). These records were developed and supplied by Lucas (2009). FFDI was calculated through a ‘reverse engineering’ approach Noble et al. (1980):

$$\text{FFDI} = 1.2753 \times \exp[0.987 \ln(\text{DF}) + 0.0338 \text{Tmax} + 0.0234 \text{V} - 0.0345 \text{RH}] \quad \text{Equation 1}$$

Where DF is a drought factor, Tmax is maximum temperature, V is 3 pm wind speed and RH is 3 pm relative humidity. This approach was developed by Noble et al. (1980) based on the operation of fire meters developed by Luke and McArthur (1978); McArthur (1967).

Where possible, these estimates used homogenised records of temperature (Della-Marta et al., 2004) and relative humidity (Lucas, 2006), but wind-speed records were more problematic (Lucas, 2009). Earlier measurements were made by human observers and later measurements were instrumental. Human observers tend to underestimate the mean and overestimate variance, therefore the change from human to instrumental measurement will flow through produce amplified increases in FFDI over the period of record. Lucas (2009) assessed the sensitivity of FFDI to changes in wind speed, concluding that variations in FFDI due to wind speed can be estimated by the relationship:

$$\delta \text{FFDI} = 0.0234 \text{FFDI} \times \delta \text{V} \quad \text{Equation 2}$$

where δFFDI is change in FFDI and δV is change in mean wind speed.

Most stations converted to instrumental measurements of wind speed using cup anemometers at around 1993 (Jakob, 2010; Lucas, 2009), either from visual estimates of wind force or pressure anemometers (Jakob, 2010; Miller et al., 2013). The preceding observer readings have a larger variance, more frequent calm days and can differ markedly between personnel (Lucas, 2009). Homogeneity tests on deseasonalised average monthly 3 pm wind speed were conducted using the Maronna-Yohai (1978) bivariate test using random numbers as a reference. Changes in station location can also affect readings but will likely affect other variables as well, so inhomogeneities in wind speed only were deemed to be due to observer and/or instrument changes.

Each time series was separated into a set of homogenous periods. Adjustments were made as simple changes in the mean between the baseline and each test period for all days with wind speed above zero and Equation 2 applied following Lucas (2009). This did not quite reproduce the change in measured mean, but differences were small (0 to 0.2 ms^{-1} on average for each month adjusted). Good quality records required no changes (Laverton) or one change (Melbourne); moderate quality records required three changes (Mt Gambier, Mildura, Nhill, Sale) and poor-quality records required six or more changes (Omeo, Orbost, Bendigo). Visually comparing the results for Bendigo with those from a recent wind climatology for Victoria VicClim3 (Mills et al., 2020), shows the adjustment produce similar changes.

The results included ΣFFDI , and annual counts of low to moderate, high, very high, severe, extreme and catastrophic fire danger each fire year (July to June 1972–73 to 2009–10). Averaged across Victoria, these were tested for regime shifts, all shifting in 2002 at $p < 0.01$ (Table 1). The implications of rapid shifts for future fire risk were discussed in Jones et al. (2013), where a slightly different configuration showed a shift in 1997–98. The different dates will be discussed later.

Table 1: Shifts in four annual records of fire indices for Victoria dating from FY 1972–73 to 2009–10, where Σ FFDI is the annual sum of daily FFDI, Hi+ days above high fire danger, VHi+ very high fire danger and Sev+ severe fire danger. T_{i0} is the bivariate test statistic, where >12.0 for time series >50 years is equivalent to $p<0.01$.

Variable	Average	Std Dev	T_{i0}	Year	Shift	Percent change
Σ FFDI	2721	655	17.6	2002	1081	44%
Days Hi+	62.38	18.77	14.8	2002	29.1	51%
Days VHi	18.33	8.47	16.5	2002	13.6	88%
Days Sev+	2.63	1.92	12.8	2002	2.8	133%

The FFDI data set of Lucas (2009) has been extended in stages (Clarke, Lucas, et al., 2013), with the latest version covering 39 stations around Australia from 1971 to early 2017 (Harris & Lucas, 2019; Lucas & Harris, 2019). This record will be referred to as LH2019. The indices most often analysed from these records are Σ FFDI and the 90th percentile, whereas the most salient values for assessing fire risk are days of high to catastrophic fire danger, although the milder fire ratings are also required to identify safe windows for fuel reduction activities (Clarke et al., 2019). Average station data for Σ FFDI from 36 stations, 35 overlapping with LH2019, was also recorded in the regional technical reports for Climate Change in Australia (2015). This data set is referred to as CCIA2015. Spatial climatologies of daily FFDI for Australia have also been constructed by Sanabria et al. (2013) and Dowdy (2018). A fire weather data set of hourly FFDI has also been constructed for Victoria on a 4 km grid from 1972 to 2012 (Brown et al., 2016) updated to 2017 (Harris, Mills, et al., 2019). This dataset has a 32-level atmosphere, making it suitable for detailed fire modelling (Brown et al., 2016).

The LH2019 record contains the lowest, 25th, 50th, 75th, 90th, 95th, 97th and highest estimate for each quarter 1971–2016. Also included are mean values of the drought factor (DF), Keetch-Byron Drought Index (KDBI), Tmax, rainfall (P), rain days, relative 3 pm humidity (RH) and 3 pm windspeed (V). Fire year median Σ FFDI ($M\Sigma$ FFDI) and the annual mean daily 97th percentile FFDI (97FFDI) were calculated from these and used in comparisons. The median estimate is not ideal, being about 80% of Σ FFDI, depending on the degree of skewness to the severe end where they are similar. 97FFDI falls between days above high and above very high fire danger, so was compared with the VHi+ data set. All these records have been calculated using Lucas (2009) original method summarised in Equation 1 with minor modifications (Clarke, Lucas, et al., 2013; Harris & Lucas, 2019).

The CCIA2015 record included average P and Tmax 1980–2010 along with Σ FFDI and days Sev+. This provided Σ FFDI and days Sev+ that could be matched with timeseries from LH2019. Of the 39 stations in LH2019 and 36 in CCIA2015, 35 were shared.

The model

The climate data used to construct the fire climate model consists of annual high-quality climate data adjusted for inhomogeneities (HQD). Variables are Tmax from the ACORN-Sat2 data set (Trewin, 2013, 2018), P from the high-resolution gridded dataset developed for the Australian Water Availability Project (AWAP) (Jones et al., 2009), the 90th percentile areal coverage of Tmax (0–100%) and high-quality 3 pm cloud (Jovanovic et al., 2011). These are all available for download from the Bureau of Meteorology climate tracker (<http://www.bom.gov.au/climate/change/index.shtml#tabs=Tracker&tracker=timeseries>).

The conceptual model used in building a fire climatology (pyroclimatology) is based on similar approaches used in hydroclimatology, originally articulated by Budyko (1974). Variables such as rainfall and potential evaporation (E_p) averaged over time incorporate general land surface characteristics via various feedback mechanisms. For example, simple models that utilise changes in mean P and E_p to estimate changes to

Constructing and assessing fire climate regimes

catchment yield, especially if more detailed models are not available or catchments are poorly monitored (Jones et al., 2006; Zhang et al., 2008). The relationship between sensible and latent heat on unsaturated land surfaces is also fairly linear (Brutsaert, 1982; Granger, 1989), resulting in meaningful correlations between variables such as Tmax and P.

Such models do not depend on detailed short-term data. For example, wind speed is essential for calculating short-term evaporation, and rainfall intensity is essential for flash flooding. But if the aim is to explore uncertainties in mean catchment runoff, average wind speed or rainfall intensity are not essential, but regional average rainfall, temperature and radiation are (e.g., Morton, 1983; Yang et al., 2006). Applied to fire, although windspeed is essential to understanding fire weather on a daily scale, it is less important over seasonal to annual timescales, because its effects have been incorporated into other climate variables. Therefore, variables from the prevailing climate need to represent all the key factors contributing to fire climates.

For energy conservation to be obeyed, point and areal relationships need to obey the distributive law. For example, daily FFDI can be converted into seasonal or annual averages at the station scale and those points averaged spatially to obtain regional values. If spatially averaged inputs can be applied to a model that produces equivalent estimates of FFDI, the distributive law has been met. This is routinely carried out for temperature and rainfall but needs to be verified for more complex variables such as fire danger indices.

To be successful, FFDI estimated using high quality data representing Victoria's average climate needs to equal FFDI averaged from an even spread of point estimates. The same data also needs to reproduce interannual variability and reliably measure change. Four indices were targeted: Σ FFDI, days Hi+, days VHi+ and days Sev+ (covering severe, extreme and catastrophic states). Because accessible high-quality regional data for relative humidity, drought indices or wind speed were unavailable, we settled on cloud amount to represent atmospheric moisture content and P to represent antecedent soil moisture.

The next step applied multiple linear regression to the following variables: Tmax measured during the main part of the fire season (TMaxFS, October to March or September to December for NSW, Qld and NT), fire year P measured as a standard anomaly, the areal coverage of 90th percentile of Tmax (90Tmax) over a calendar year and 3 pm cloud (C3pm). Cloud amount was tested for the fire year, but the lag of six months in the calendar year preceding gave slightly better results. Cloud amount was available from 1957 to 2014, so from 2015, we estimated it from maximum temperature and rainfall. The error introduced by this substitution is small, and does not affect the overall results. The regression relationship is described by the following:

$$\text{FFDI} = A + B \times P + C \times \text{TmaxFS} + D \times 90\text{Tmax} + E \times \text{C3pm} \quad \text{Equation 3}$$

The same relationship was used for all four indices and the t-statistics for constants B to D were generally well below $p=0.05$, except for Sev+ index where both TmaxFS indices increased to $p=0.18$ for the C constant and $p=0.35$ for the D constant but were used for convenience. Note also, that the A constant had high p values in each case, showing that the intercept has little influence on the results.

Comparing the results with the 35 stations in common from CCIA2015 and H&L2019, average Σ FFDI and days Sev+ for an individual station or region was best described by average annual RH, Tmax and V.

$$\text{Av FFDI} = A + B \times \text{RH} + C \times \text{Tmax} + D \times \text{V} \quad \text{Equation 4}$$

Model results

The results are shown in Table 2. For Equation 3, r^2 results are >0.9 for Σ FFDI, days Hi+ and days VHi+, and 0.75 for days Sev+. For Equation 4, they show that average fire climates over Australia can be reasonably well described by relative humidity, maximum temperature and wind speed with a few outliers, the latter mainly

near the coast. The standard error of 75% for areally-averaged days Sev+ is due to its highly skewed distribution. This may be improved using higher quality data and possibly different or additional variables.

Table 2: Vital statistics for the regression model results for four FFDI indices for Victoria (Equation 3) and for FFDI indices averages over time (the A constant in Equation 3) across Australia. Changes per unit are shown in the last four columns with error margins. Int is intercept.

Variable	Multi r	r ²	SE	SE (%)	P (St anom)	TmaxFS	90Tmax	C3pm
Equation 3								
ΣFFDI	0.97	0.93	181	6.7%	-326±33	137±66	4.4±1.3	-488±181
Days Hi+	0.97	0.94	5.0	8.0%	-9.2±0.9	5.4±1.8	0.08±0.04	-14.3±5.0
Days VHi+	0.96	0.91	2.6	14.2%	-3.7±0.5	2.2±1.0	0.06±0.02	-7.7±2.6
Days Sev+	0.86	0.75	1.0	38.0%	-0.57±0.19	0.52±0.37	0.007±0.008	-2.61±1.03
Equation 4					Int	RH	Tmax	V
Av ΣFFDI	0.98	0.96	423	12.1%	6661±703	-185±9	111±18	163±25
Av med ΣFFDI	0.98	0.95	556	16.3%	6546±877	-175±10	137±23	90±32
Av 90FFDI	0.96	0.91	3.9	14.2%	44.9±6.0	-1.13±0.07	0.30±0.16	1.49±0.22
Av Days Sev+	0.86	0.75	2.9	75.5%	16.2±4.8	-0.53±0.06	0.02±0.13	0.67±0.17

These results show the potential to combine Equations 3 and 4 to estimate indices except for days Sev+ if high quality data for RH and V becomes available. Each of Equations 3 and 4 follow the distributive law, obeying the linearity expressed both regressions, point- and areally-averaged approaches yielding identical results. However, without high-quality spatial data for RH and V, we could not put this into operation, merely show that it works.

Table 2 also shows sensitivity measured as change per unit inputs in Equations 3 and 4. For Equation 3, C3pm has the strongest effect per unit (being measured in octas). The standardised results are in Table 3, showing standard deviation for each variable as a percentage of each index. P is the strongest input into FFDI but declines with the higher risk indices – its standard deviation accounts up 58% of ΣFFDI but only 33% of days Sev+. TmaxFS is surprisingly low, but is augmented by the spatial component of 90Tmax, so combined, Tmax accounts for roughly 40% using the same measure. C3pm is roughly half that, but for days Sev+ combines strongly with P. This represents conditions with low rain and low cloud amount.

Table 3: Standard variance of the input variable as a proportion of the mean for each variable. This is essentially the weight of the standard deviation of the inputs. E.g., the standard deviation of P is equal to 58% of the mean ΣFFDI. Note that Tmax is p>0.10 for 97FFDI and days Sev+ in a multiple regression.

	ΣFFDI	Days Hi+	Days VHi+	Days Sev+		ΣFFDI	MΣFFDI	97FFDI	Days Sev+
P	-58%	-57%	-50%	-33%	RH	58%	91%	110%	103%
TmaxFS	17%	23%	21%	21%	Tmax	13%	25%	9%	2%
90Tmax	23%	15%	24%	12%	V	16%	14%	41%	42%
C3pm	-18%	-19%	-22%	-32%					

For mean values of FFDI at a location (Equation 4), RH is the most important input, Tmax less important and V becomes more important with higher fire risk. Note that V is actually inversely correlated with FFDI both for the mean and is mostly closely correlated with RH of the various inputs into Equation 4. It acts as a counterbalance to RH in coastal regions, so its contribution to Equation 4 is opposed to its correlation. The greatest outliers in percentage terms were Mackay and Coffs Harbour where windspeed overcompensated in the results. Interannually, the correlation is positive, slightly higher at the lower risk end. For the adjusted

Constructing and assessing fire climate regimes

Victorian windspeed 1971–72 to 2009–10 this is 0.53, 0.48, 0.49 and 0.44 from Σ FFDI to days Sev+. Modelling studies such as those conducted by Clarke, Evans, et al. (2013) find a stronger positive relationship with V and severity on an event basis as in Equation 1.

Figure 1 compares Equation 3 results for Victoria (the blue line) with the station averaged data for the state (red line) for four FFDI indices. They all have relatively close fit, including days Sev+ despite having the poorest r^2 value of 0.75 (Figure 1d).

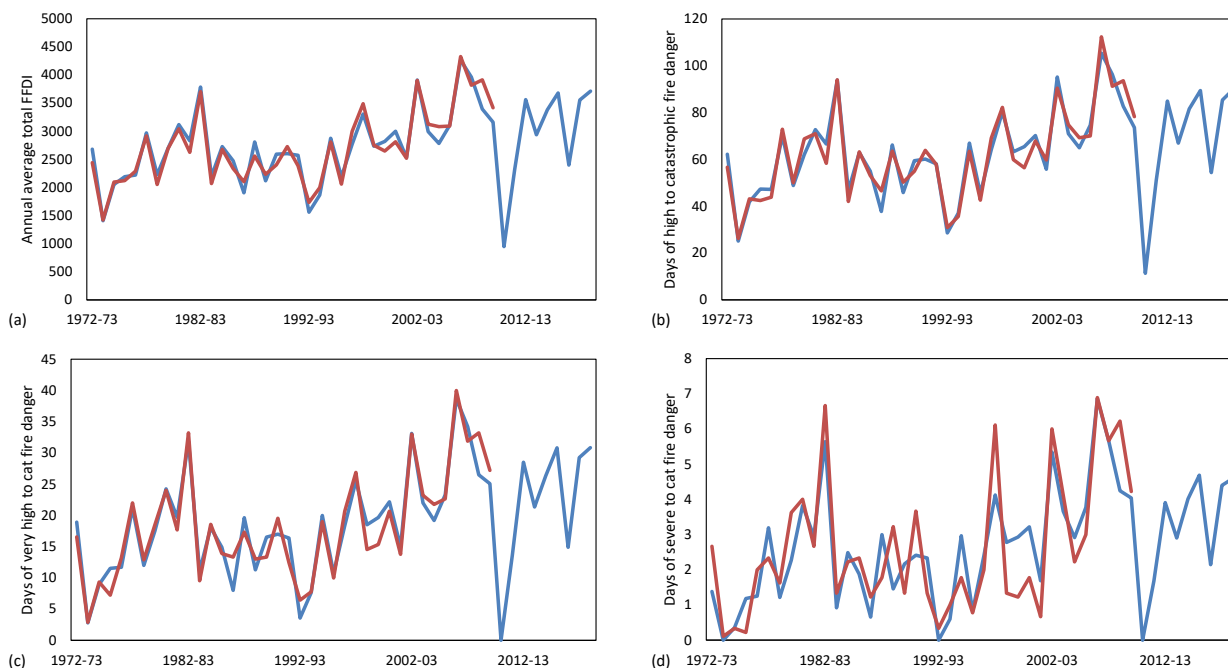


Figure 1: Regression model results for Victoria covering (a) total FFDI, (b) days above high fire danger, (c) days above very high fire danger and (d) days above severe fire danger.

The residuals were investigated to identify missing elements. The only non-random effects showed a 2-year lag effect from rainfall for Σ FFDI, days Hi+ and days VHi+ (correlation -0.31, -0.22, -0.22, respectively) and a one-year lag for Sev+ (-0.23). Higher rainfall has a suppressing effect on FFDI that is not fully represented by the model. However, the relationship was weak ($p > 0.05$), resulting in a low t-statistic. Adding lagged rainfall to the regression had little effect, so the model was left as is. This lag may be compensated for in the future by adding a drought factor if high quality data becomes more widely available.

Further comparisons were made between Σ FFDI and the annual median Σ FFDI from LH2019 and the days VHi+ and 97th percentile from LH2019 averaged from the four Victorian stations common to both data sets (Melbourne, Laverton, Mildura and Sale). Because the totals differ, anomalies were used (Figure 2). The level of agreement between $M\Sigma$ FFDI from JH2019 and Σ FFDI has an r^2 of 0.88 and between 97FFDI and days VHi+ has an r^2 of 0.81. For seven years from the end of the regression period (2010 to 2016 inclusive), these r^2 values are 0.97 and 0.87, respectively, both at the $p < 0.01$ level. This serves as an independent test as it lies outside the model calibration period.

This result, combined with r^2 values > 0.9 for three of the four main FFDI indices, shows that the regressions remain robust following the base period (i.e., 2010–11 to 2015–16). The capacity of the regression model to reproduce the low fire danger year of 2010–11 and high fire danger year of 2015–16 shows that it can be used to extend the FFDI record from fire years beginning in 1957 to 2018–2019.

Constructing and assessing fire climate regimes

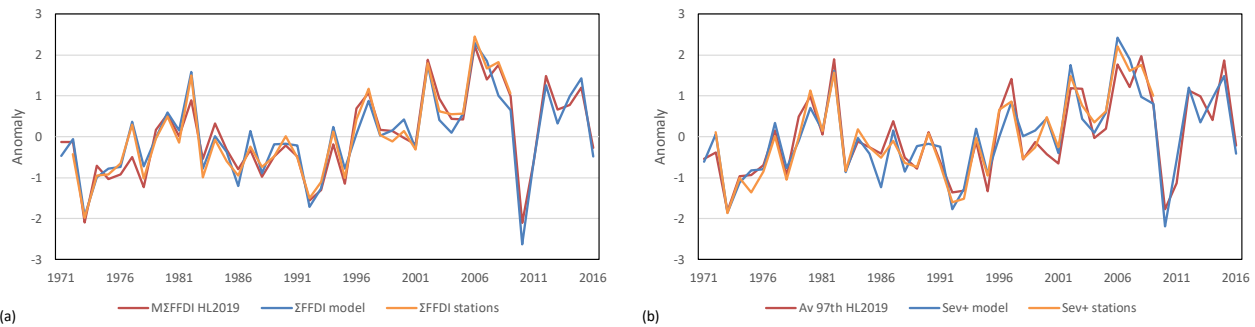


Figure 2. Comparison of anomalies for (a) station-averaged Σ FFDI for Victoria (orange), modelled Σ FFDI from areal averages (blue) and station-averaged median Σ FFDI (red), and (b) the same comparing days Hi+ and the 97th percentile FFDI.

Extending the model to other regions

The model in Equation 3 was applied in other states and regions around Australia. It was expected to do reasonably well in similar climates, but less well in regions with different seasonality. Median Σ FFDI and 97FFDI were averaged for each state or region. The numbers of stations in each region and brief comparisons are listed in Table 4. M Σ FFDI and Σ FFDI, and 97FFDI and days VHi+ were compared for each region. The r^2 results (including 97FFDI and days Sev+) are shown in Table 4 and shown in Figures 3 and 4.

Southeastern Australia covers NSW to just north of Sydney, SA just west of the Eyre Peninsula, Victoria and Tasmania. This region contains 12 stations with an even geographic spread so is likely to be close to the regional average climate. Tmax and P data for the 1971–2016 period are 20.6 °C and 21.0 °C and 638 and 627 mm, respectively. The Σ FFDI r^2 is 0.88 and 97FFDI/VHi+ is 0.86. These are similar to the results for Victoria, showing the impact of good regional coverage.

Table 4: Comparison between HQD FFDI and the 39 station LH2019 data (1971–72 to 2015–16), pairing regional average Σ FFDI with M Σ FFDI, and days VHi+ and days Sev+ with 97th percentile FFDI, results as r^2 values. Station numbers in brackets are those in common with the CCIA2015 and LH2019 data sets.

Region	Stations	r^2 Σ FFDI, M Σ FFDI	r^2 97FFDI, days VHi+	r^2 97FFDI, days Sev+	Notes
Victoria	4	0.88	0.81	0.79	Moderate coverage; state wetter, cooler
New South Wales	9 (9)	0.88	0.87	0.81	Good coverage; state drier, hotter
South Australia	4	0.69	0.65	0.58	Biased coverage; state drier, hotter
Tasmania	2	0.57	0.49	na	Biased coverage (warm, dry); state wetter, cooler
SE Australia	12	0.88	0.86	0.86	Good coverage; climates similar
SW Western Australia	3	0.39	0.25	0.21	Two of three stations differ from regional climate
Queensland	8 (7)	0.87	0.68	0.68	Broad coverage; state drier, hotter
Western Australia	9	0.35	0.44	0.45	Biased coverage (coastal), inhomogeneities
Northern Territory	3 (1)	0.84	0.76	0.73	Even coverage

New South Wales, with nine stations, produces similar r^2 values of 0.88 and 0.87. This is despite a slightly warmer and drier climate represented in the state averages (+1.1 °C and 61% P). There is a subtle change of balance between the two over the period of record where M Σ FFDI increases faster than Σ FFDI.

Constructing and assessing fire climate regimes

For **South Australia**, the result is poorer, with r^2 results of 0.69 and 0.65, possibly due to having two arid zone and two temperate stations in a state with a very large arid zone. There are large differences between Tmax and P between the station and state averages as a result.

Tasmania has the reverse issue, with the two stations (Launceston, Hobart) being warmer and drier than the state average. R^2 values are 0.57 and 0.49. Windspeed registers a shift of 17% in 1993, possibly influencing the balance between the two data sets.

For **SWWA**, the individual stations do not represent the regional average very well, with r^2 values of 0.39 and 0.25 for the two comparisons. Of the three stations, Perth represents regional temperature and rainfall better than Albany or Esperance. Most of the differences are due to rainfall patterns; Albany and Esperance are not very representative of the regional pattern.

Queensland shows r^2 values of 0.87 and 0.68. The former is probably due to more comprehensive state coverage of eight stations despite differences in Tmax (28.3 °C and 30.3 °C) and P (1053 mm and 647 mm, stations and state, respectively). This presents a coastal bias.

Western Australia has low r^2 values of 0.35 and 0.44, the only case where median/mean Σ FFDI fares worse than the extremes. These values change over time; for 1971–1995, they are 0.39 and 0.33 respectively and from 1996 both are 0.69. WA contains several climates, which may be unevenly represented (as was the case for SWWA) but inhomogeneities may also be affecting the results, including an 8% shift in windspeed in 1994.

Northern Territory shows r^2 values of 0.84 and 0.76, the good result probably due to the three evenly spaced stations, even though the fire season in Darwin is distinctly different to that in Tennant Creek and Alice Springs. This also demonstrates the capacity for Equation 3 to represent different climatic patterns.

We calculated mean Σ FFDI and days Sev+ for each station in the LH2019 dataset using Equation 4, then averaged it across each state and region. We compared this with Σ FFDI and days Sev+ calculated with the HQD and averages reported in CCIA2015. The base years were 1981–2010 for CCIA2015 and displaced six months earlier into fire years 1980–81 to 2009–10 for the other two measures. This involved a slight loss of accuracy. The results are shown in Table 5.

Only the 35 stations common to both LH2019 and CCIA2015 could be used, so that coverage some regions is slightly more constrained. When Equation 4 is applied to each station, the resulting regional averages for Σ FFDI is within 10% of the regional station averages from CCIA2015 (Table 5). Days Sev+ are less accurate, with SA under-estimated by 1.7 days, SWWA over by 1.3 days and NSW over by 1.1 day the rest within ± 1 day. The point and areal outcomes for Equation 4 obey the distributive law perfectly and days Sev+ is close but shows a small amount of nonlinearity. Compared with the HQD results, differences in climate expressed as P and Tmax result in higher or lower estimates for Σ FFDI, depending on the direction of bias.

The days Sev+ index is prone to overestimation in warmer and drier conditions. We are reasonably confident that having high-quality RH and V available at both the station and regional scale will help to constrain these estimates. However, the results show that interannual variability is being relatively well captured by the Equation 3, so estimates of relative change over time can be relied upon.

Constructing and assessing fire climate regimes

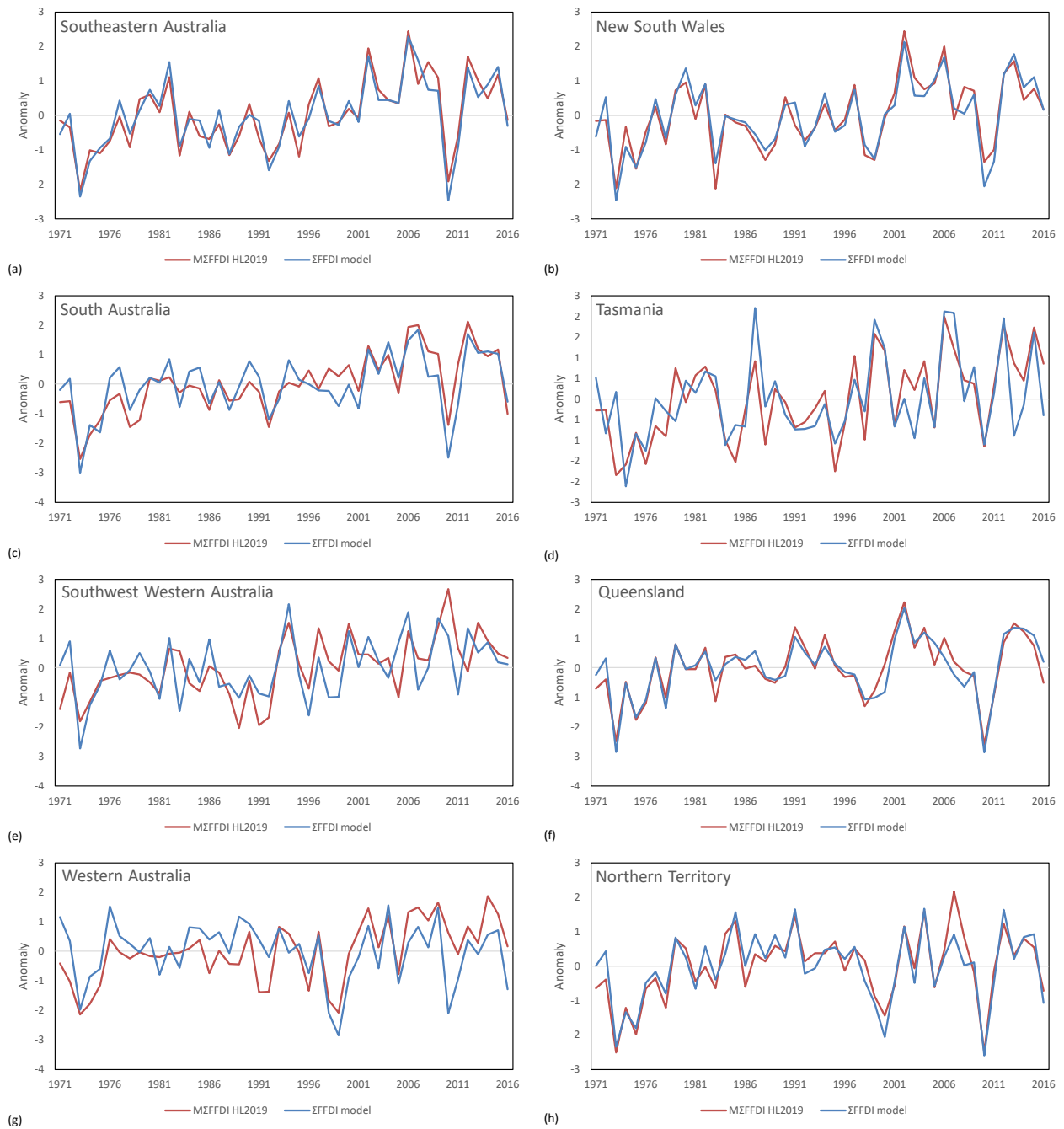


Figure 3. Comparisons of anomalies for median Σ FFDI from LH2019 (station data averaged for the region) and Σ FFDI calculated from regional average climate for (a) southeastern Australia, (b) New South Wales/ACT, (c) South Australia, (d) Tasmania, (e) southwest Western Australia, (f) Queensland, (g) Western Australia and (h) Northern Territory.

Constructing and assessing fire climate regimes

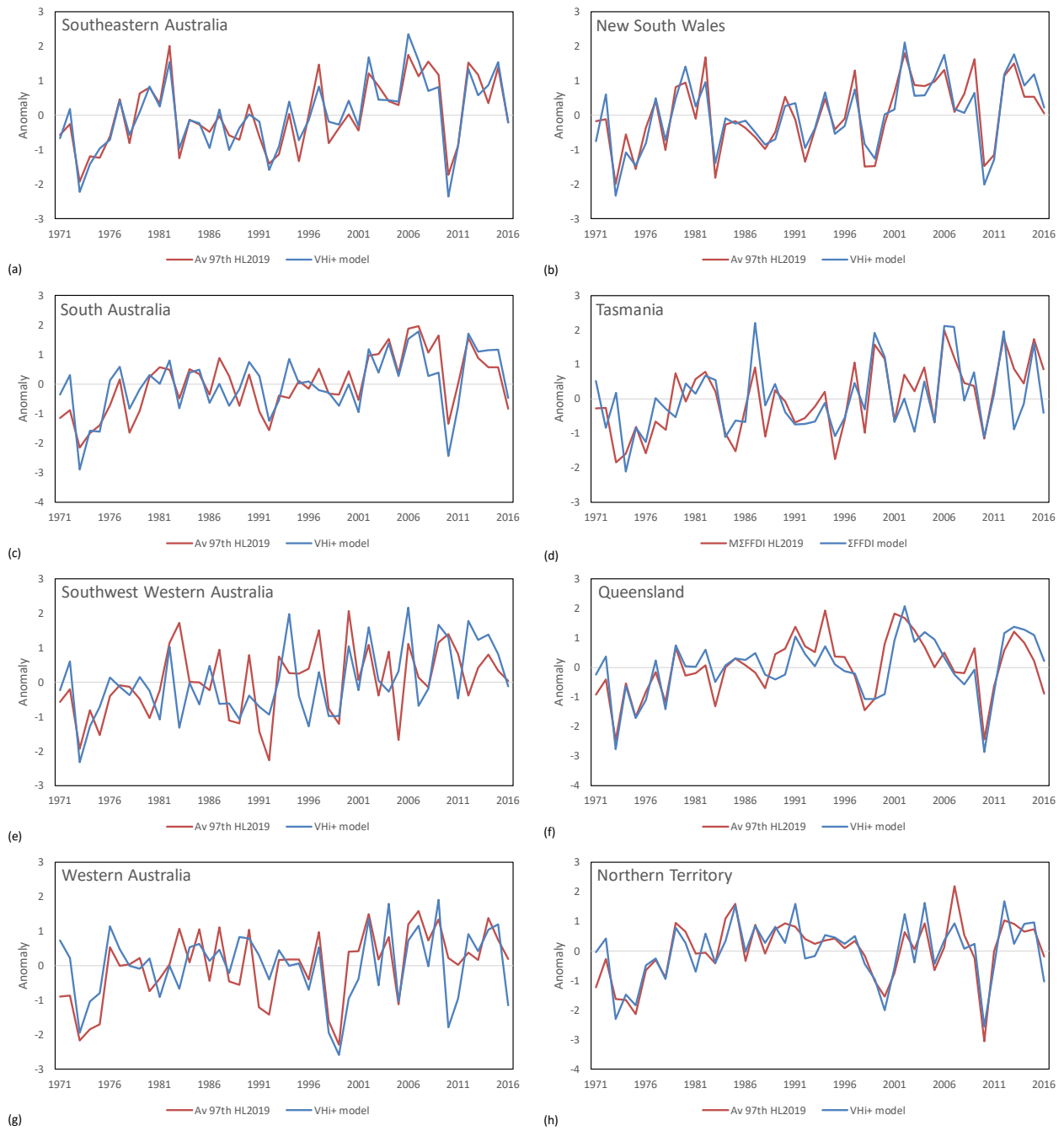


Figure 4. Comparisons of anomalies for the average 97th percentile of FFDI from LH2019 (station data averaged for the region) and days VHi+ calculated from regional average climate for (a) southeastern Australia, (b) New South Wales/ACT, (c) South Australia, (d) Tasmania, (e) southwest Western Australia, (f) Queensland, (g) Western Australia and (h) Northern Territory.

Table 5. Comparison of estimates for Σ FFDI and days Sev+ (1980–81 to 2009–10) from regressions at individual stations and averaged over a state or region, estimating both from state or regional average climate and averaged station Σ FFDI and days Sev+ from CCIA2015.

Method	Tmax	P	Daily Σ FFDI	Model Σ FFDI	Daily Sev+	Model Sev+
Victoria						
Station daily data*	20.9	453	2691		3.4	
State regression HQD	20.2	642		2723		2.9
CCIA2015/LH2019 station av	20.9	500	3025	2993	3.0	3.8
Southeastern Australia						
Regional regression HQD	21.0	605		3054		3.8
CCIA2015/LH2019	20.8	670	2579	2569	1.9	2.4
New South Wales						
State regression HQD	24.4	527		3614		7.0
CCIA2015/LH2019	23.4	861	2923	3047	1.9	2.6
Tasmania						
State regression HQD	14.9	1336		1616		0.0
CCIA2015/LH2019	17.2	652	1415	1318	0.1	0.0
South Australia						
State regression HQD	27.2	222		4437		10.3
CCIA2015/LH2019	22.7	434	4437	4097	8.0	6.3
Southwest Western Australia						
Regional regression HQD	22.5	631		3561		6.7
CCIA2015/LH2019	22.1	734	2399	2562	1.4	2.7
Queensland						
State regression HQD	30.3	616		4504		10.2
CCIA2015/LH2019	28.4	1136	3193	3239	2.2	1.9
Western Australia						
State regression HQD	29.6	377		4408		10.9
CCIA2015/LH2019	26.6	477	4571	4583	6.6	6.7
Northern Territory						
State regression HQD	32.3	579		4765		11.5
CCIA2015/LH2019	32.2	1702	3186	3332	0.4	1.0

3. Assessing Fire Climate Regimes for Australia

Current understanding of fire climates and climate regimes

Existing records of historical Forest Fire Danger Index (FFDI) and Grass Fire Danger Index within the Bureau of Meteorology date from 1972 for a number of sites around the country (Lucas, 2009), later updated (Clarke, Lucas, et al., 2013; Harris & Lucas, 2019). Dowdy (2018) produced a gridded daily record 1950–2016 for the whole country. Custom regional station-based records have also been created for research purposes (Fox-Hughes, 2008) along with downscaled results from climate models. State fire agencies assess spatial fire risk using tools like the Phoenix fire model (Duff et al., 2014).

Despite all this work, the scientific understanding of fire climates and their relationship with changing fire risk is limited. The relationship between climate change and changing fire risk is widely acknowledged (Abram et al., 2021; Clarke & Evans, 2019; Clarke et al., 2016; Hennessy et al., 2005; Lucas et al., 2007; Williams et al., 2013) but without a clear baseline and reliable methods to measure that change, it difficult to know how fast fire risk is changing and what future risks may be. The standard method is to assess the linear trend, but decadal variability, data quality and a comparatively brief record complicate this.

These limitations can be overcome by using high quality data to identify regime changes and attributing those to external forcing. Temperature follows a staircase-like pattern of change (Belolipetsky et al., 2015; Jones, 2012; Jones & Ricketts, 2017). Figure 5 shows maximum temperature (Tmax) for Victoria 1910–2019, detected using the Maronna-Yohai (1978) bivariate test. Limited change occurred from 1910 to 1996 when a regime change resulted in Tmax increasing by almost 1°C (Jones, 2012), followed by a shift of 0.5°C in 2013. The shift in 1997–98 extended across SE Australia, part of a phenomenon that affected global climate. The shift in 2013–14 ended the so-called hiatus in warming that began in 1997–98 (Jones & Ricketts, 2019).

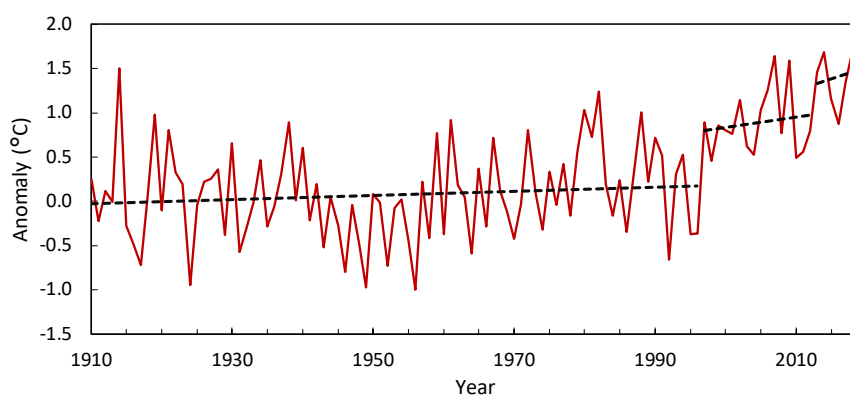


Figure 5: Average maximum temperature for Victoria 1910–2019, showing regime changes detected to a level of $p < 0.01$.

An assessment of regime changes in the Australian region to 2019 show shifts commencing in the late 1950s, mainly in minimum temperature in the north of Australia; widespread shifts in the late 1960s–early 1970s in both maximum and minimum, 1979 in mainly minimum temperature (Tmin) in the north, 1996–98, and most recently Tmax during 2008 to 2010 in western Australia and 2013–14 in eastern Australia. Rainfall (P) shifted downwards in SW Western Australia (SWWA) in the late 1960s and upwards in northern Australia in 1973. How have these changes influenced fire regimes?

Assessing climate fire regimes

The baseline data set presented in the previous chapter is referred to in the following as VicSD72–10, SD for station data. The full model data set built from the high-quality data extends from 1957–58 to 2019–20. For Victoria the full data set is referred to as VicHQD with years shown as 72–10 for the series matching VicSD72–10, and VicHQD57–19 for the extended record. Unless otherwise indicated, all data is in fire years from July to June the following year.

Constructing and assessing fire climate regimes

From the LH2019 data set we extracted the median Σ FFDI (M Σ FFDI) and the 97th percentile (97FFDI) variables contributing to FFDI from the 39 stations around Australia for the fire years 1971–72 to 2015–16. Averages were calculated to each state and territory. The Victorian average is from four stations and is labelled VicLH. For both the HQD and LH data sets, the prefix changes with region (e.g., NSWHQD, NSWLH) and suffix with time period. The other data set used in comparisons are from Climate Change in Australia (CCIA) (CSIRO & Bureau of Meteorology, 2015), which contains 1981–2010 means for Σ FFDI, days Sev+, Tmax, P and DF for 36 stations nationally. These data sets have substantial but not complete overlap.

The level of agreement between median Σ FFDI from VicLH and Σ FFDI from VicHQD has an r^2 of 0.88 and between the 97% FFDI percentile and VHi+ is 0.81. For seven years from the end of the regression period (2010 to 2016 inclusive), r^2 values are 0.97 and 0.87, respectively. All results are at the $p < 0.01$ level. This serves as an independent test – the latter r^2 results are higher than for the original multiple linear regression. This suggests the later data is more reliable than the earlier record.

Shift results for the four FFDI indices averaged from the station data Figure 6 are similar to those in Figure 1, showing regime changes as successive means. The magnitude of change is nonlinear with respect to higher fire risk. Σ FFDI increases by 44%, whereas Sev+ shifts up by 133%, shifting from 2.1 days per year to 4.8 days.

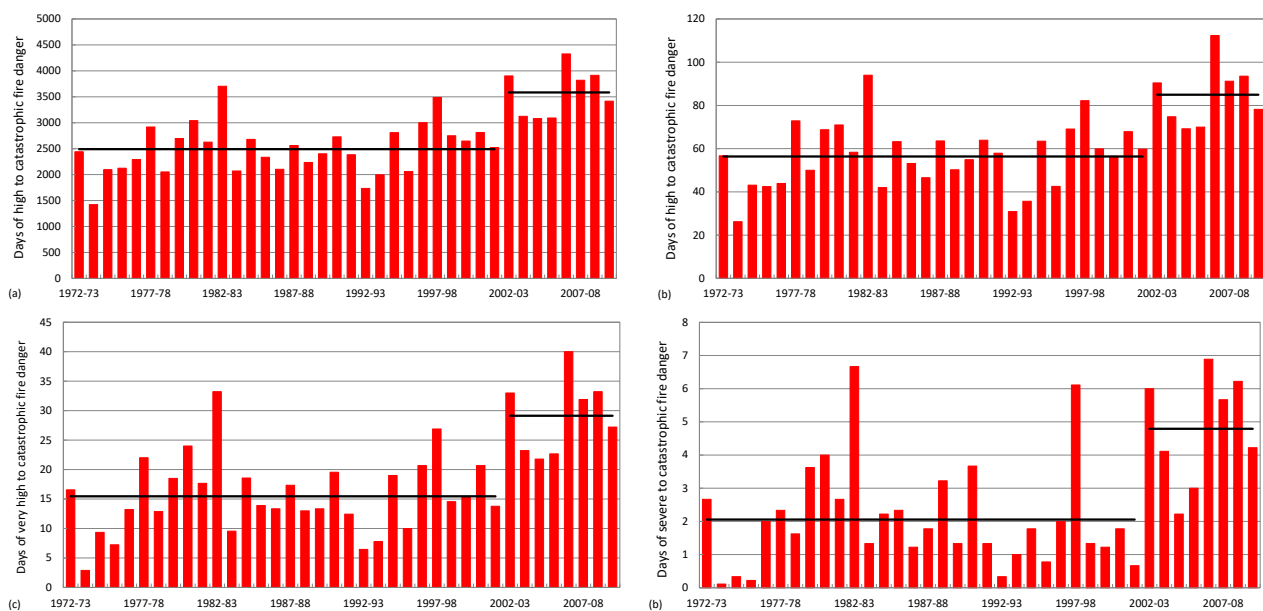


Figure 6: Measures of FFDI 1972–73 to 2009–10 from VicStations72–10, adjusted for windspeed inhomogeneities, averaged across Victoria without area weighting, covering (a) total FFDI, (b) days above high fire danger, (c) days above very high fire danger and (d) days above severe fire danger.

The extended climatology

The full data set 1957–2019, of 62 years' duration allows regime shifts to be analysed with greater confidence. The starting date coincides with the earliest detected regime shifts for Australia: Tmin and average temperature (Tav) in northern and western Australia in 1957–58 (Records begin in 1910). These vary between 0.4 °C to 0.6 °C for Aust Tmin, and WA and SA Tmin and Tav. Changes in Tmin are not anticipated to greatly affect fire regimes and are considered to be related to large-scale shifts in sea surface temperatures.

The analysis of time series for step changes can be influenced by end effects, affecting shorter records so that short runs of anomalous data are detected as regime shifts. Interannual climate variability can also affect the timing of detection – adjacent extremes to an underlying regime shift can lead to the break point being displaced by several years. This has little effect on the size of the shift, only its timing. If available, monthly data can be used to pinpoint change dates.

Constructing and assessing fire climate regimes

We conducted tests with different combinations of data to test the robustness of shift dates and to detect shifts in the input data. VicSD and VicHQD 1972–73 to 2009–10 both shift in 2002, shifts in the latter being 15–11% smaller (Table 3). The extended climatology was then tested in two forms: (1) VicHQD57–19 with VicSD72–10 inserted (blended) and (2) VicHQD57–19 only. The blended set shows the shift date moving back to 1996–97 for Σ FFDI and days Hi+ time series and remaining at 2002–03 for the higher risk ratings. Three indices for VicHQD57–19 shift in 1997–98 and days Sev+ in 2002–03. The shifts are larger for point-sourced data.

Table 6: Shift year, size of shift estimated by the bivariate test for FFDI from observations and regression model for the period 1972–73 to 2009–10 and a blended time series from the models and observations and the modelled time series 1957–58 to 2017–18. All shifts $p < 0.01$.

Period Variable	1972–73 to 2009–10			1957–58 to 2019–20			
	Shift year	VicSD shift	VicHQD shift	Shift year	VicBlend shift	Shift year	VicHQD shift
Σ FFDI	2002	1081	919	1996	734	1997	659
Days Hi+	2002	29.1	25.6	1996	19.8	1997	18.6
Days VHi+	2002	13.6	11.8	2002	10.2	1997	9.0
Days Sev+	2002	2.8	2.5	2002	2.0	2002	1.8

The LH1097 1971–2016 M Σ FFDI and 97FFDI records for Victoria show shifts in 1996–97 and 2002–03, respectively $p < 0.01$ and $p < 0.05$, following a similar pattern to the blended record. The inputs to that record, DF, KDBI, RH and V all shifted in 1996–97, and Tmax in 1998–99 at $p < 0.01$. The full record of VicHQD inputs from 1957 show shifts in TmaxFS in 2002–03 and Tmax90 in 2005–06, P in 1994–95 at $p > 0.1$ (10% decrease) and no result for C3pm (no result returns a $p > 0.1$ and shift/standard deviation ratio of < 1).

Comparing three different data sets, point-averaged and spatially-averaged, with different lengths and variables is hard to follow, but we present these comparisons to show that (1) the climatology is robust and (2) the underlying climate regime change most probably occurred in 1996–97. October 1996 was nominated as the date when relative humidity shifted downwards (Bureau of Meteorology, 2006), heralding the beginning of the Millennium drought. This shift has been associated with a climate regime change across SE Australia, affecting Tmax in particular (Jones, 2012).

In Figure 7a–c, shifts detected 1996–97 in the longer data set, indicates the variations above may be due to small differences between shorter time series. These longer records are finely balanced as to whether 1995–96 or 1996–97 is preferred. Days Sev+ stays at 2002–03 for all versions (Figure 7d). Years of high risk become more apparent through Figures 7a–d as standard deviation increases with severity. We contrasted the size of the shifts with the co-efficient of variation (C_v) for each index. This progression follows a power relationship, where the change in mean in percentage equals $C_v^{1.45}$, where C_v is the co-efficient of variation (r^2 0.99 for four points, $p < 0.01$). Relative changes in regions with low fire risk are proportionally greater than those with high fire risk. This result has far-reaching outcomes for regions where fire risk may shift from negligible or rare events to a much higher frequency.

Constructing and assessing fire climate regimes

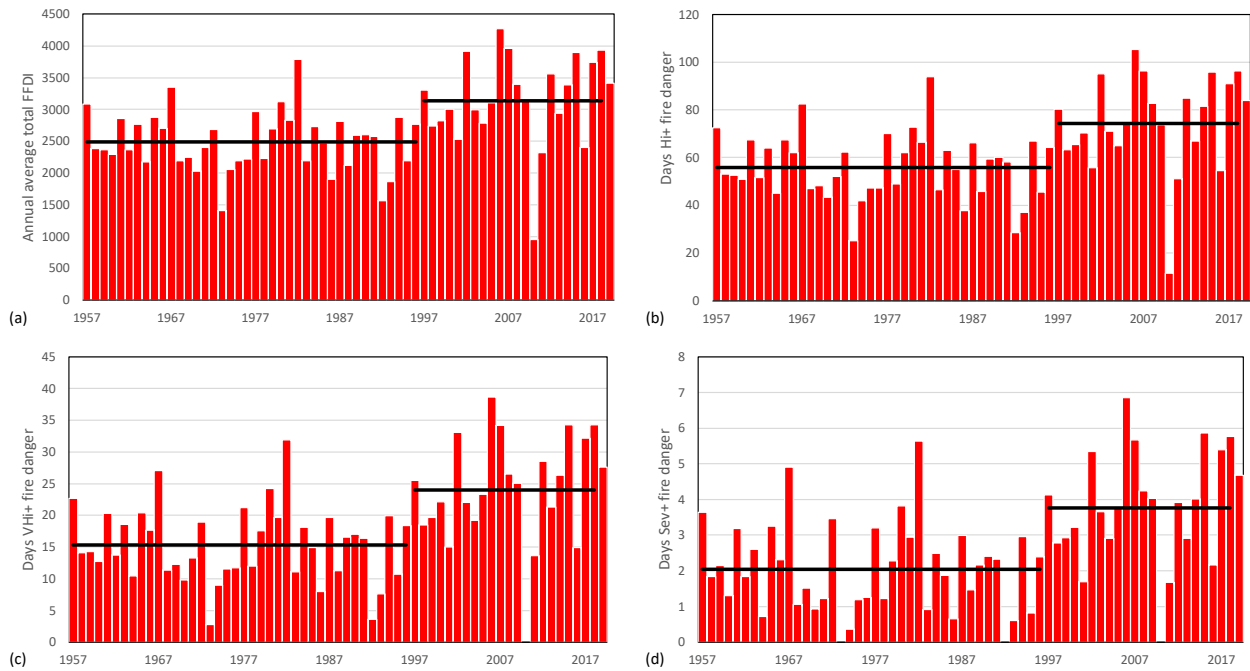


Figure 7: Regression model results for Victoria 1957–58 to 2019–20, showing regime averages (black lines) for (a) total FFDI, (b) days above high fire danger, (c) days above very high fire danger and (d) days above severe fire danger.

Extending to other regions

Table 7 summarises the results of bivariate testing to the regions outside of Victoria, where the HQD1957–2019 FFDI indices were tested for shifts in mean. NSW and SA both show shifts in 2012–13, but testing also showed a secondary shift in 2002–03. The reasons for pursuing this earlier shift are outlined next. Queensland FFDI indices also shift, but less definitively, in 2012–13. Victoria Σ FFDI and days Hi+ shift in 1996–97 or 1997–98 depending on the data set and days VHI+ and Sev+ in 2002–03. SEA shifts at the time and SWWA two years year earlier, except for days Sev+ on 2004–05. Tasmania shows shifts with varied timing. WA and NT shod no shifts of note.

Attributing regime changes depends on the influence of other climate variables. If co-dependent or physically-related variables show similar timing, and those shifts can be attributed to forcing, then changes in fire regimes can also be attributed to forcing if there is no other plausible explanation. Timeseries from the HQD inputs to Equation 3 can be tested either for the period of FFDI record or the whole record from 1910 (C3pm from 1957). The whole record is preferred because it includes an extended period of stationary climate and is less prone to end effects. The LH2019 data set provides 46 fire years, allowing regime changes in the input variables to also be tested. Table 8 lists station-averaged variables for the regions listed in Table 7 plus Victoria.

For the variables in Equation 3, only Tmax and Tmax90 are strongly nonlinear; Tmax via regime changes and Tmax90 through rapid acceleration in the last two decades. A sensitivity assessment carried out by subtracting each of the variables from Equation 3 for HQD Σ FFDI shows that although Tmax and Tmax90 are influential, P and C3pm both contribute to the shift date, although with varying p values. This is important, because all four inputs are required to reproduce the regime shift in the original data through a combinatory effect.

Omitting each of the four variables for Victoria produces all the shift dates represented in Table 1. NSW and Qld all select 2012–13, SA 2002–03 and 2012–13, Tasmania 1996–97 and 2005–06 and SWWA 2002–03, 2000–01 and 1968–69, the latter if C3pm is omitted. The timing of the latter coincides with the drying of the region, where P decreased but with little effect on temperature.

Table 7: Regime detection of FFDI derived from mean annual climate data from selected states and regions using the bivariate test, showing the year of shift, p level attained (<0.1, <0.05 or <0.01) and change differenced from the regime means.

Variable	Shift year	P level	Regime 1	Regime 2	Change	Change (%)
New South Wales (primary) 1957–58 to 2019–20						
ΣFFDI	2012–13	p<0.01	3549	4431	882	25%
Days Hi+	2012–13	p<0.01	92.3	117.5	25.2	27%
Days VHi+	2012–13	p<0.01	31.8	43.9	12.1	38%
Days Sev+	2012–13	p<0.05	6.6	9.0	2.4	37%
New South Wales (secondary) 1957–58 to 2009–10						
ΣFFDI	2002–03	p<0.05	3489	4135	646	19%
Days Hi+	2002–03	p<0.05	90.5	110	19	21%
Days VHi+	2002–03	p<0.05	31.0	39.9	8.9	29%
Days Sev+	2002–03	p<0.05	6.4	8.3	1.9	30%
South Australia (primary) 1957–58 to 2019–20						
ΣFFDI	2012–13	p<0.01	4331	4950	620	14%
Days Hi+	2012–13	p<0.01	119.8	137.2	17.4	15%
Days VHi+	2012–13	p<0.01	44.3	53.0	8.7	20%
Days Sev+	2012–13	p<0.05	10.1	11.8	1.7	17%
South Australia (secondary) 1957–58 to 2009–10						
ΣFFDI	2002–03	p<0.05	4282	4814	533	12%
Days Hi+	2002–03	p<0.05	118.5	133	15	13%
Days VHi+	2002–03	p<0.05	43.6	50.9	7.3	17%
Days Sev+	2002–03	p<0.05	10.0	11.4	1.4	14%
Tasmania 1957–58 to 2019–20						
ΣFFDI	1999–2000	p<0.05	1403	1792	390	28%
Days Hi+	1997–98	p<0.10	15.3	25.1	9.7	64%
Days VHi+	2006–07	p<0.05	1.5	5.6	4.1	271%
Days Sev+	nr	nr	nr	nr	nr	nr
Southeastern Australia 1957–58 to 2019–20						
ΣFFDI	2002–03	p<0.05	2780	3404	624	22%
Days Hi+	2002–03	p<0.01	65.4	83.1	17.6	27%
Days VHi+	2002–03	p<0.01	19.8	28.2	8.4	43%
Days Sev+	2002–03	p<0.01	3.3	5.0	1.7	52%
Southwest Western Australia 1957–58 to 2019–20						
ΣFFDI	2000–01	p<0.05	3406	3769	363	11%
Days Hi+	2000–01	p<0.01	87.4	102.5	15.0	17%
Days VHi+	2000–01	p<0.01	29.9	37.0	7.0	23%
Days Sev+	2003–04	p<0.01	6.3	7.5	1.2	19%
Queensland 1957–58 to 2019–20						
ΣFFDI	2012–13	p<0.1	4500	5026	626	14%
Days Hi+	2012–13	p<0.1	124.4	141.6	17.2	14%
Days VHi+	2012–13	p<0.1	45.4	53.7	8.3	18%
Days Sev+	2012–13	p>0.1	10.1	11.6	1.5	15%
Western Australia 1957–58 to 2019–20						
All	nr	nr	nr	nr	nr	nr
Northern Territory						
All	nr	nr	nr	nr	nr	nr

Table 8: Results of bivariate testing for the HL2019 inputs averaged for the regions in Tables 6 and 7 showing the year of the shift and p values (null hypothesis, or a random change in mean). Above p=0.1 no result (nr) is given. Single years are calendar years and ranges denote fire years (July to June). HQD denotes high quality data from the Bureau of Meteorology 1910–2019.

	DF		KDBI		P		Days P	
	Date	P value						
Vic	1996–97	<0.01	1996–97	<0.01	nr	nr	nr	nr
NSW	nr							
SA	1974–75	<0.05	1974–75	<0.01	nr	nr	1993–94	<0.05
Tas	nr							
SE Aust	1996–97	<0.05	1996–97	<0.05	1977–78	<0.05	nr	nr
SW WA	nr	nr	nr	nr	nr	nr	1993–94	<0.05
Qld	nr							
WA	nr							
NT	nr	nr	1976–77	<0.1	nr	nr	nr	nr

	RH		Tmax (HQD)		Tmax FS (HQD)		V	
	Date	P value	Date	P value	Date	P value	Date	P value
Vic	1996–97	<0.01	1997	<0.01	2002–03	<0.01	1996–97	<0.01
NSW	2001–02	<0.01	2001	<0.01	2002–03	<0.01	1994–95	<0.01
SA	1996–97	<0.01	2001	<0.01	2002–03 1965–66,	<0.01	1991–92	<0.01
Tas	1996–97	<0.01	1999	<0.01	2006–07	<0.01	1993–94	<0.01
SE Aust	1996–97	<0.01	1997	<0.01	2002–03	<0.01	1994–95	<0.01
SW WA	1993–94	<0.01	1994	<0.01	1993–94 1979–80,	<0.01, <0.05,	1976–77	<0.01
Qld	nr	nr	2001, 2013	<0.01	2011–12	<0.01	1992–93	<0.01
WA	2001–02	<0.01	2001	<0.01	2002–03	<0.01	1994–95	<0.01
NT	1979–80	<0.05	1979, 2013	<0.01,<0.05	1979–80	<0.01	1990–91	<0.01

Matching shift dates in Table 8 with those in Table 7 indicates that shifts in TmaxFS and RH have the most influence on FFDI shift dates. Windspeed (V) shows a strong influence of the introduction of instrumentation in 1993–94, indicating that more quality control of this variable is needed. Comparisons between fire year and fire season Tmax shows that annual and winter season Tmax (the latter not shown) coincides with downward shifts in RH. Compared to Tmax, TmaxFS is delayed by a few years in the southern and eastern regions. These were years of successive relatively dry La Niña events, where three of four summers were cooler and P remained close to the long-term mean. The 2012–13 peak is associated with the return of high FFDI conditions after the two wet years and suppressed Tmax during 2010–2012. These were initiated by the most powerful La Niña in 50 years, a negative Indian Ocean Dipole and strong positive Southern Annular Mode combining with record sea surface temperature of NW Australia (Hendon et al., 2014). A regime shift in sea surface temperature preceded these events in 2009. Annual Tmax also shifted warmer in the eastern states in 2013, likely to have contributed to sustained high FFDI levels since that time.

Victoria: The current fire regime commenced in 1997–98. While the change in Σ FFDI average from seven stations is an estimated 44% from 2002–03 to 2009–10, the shift from the full HQD57–18 reconstruction is 26%. The lower shift is due to the longer time series that includes the cooler years of 2010–2011. The HQD data set is also slightly cooler and wetter than the station data set. The higher risk indices follow a power law with increasing severity.

New South Wales: A shift was initially detected in all four variables of FFDI 2012–13, three at p<0.01 and Sev+ at p<0.05. When tested to mid-2010, thus avoiding the two wet years to mid-2012, a shift in 2002–03 at p<0.05 is detected in all indices. Based on underlying shifts in fire season Tmax and RH at the same time,

we conclude that the current fire regime in NSW began in 2002–03. Further work is needed to determine whether warmer conditions after 2013 are leading to even greater fire risk. Figure 8 shows these regimes for Σ FFDI and days Sev+.

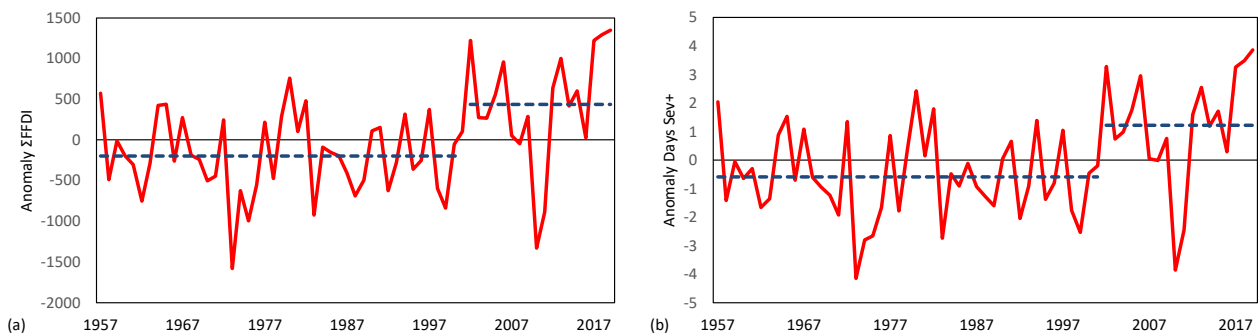


Figure 8: Annual anomalies and regimes for New South Wales for (a) Σ FFDI and (b) days Sev+ with the current fire season added in to the end of January 2020, scaled to the annual average. Anomalies from a baseline of 1980–81 to 2009–10.

South Australia: As for NSW, the bivariate test selects 2012–13 with the full data set for all FFDI indices, but cropped to 2009 shows a shift in 2002–03 at $p < 0.05$. Increases vary from 14% to 20% for the earlier date. RH shifts in 1996–97 and TmaxFS in 2002–03. Estimated Σ FFDI for the HQD data is close to the average from the four climate stations, even though mean state Tmax is higher than station mean Tmax. Figure 9 shows these regimes for Σ FFDI and days Sev+ with the current fire season added in to the end of January 2020, scaled to the yearly average.

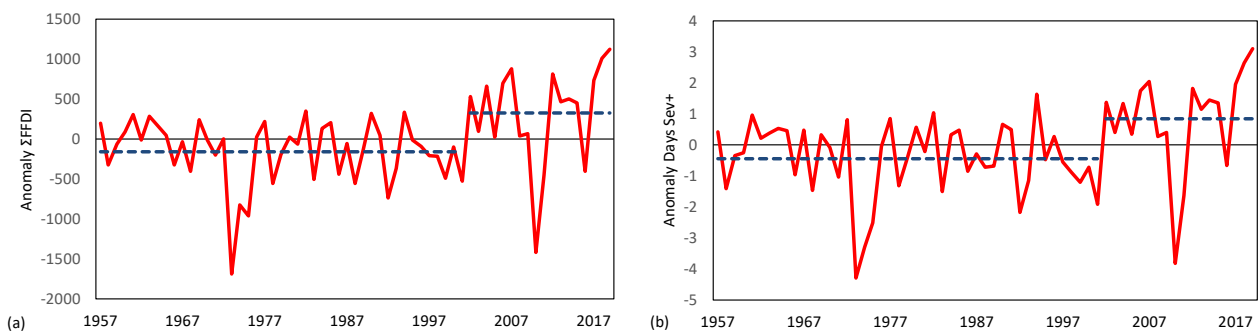


Figure 9: Annual anomalies and regimes for South Australia for (a) Σ FFDI and (b) days Sev+ with the current fire season added in to the end of January 2020, scaled to the annual average. Anomalies from a baseline of 1980–81 to 2009–10.

Tasmania: The results do not show a consistent pattern, with Σ FFDI shifting in 1999–2000 at $p < 0.05$, days Hi+ in 1997–98 at $p < 0.01$ and days VHi+ in 2006–07 at $p < 0.05$. The latter date is sensitive and in 100 trials using a random timeseries reference approximately one-third of the time 1999–2000 is selected. No useful results were produced for days Sev+. Shifts in key input data show a shift in RH in 1996–97, Tmax in 1990 and TmaxFS in 2006–07 all at $p < 0.01$. These are reasonably close to the above dates. Fox-Hughes (2008) noted that severe events increase faster than the mean in SE Tasmania, and that spring events in Hobart increased during the mid-1990s. Changes may not have been uniform across the island and projections of future change vary widely from the southwest to the northeast (Fox-Hughes et al., 2014).

Figure 10 shows these regimes for Σ FFDI and days VHi+. The regime shift in days VHi+ has been moved back to coincide with that in Σ FFDI, to provide a consistent comparison. This figure emphasises a result that was also evident for Victoria. Extreme hot, dry departures in cool, wet climates can be dramatic, leading to disproportionate changes in mean following regime changes. The r^2 value between days VHi+ and FFDI97 in the HL2019 dataset is 0.41, $p < 0.01$. Further work would be required to provide a more reliable estimate of days VHi+ fire risk, but the principle of proportionally larger changes in cool, moist climates holds, especially where conditions are becoming more variable.

Constructing and assessing fire climate regimes

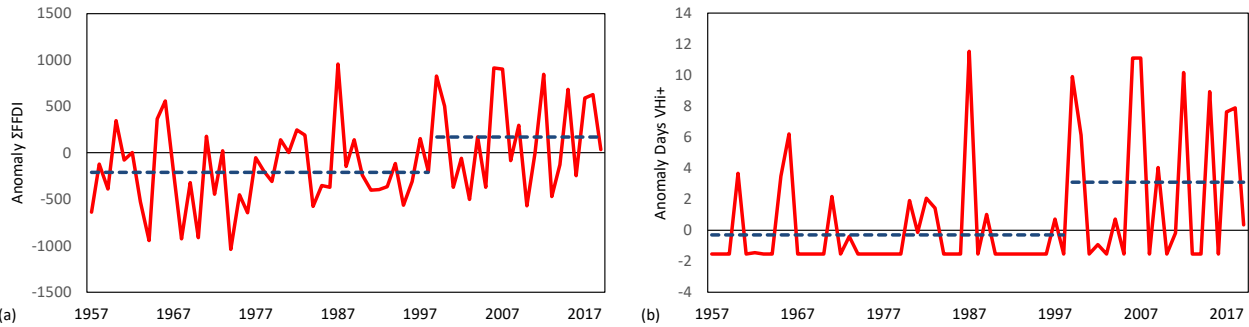


Figure 10: Annual anomalies and regimes for Tasmania for (a) Σ FFDI and (b) days VHi+ with the current fire season added in to the end of January 2020, scaled to the annual average. Anomalies from a baseline of 1980–81 to 2009–10.

Southeastern Australia: covering southern NSW, SE South Australia, Victoria and Tasmania, this region underwent a fire regime shift in 2002–03, but the underlying variables indicate this was in response to a general climate regime shift in 1997–98. Figure 11 shows these regimes for Σ FFDI and days Sev+.

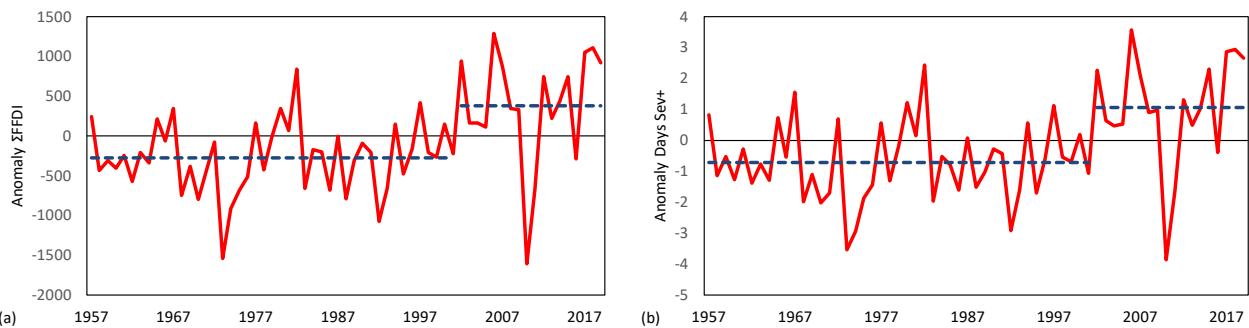


Figure 11: Annual anomalies and regimes for southeastern Australia for (a) Σ FFDI and (b) days VHi+ with the current fire season added in to the end of January 2020, scaled to the annual average. Anomalies from a baseline of 1980–81 to 2009–10.

Southwest Western Australia: this region shows a similar pattern to SE Australia, shifting one year earlier in 2001–02, whereas the underlying climate data shows shifts in RH and TmaxFS 1993–94. In Figure 12, which shows regimes for Σ FFDI and days Sev+, 1993–94 forms a peak, but is followed by several years of lower fire danger before consistently forming a consistent change in mean, as indicated by the bivariate test. Severe fires occurred in 2002–03, the worst since 1960–61 (Bryant, 2008), which marks the regime shift in days Sev+. According to these records, the late 1960s downward shift in rainfall seems to have had no impact on FFDI. Enright and Fontaine (2014) describe fire activity as quiescent for a long period before reporting a succession of fires in the 2000s.

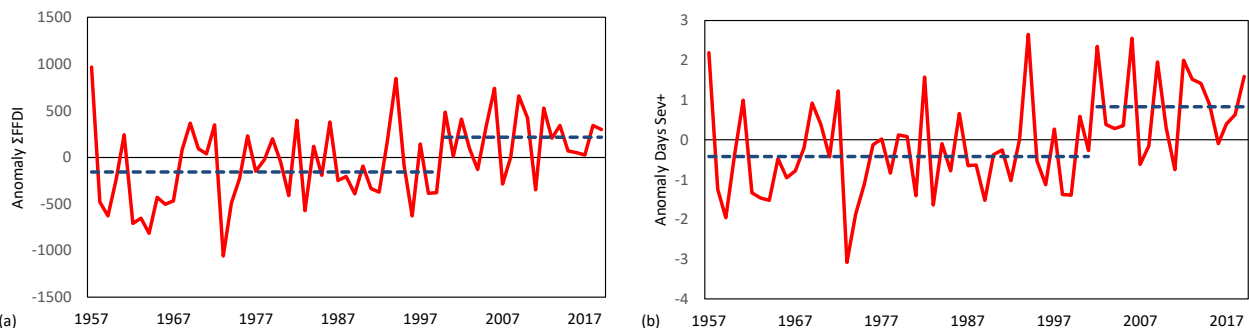


Figure 12: Annual anomalies and regimes for Southwest Western Australia for (a) Σ FFDI and (b) days VHi+ with the current fire season added in to the end of January 2020, scaled to the annual average. Anomalies from a baseline of 1980–81 to 2009–10.

Queensland: From Table 7, Queensland FFDI indices shifted in 2012–13 at $p < 0.01$, but Table 8 indicates shifts in T_{max} in 2001 and T_{maxFY} in 2001–02. Figure 13 shows that although there was a peak in the early 2000s, sustained high FFDI indices have only been maintained since 2012–13. An important question is whether the shift in T_{max} from 2013 affecting eastern Australia is influencing higher levels of FFDI in Queensland. If so, that might justify using the period since 2012–13 as a baseline for estimating current levels of risk.

As Queensland contains both spring-summer and winter-spring fire regimes further north, carrying out a single state analysis is difficult. We have not addressed winter-spring regimes in this paper, so more work may be needed to ensure that the fire climatology is robust in these regions.

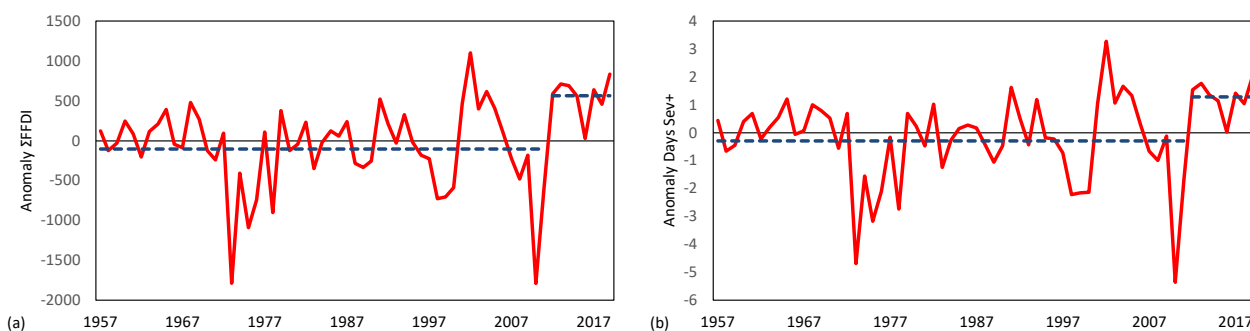


Figure 13: Annual anomalies and regimes for Queensland for (a) Σ FFDI and (b) days VHi+ with the current fire season added in to the end of January 2020, scaled to the annual average. Anomalies from a baseline of 1980–81 to 2009–10.

Western Australia: There is no detectable regime behaviour in the state average, which covers three seasonal fire regimes: summer-autumn, spring-summer and winter-spring. Given the size of the state, five stations from the NW from the HL2019 data set were averaged and tested (Broome, Carnarvon, Geraldton, Meekatharra and Pt Hedland). They show shifts in 2001–02 for median Σ FFDI and 97% FFDI of 12% and 9% respectively, the same timing as for SW WA, but the main inputs of RH shift in 2000–01 and T_{max} in 2006–07 (all $p < 0.01$).

Northern Territory: As for WA, there is no detectable regime behaviour. Four stations from the HL2019 data set for central Australia were averaged and tested (Alice Springs, Mt Isa, Tennant Creek and Woomera). They show shifts in 1979–80 for median Σ FFDI and 97% FFDI of 26% and 22% respectively, along with KBDI, RH and T_{max} (all $p < 0.01$). This is the most closely linked set of variables tested, but as the time series only began in 1971, this result may be due to being close the start of a relatively brief time series. On the other hand, T_{max} does shift across northern Australia in 1979 by 0.76 °C, so a new fire regime may have been established in central Australia at this time.

Studies of changes in FFDI

Most previous studies assume that the underlying response of historical FFDI to forcing has been trend-like with variability superimposed, the exception being Jones et al. (2013). However, many papers explicitly refer to the nonlinear nature of recent changes (Clarke, Lucas, et al., 2013; Dowdy, 2018; Harris & Lucas, 2019; Harris, Mills, et al., 2019; Harris, Nicholls, et al., 2019; Lucas et al., 2007; Sharples et al., 2016; Williams et al., 2013).

Lucas et al. (2007) recorded a change in trend of 10–40% between 2001–07 compared to 1980–2000 across various sites in their study, suggested a role for decadal climate variability where decadal cycles were enhanced by anthropogenic change. They also noted that some of the events between 2000 to 2006–07 exceeded the conditions projected for 2050 presented in the same report. Clarke, Lucas, et al. (2013), analysing the high-quality data set developed by Lucas (2009) that extended to 2009–10 noted the ‘jump’ around 2000, and speculated whether it was due to decadal variability combining with climate change. Using trend analysis, the 90th percentile daily FFDI reached the $p = 0.05$ level in about half the records examined.

These estimates cannot be directly compared with those here because they use different a different index. Clarke, Lucas, et al. (2013) also noted the recent changes rival future projections. Sharples et al. (2016) also noted this nonlinear increase, which included an increase in extreme bushfires and pyroconvective events.

Sanabria et al. (2013) constructed a national spatial climatology from the 78 stations developed by Lucas (2010), interpolating the input data then calculating FFDI. They used an additional 35 secondary variables to fine-tune the drought factor to account for fuel dryness. They tested the surface with the larger set of stations then narrowed it down to the 38 of high quality used by Clarke, Lucas, et al. (2013), which provided a smoother surface when interpolated and lower values, concluding that the better-quality but sparser network was preferable. They investigated return periods of up to 500 years using different extreme event formulations, producing estimates of different 50-year return periods (Sanabria et al., 2013). However, nonstationarity in the input data will skew the results.

Williamson et al. (2016) built a national dataset of FFDI from the SILO database of daily data (Jeffrey et al., 2001) 1900–2011 using the Noble et al. (1980) formulation of FFDI. They coupled this with a satellite record of fire activity from 2000–2011 (hotspot detection) to better understand the climate influence on regional fire activity over 61 regions based on similarity between a set of climate indices. These were then compared with the ENSO and Indian Ocean Dipole (IOD) indices to determine interannual influences on fire behaviour, with strong relationships identified, particularly in southern regions. There were clear relationships between fire activity and FFDI across different zones, and fire was associated with different FFDI thresholds across these zones. They did not investigate longitudinal change, relying on the Jolly et al. (2015) conclusion that the high interannual variability they detected obscured any underlying trends.

Dowdy (2018) constructed a gridded record of FFDI from data contained in the Australian Water Availability Project database with wind taken from an NCEP-NCAR reanalysis extending from 1950 to 2016. The length of recorded allowed differencing between blocks of two to three decades each without resorting to trend analysis. When divided into halves (1951–1983 and 1984–2016), increases in mean FFDI at the $p < 0.05$ level were detected in the south, mainly in the SA region, with decreases in north and northwest (Dowdy, 2018). This may be due to an upward shift in rainfall of 94 mm or 18% in 1973 in northern Australia (our analysis). Separating the last half period into quarters, change was dominated by more widespread increases across southern Australia than earlier, with some northern areas experiencing decreases and other increases. Dowdy (2018) also pointed out the nonlinear increases in FFDI after 1999, especially in southern Australia.

Dowdy (2018) presented rarer events such as 1, 5 and 10-year return periods, stating that the longer time series could produce “climatological analysis with minimal influence from natural variability”. However, he also referred to the nonstationary nature of the time series, saying that after 2000 in some SE Australian locations during spring, extreme values were similar to those formerly seen in summer. These conclusions are inconsistent. Nonstationarity will also affect long-run statistics because return periods of extreme events can change dramatically. Extracting the less common events from long records is problematic unless it is possible to distinguish nonlinear forced change from internal variability.

Harris and Lucas (2019) analysed their national high-quality FFDI station dataset to 2017. Similar to Dowdy (2018), they detected larger increases in the south, especially in spring. They recorded trends meeting the $p < 0.05$ level in the 90th percentile FFDI in 44% of the all-station network (17/39) and in the all station average (Harris & Lucas, 2019). They assessed the influence of the Southern Annular Mode, Indian Ocean Dipole and El Niño – Southern Oscillation on detrended data, finding that all three had strong seasonal and regional influences on interannual variability, separately and in combination, useful for seasonal forecasting. They also assessed whether these variables could contribute to the long-term linear trend or whether the Interdecadal Pacific Oscillation (IPO) could contribute to decadal variability, finding neither could explain the observed changes. Anthropogenic change was identified as the cause of the upward trend without the

authors being able to pinpoint the specific mechanism (Harris & Lucas, 2019). They concluded that observed trends have generally been in excess of projections from climate modelling studies.

Hope et al. (2019) simulated the February 2017 Sir Ivan fire in NSW as a first study examining event attribution, modelling FFDI and fuel dryness. They used a seasonal forecasting model, with an external drought factor calculated separately because of the limited initialisation time available to stabilise soil moisture. The model’s ability to reproduce windspeed in realistic detail was also limited. The model was run with current (400 ppm) and 1960-equivalent CO₂ (315 ppm), initialised from long runs. The 1960-equivalent run had temperatures removed through the ocean profile to represent the difference in atmospheric CO₂ forcing over time. The results showed differences in Tmax and FFDI to the p<0.1 level in the region of interest, along with reduced RH, so the aim of the study was deemed successful, that models have the capacity to carry out event-based attribution assessments on extreme bushfires.

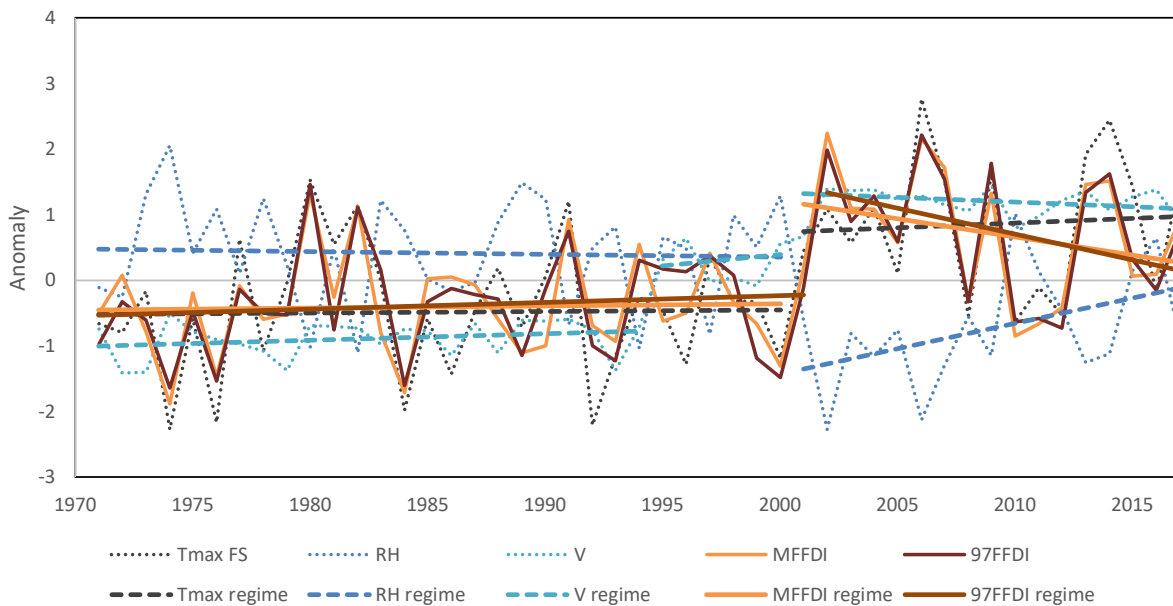


Figure 14: Observations for Tmax FS, RH and V and calculated MFFDI and 97FFDI averaged from four climate stations surrounding the Sir Ivan area drawn from the LH2019 dataset (Cobar, Dubbo, Moree, Wagga Wagga), with regime shifts and internal trends.

Despite modelling the fire as two discrete events, they described the recent event as occurring on the back of an upward trend in FFDI from 1960 to 2017 based on analysis of the Dowdy (2018) climatology (Hope et al., 2019). They also described the inputs such as Tmax in terms of trends. We tested this for Tmax FS, RH, V, MFFDI and 97FFDI averaged from four climate stations surrounding the Sir Ivan area from the LH2019 dataset (Cobar, Dubbo, Moree, Wagga Wagga; Figure 10). All were analysed for shifts, with TmaxFS, RH and MFFDI shifting in 2001 and 97FFDI in 2002. V shifted in 1995, most likely an inhomogeneity due to a change in instrumentation, and in 2001 (All shifts p<0.01). DF, P and raindays showed no notable trends or shifts. Tmax and RH strongly influenced the outcome. The inhomogeneity for windspeed in 1995 and the later shift had little influence on the results, despite being positively correlated with annual 97FFDI. RH increased after 2010 and both FFDI measures decreased, but this is due to three anomalous wet years; warm and dry conditions in the region have continued after 2017. The results could therefore be interpreted as the before and after case of a regime shift.

Brown et al. (2016); Harris and Lucas (2019); Harris, Mills, et al. (2019); Harris, Nicholls, et al. (2019) produced and analysed a downscaled climate and fire weather data set VicClim, combining the output of a mid-scale numerical weather forecasting model, global reanalysis data, and observational and historical data. The outputs include the inputs to FFDI, multiple FFDI indices and a 32-layer atmosphere, including the difficult to

manage variables of windspeed and relative humidity. The data set was evaluated using selected fire events and the overall climatology. While it revealed known high resolution features resulting from topographic effects, it also retained some biases, especially for rainfall (Brown et al., 2016).

Investigating this dataset for its climatology, Harris, Mills, et al. (2019) compared trends and variability 1972–2017 with number of fires (ignition), and total area burnt. However, they removed the trend from the data before presenting the results so they cannot be compared with those here. They commented on the strong decadal variability but did not consider this as part of the response to climate change.

Harris, Nicholls, et al. (2019) assessed the sensitivity of fire activity: total number of fires, area burned and mean fire size 1972–73 to 2013–14 with stepwise multiple regression using a wide range of climate variables, testing sensitivity on a quarterly to annual basis. Their aim was similar to ours – to assess the effect of the broader climate on fire activity. They did so by undertaking a first-difference approach, measuring the change from the preceding period. They measured total number of fires as a trend, increasing from 192 to 522 over that period.

From the VicClim climatology, Harris, Nicholls, et al. (2019) identified the largest changes in Tmax and RH (as vapour pressure, VP) as occurring in spring followed by summer and least in winter. Few trends were significant. For correlations with the annual fire season (Nov–Mar) number of fires, the largest influences were changes in Tmax, 3 pm vapour pressure and P. All months in three monthly running means for P and 3pm VP were highly correlated whereas November to January was for Tmax (covering the early part of the fire season). For area burned and average fire size, the main influences were spring VP and P and summer Tmax (Harris, Nicholls, et al., 2019). The multi-variate regression models developed were (1) for change in number of fires, Oct–Dec δP , Jan–Mar δT_{max} and Jun–Aug δP , $r^2=0.66$; (2) for changes in area burnt, Oct–Dec $\delta 3pm VP$, Jan–Mar δT_{max} and Jun–Aug δT_{max} , $r^2=0.61$.

For number of fires, Harris, Nicholls, et al. (2019) then used each of the predictors to calculate change over time, to see if they could reproduce the observed trend. The selected model estimated 26% of the total change measured as a trend (86 of 330 fires per year), attributing 19% of that to Jan–Mar δT_{max} . The remainder of the increase, they attributed to non-climatic factors. However, the number of fires shows a clear shift in 1996–97, consistent with the identified shift in fire climate regime.

The total area burned and mean fire size, derived from number of fires and total area burned shown in Harris, Nicholls, et al. (2019), occupy three distinct regimes. Total area burned peaked at 500,000 ha between 1973–74 and 1984–85, and mean fire size peaked at just over 1,000 ha during this period. From then to 2002–03, both variables were very low, almost background noise. In 2002–03, total area burned peaked at over 1.2 million ha, and at over 1 million ha in 2006–07 (Harris, Nicholls, et al., 2019). Average fire size was almost 2,500 ha and about 1,500 ha for both these dates. Subsequently, over 1.2 million ha was burned in 2019–20. Harris, Nicholls, et al. (2019) used the same method of linear regression for climate variables using natural logarithms for the area burned and fire size. This assumes a power law relationship between linear forcing and nonlinear response. Their results show a close fit for short periods but not the whole time series (Their Figures 4 and 5). The regression model reproduced total area burned fairly well after 2002–03 but only 1982–83 was close beforehand. Mean fire size was predicted less well, producing a reversal of trend between data and prediction.

The use of differences in regression analysis avoids imposing a calculated trend but reproduces the underlying linear structure of the data. If the data contains a genuine trend, then differencing will infer a strong cause-and-effect relationship by reproducing that trend. However, if the underlying data is nonlinear, differencing will only identify the component of gradual change in that data because the absolute measure is the driver, not the incremental change. If there is only one shift in a data series associated with a change, regression analysis will not identify it.

Constructing and assessing fire climate regimes

Our interpretation of the Harris, Nicholls, et al. (2019) fire activity is that number of fires underwent in regime shift in 1996–97, and area burnt and average fire size followed in 2002–03. As this latter period contains the largest responses in the time series, it defines the regression relationships, so is the best reproduced in the sequence. The variations in area burned and average size before the mid-1980s, probably relate to management and response, with only 1982–83 carrying a strong climate signal. Reforms following the Ash Wednesday fires appear to have largely suppressed large fires from the mid-1980s until the fire climate regime shift in the late 1990s. An increase in the number of fires was the first response, followed large fires increasing at the same time as the regime shift in days Sev+ in 2002–03, partially exacerbated by large-scale drying associated with the Millennium drought.

The focus on these examples is not to single out particular studies, because all the above have analysed changes in fire danger indices as trends. The important conclusion is that by attributing the underlying influences of climate change on fires as being gradual, they reach different conclusions to this report.

4. Comparing recent regime change with projected future change

Comparisons with future projections

Studies describing future projections of fire weather previously described cover SE Australia (Clarke & Evans, 2019; Clarke et al., 2011; Hennessy et al., 2005; Lucas et al., 2007) and nationally (Clarke et al., 2016; CSIRO & Bureau of Meteorology, 2015). Climate model-based studies for specific regions include a future fire danger climatology for Tasmania (Fox-Hughes et al., 2014), projections for Victoria (Timbal et al., 2016), New South Wales (Clarke & Evans, 2019), and nationally (Clarke et al., 2016).

The most recent national projections were carried out for Australia's natural resource management regions (CSIRO & Bureau of Meteorology, 2015), adapting the Clarke, Lucas, et al. (2013) data. These regions are not congruent with state boundaries. Days above the severe fire danger rating (FFDI >50, days Sev+) were projected over eight clusters. The baseline used was 1981–2000 with a midpoint of 1995.

For the southern cluster, covering most of Victoria and some of SE Australia the estimated baseline was 2.8 days Sev+ per year. Comparing that with the HQD estimate for SE Australia, offset by the six-month difference between fire and calendar years, estimated days Sev+ were 2.9 per year, statistically equivalent. For 2030, projected Sev+ was 3.5–3.6 days and for 2070 3.8–5.3 days (CSIRO & Bureau of Meteorology, 2015). For the original record used to build the climatology for Victoria, the period 2002–03 to 2009–10 averaged 4.8 days per year and for the longer record VicHQD 1996–97 to 2019–20 days Sev+ averaged 3.8 days per year and for SE Australia 2002–03 to 2019–20 was 5.0 days per year.

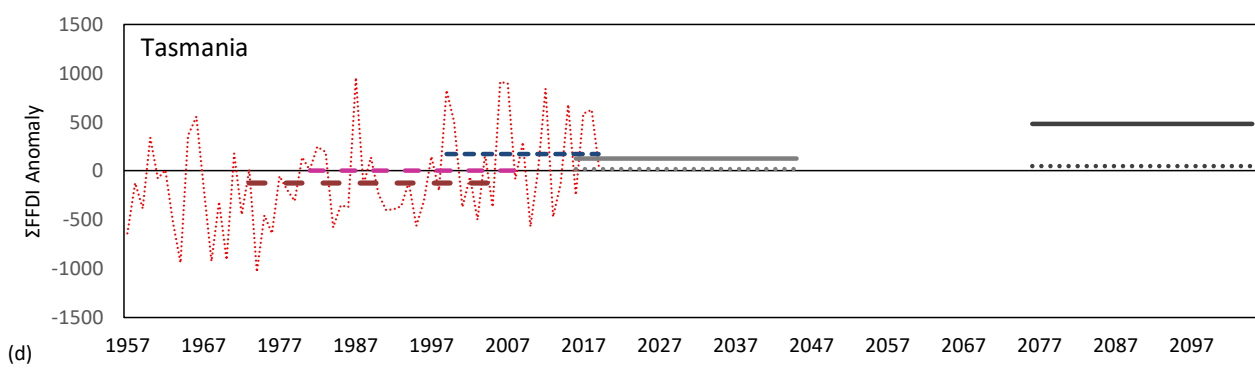
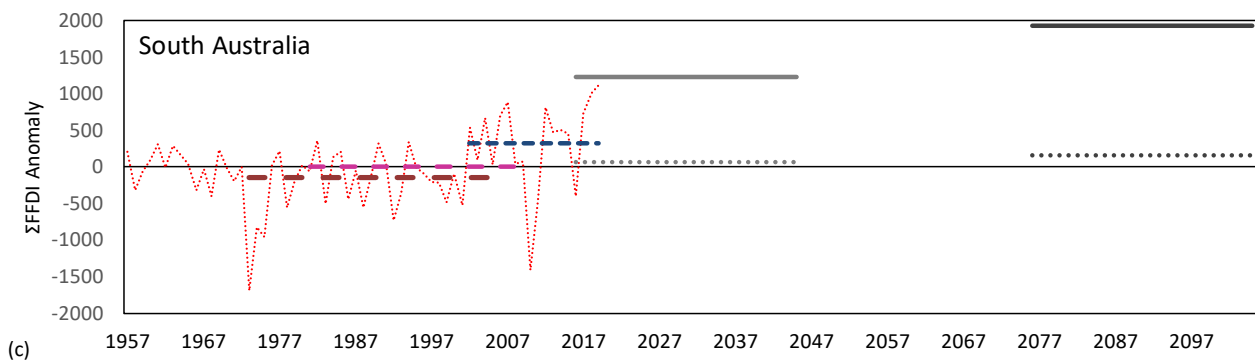
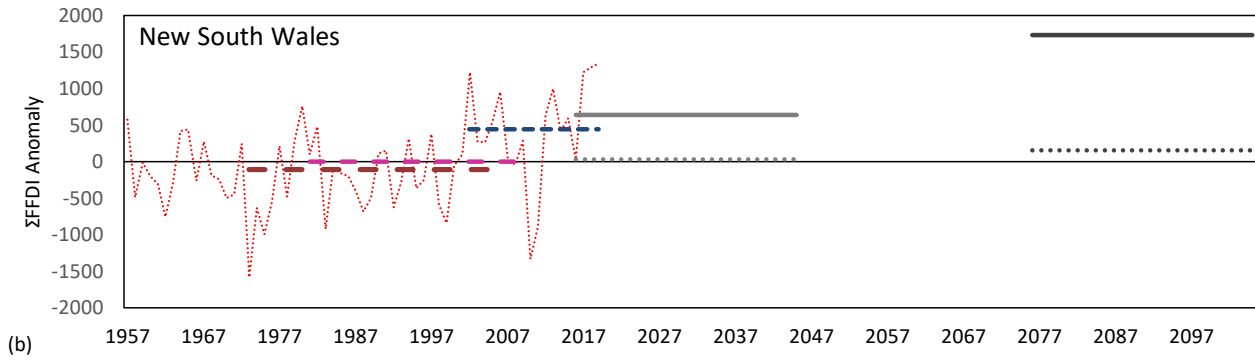
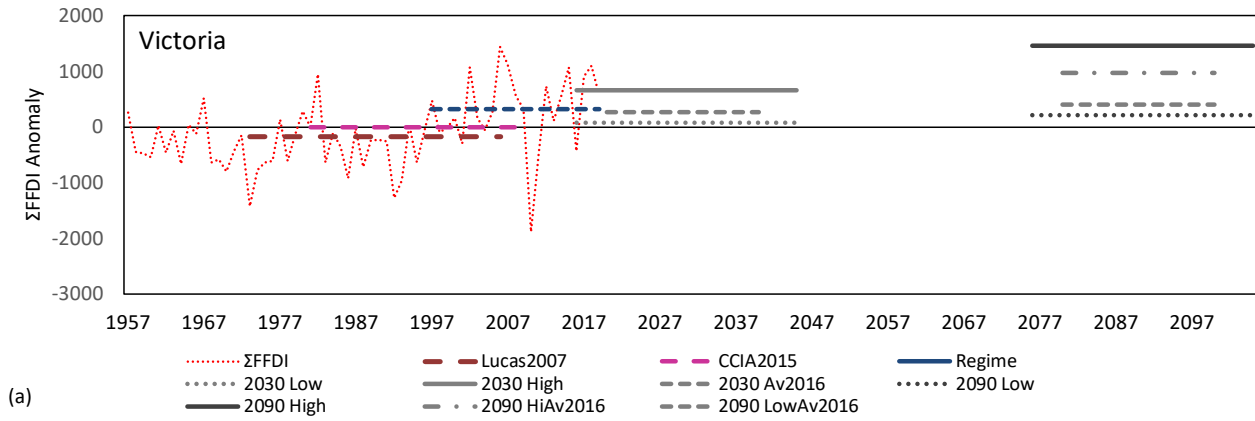
The current fire regime in this region therefore rivals the CCIA2015 projections for 2030. The 2030 increase from CCIA2015 is proportionally less than the earlier Lucas et al. (2007) study because of the difference between the baseline periods 1973 to 2006–07 and 1981–2010 used in the two studies. For Victoria, for the indices Σ FFDI and days Hi+, VHi+ and Sev+, the difference between the two baselines is 8%, 9%, 14% and 20% respectively. This shows the difficulty in comparing projections that have different baselines, particularly when the model of change is based on the climate system responding gradually and those baselines straddle regime shifts in different ways. This is compounded by regions of interest also changing over time.

Comparing baselines, regimes and projections

This section compares baselines from Lucas et al. (2007) and CCIA2015 with the current regime and future projections from CCIA for 2030 and 2090 for each state and selected regions. For regions that have undergone a confirmed regime change, two baselines were calculated: one from Lucas (2007) and the other from CCIA2015. They are averaged from the HQD Σ FFDI and days Dev+ datasets for the periods 1972–73 to 2006–07 for Lucas07 and 1980–81 to 2009–10 for CCIA2015. These are compared with the current regime. Projections for 2030 and 2090 were averaged from individual station projections for each state/region from CCIA2015. Simple averages were calculated without any weighting, and absolute values were used as this had been successful in calculating the climatologies. For Victoria, projections from Timbal et al. (2016) are added. These have the same baseline as CCIA2015 and provide average projections for 2030 and high and low average projections for two emissions pathways for 2090.

In Figure 15, for all regions that registered a shift in Σ FFDI, the current regime exceeds the 2030 and 2090 low estimates. Victoria is at about halfway up the 2030 range, Tasmania and SE Australia exceed it, Queensland is equal, SW Western Australia is just below the upper limit and South Australia is partway up the range, but it has the largest projected uncertainties of all the states.

Constructing and assessing fire climate regimes



Constructing and assessing fire climate regimes

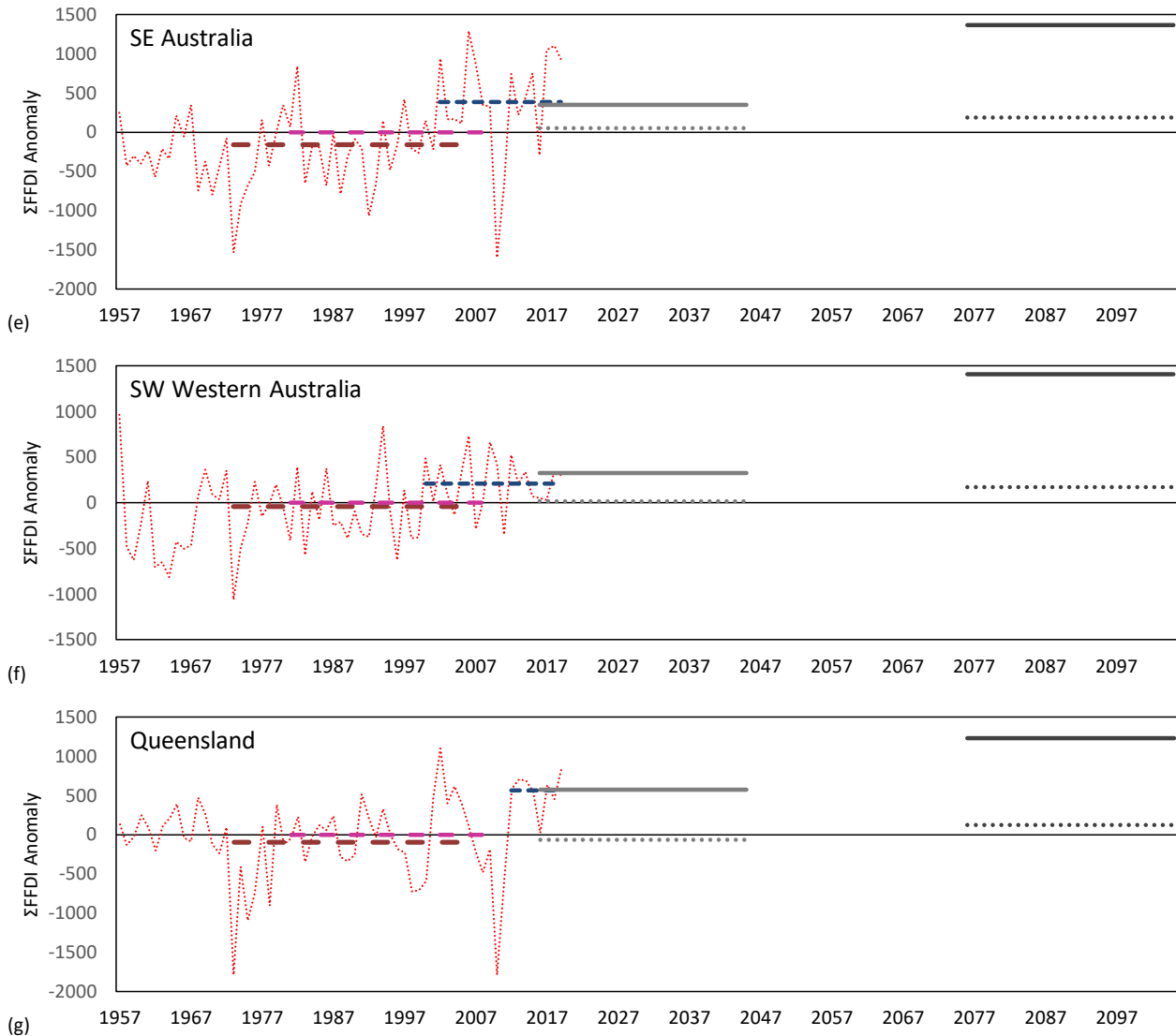


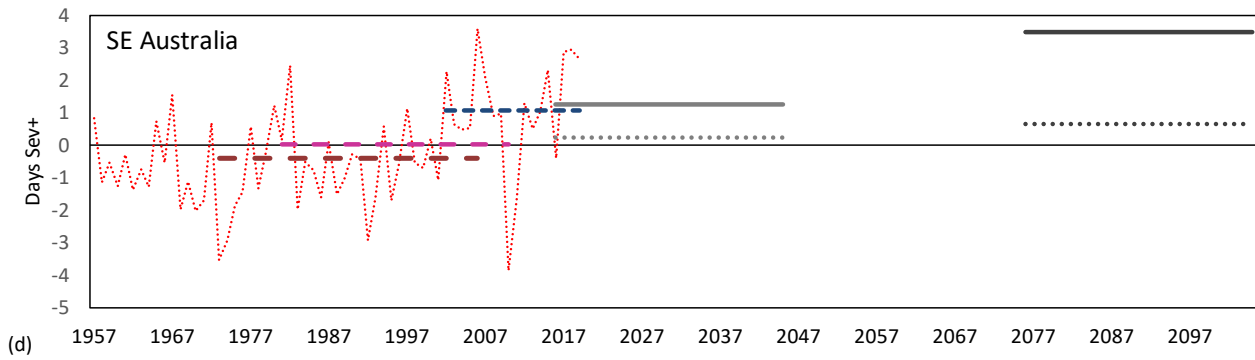
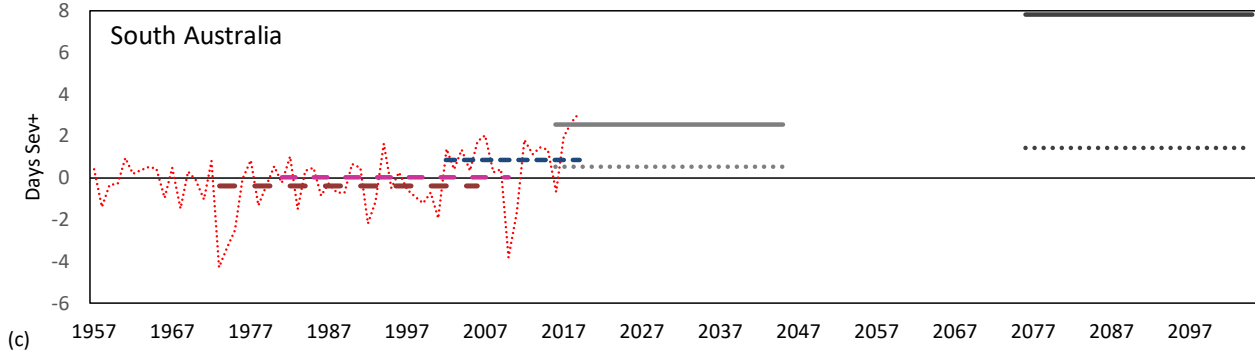
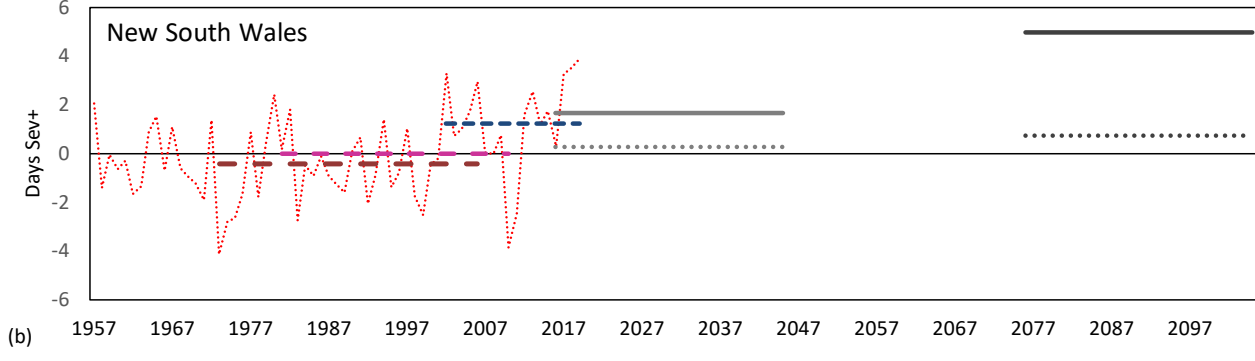
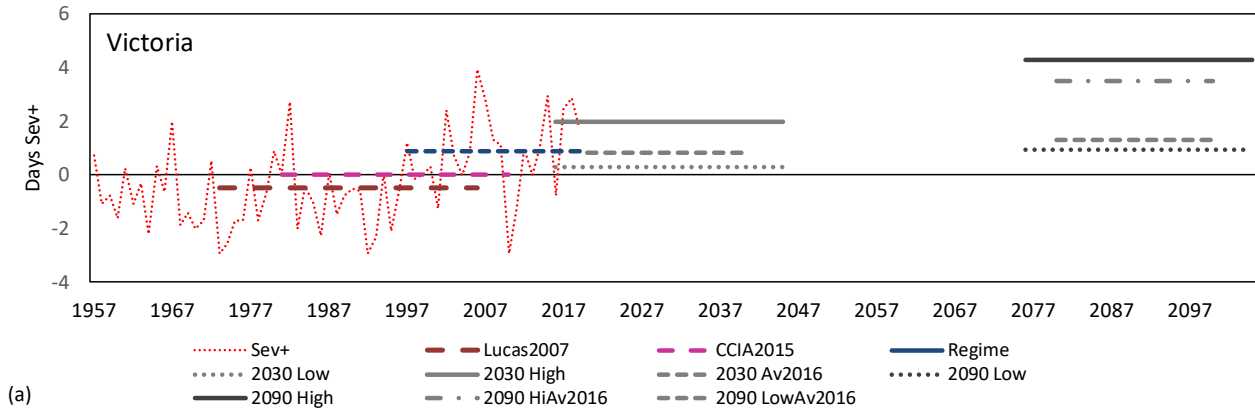
Figure 15: HQD Σ FFDI anomalies set to the baseline 1980–81 to 2009–10 (CCIA20151 offset by six months, magenta dashed line) showing the baseline 1972–73 to 2006–07 (Lucas07, brown dashed line) and most recent regime (dark blue dashed line), shown with the 2030 projected range of change (mid grey lines) and 2090 (dark grey lines) for (a) Victoria, (b) New South Wales, (c) South Australia, (d) Tasmania, (e) SE Australia, (f) SW Western Australia, (g) Queensland.

For days Sev+ in Figure 16, the pattern is similar but Queensland and SW Western Australia are near the upper limit, SE Australia, New South Wales, Victoria and South Australia in decreasing order. Tasmania is not included because of data limitations but eastern Tasmania is known to experience these conditions. Only South Australia does not exceed the lower 2090 limit.

These results benchmark recent changes against the Lucas et al. (2007) and CSIRO and Bureau of Meteorology (2015) projections for future change. They confirm earlier commentary on future projections rivalling current change (Clarke, Lucas, et al., 2013; Jones et al., 2013; Lucas et al., 2007). They also show that the later baseline used in CCIA2015 took up some of the observed regime change. When those projections were being made (2014–15), most regions in Australia had been in a regime that exceeded the average baseline by the amounts shown in Figs 15 and 16 for over a decade and for Victoria, almost two. This is a weakness of the scaling method that updates projections based on the assumption of gradual change, where differences in the same time periods in models are applied to observation, when observations had already shifted into the 2030 range in most places.

Constructing and assessing fire climate regimes

This reveals an important advantage of regimes over trends. If a shift to a new regime can be identified and attributed, then the prevailing climate-related aspect of fire risk can be re-evaluated immediately, rather than dealing with the signal to noise problem presented by short-run trends.



Constructing and assessing fire climate regimes

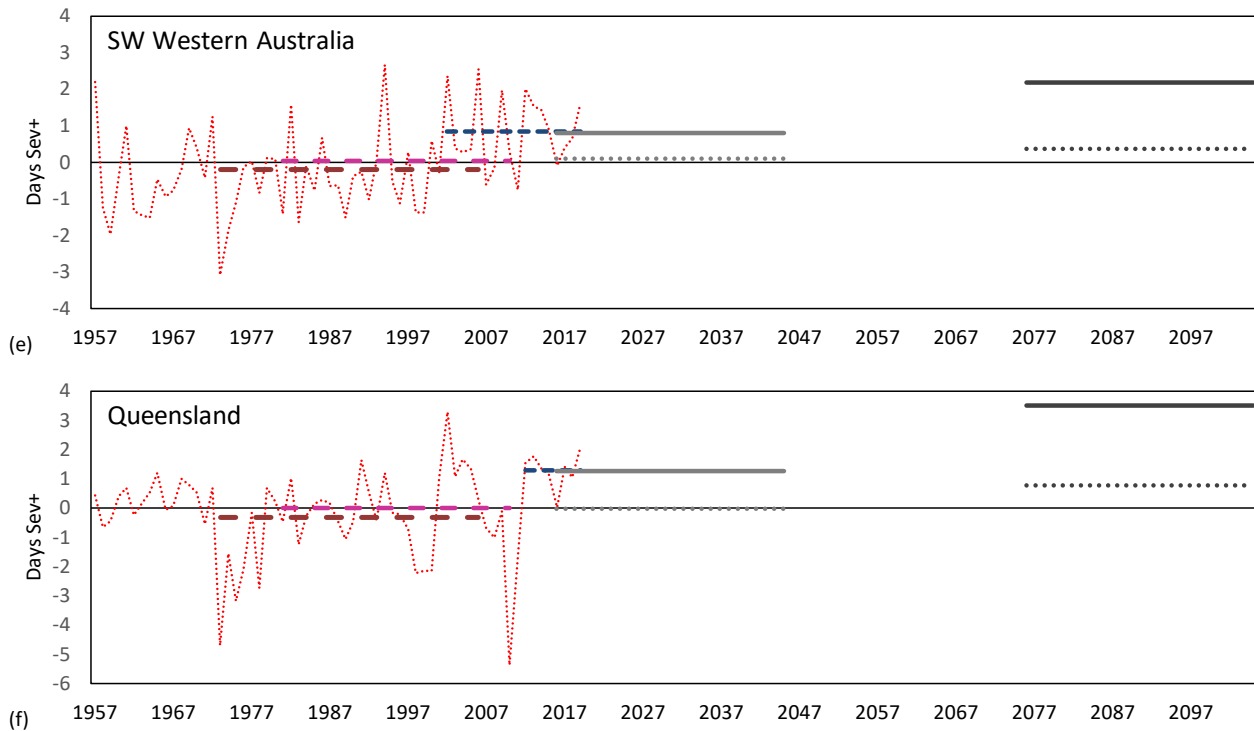


Figure 16: HQD days Sev+ anomalies set to the baseline 1980–81 to 2009–10 (CCIA20151 offset by six months, magenta dashed line) showing the baseline 1972–73 to 2006–07 (Lucas07, brown dashed line) and most recent regime (dark blue dashed line), shown with the 2030 projected range of change (mid grey lines) and 2090 (dark grey lines) for (a) Victoria, (b) New South Wales, (c) South Australia, (d) SE Australia, (e) SW Western Australia, (f) Queensland.

Comparisons with regional studies

Victoria

Lucas et al. (2007) assessed future changes in FFDI across Australia, with six locations in common with the wind-adjusted set used to construct the HQD model, building on Hennessy et al. (2005) who assessed projections for SE Australia. Their study used FFDI. Table 9 compares days VHi+ from both datasets using the 1973 to 2006–07 baseline. Both average 19 days per year for Victoria. If the recent regime is taken as dating from 1996–97, the changes from the baseline are approaching the high-case for 2050. Clarke, Lucas, et al. (2013), analysing the high-quality data set developed by Lucas (2010) that extended to 2009–10, also noted that recent changes rival future projections.

Timbal et al. (2016) analysed Melbourne, Laverton, Mildura, Sale and Mt Gambier stations to 2015, estimating an average linear trend of 28% in Σ FFDI and 3.6 days in Sev+. They also estimated future changes applying monthly mean changes to maximum temperature, rainfall, relative humidity and wind speed to the same baseline used in CCIA 2015, from three climate models taking the average of those. Two forcing pathways were used: RCP4.5 and RCP8.5 (Moss et al., 2008), averaged in 2030 and presented separately in 2090. For 2030 they estimated a state-average increase of 9.3% for Σ FFDI in 2030 and 14.1% and 34.4% for RCP4.5 and RCP8.5 in 2090, respectively. For days Sev+, projections were 28%, 45% and 120% in that order.

Lucas et al. (2007) also considered the return periods for catastrophic conditions, the worst case for 2050 summarised in Table 9. They range from one every ten years for Bendigo to 1.2 per year in Mildura. Some stations will be approaching this frequency, which is equivalent to once in every 2.5 years when averaged over the state, but as discussed earlier, the short time series and data quality make return period difficult to assess at individual locations with any confidence.

Victorian Country Fire Authority days of declared total fire bans dates back to 1947. Correlation of annual total fire ban days with HQD days Hi+ showed a shift from 0.26 to 0.81 after 1977–78 ($p=0.002$). A search

could not locate evidence of a change in forecasting methods but one must have occurred to produce a change of this magnitude. The subsequent move from total state bans to district bans from 1986–87 had little effect on the results. Total fire ban declarations since 1978–79 shifted in 1997–98 from 7.7 to 13.6 days per fire year at $p < 0.05$, an increase of 78%. A running correlation of 21 years since 1978 shows that the relationship between HQD-derived FFDI and declared days of total fire ban remains around 0.8. This is consistent with total fire ban days being declared in the mid-range of state-wide FFDI of 25–49 and shows that the declaration of total fire ban days in Victoria has followed the regime shift.

Table 9: Average number of days VHI+ per year in FFDI for selected locations in Victoria 1971–73 to 2006–07 from this report and Lucas et al. (2007) with 2020 and 2050 projections in percentages.

	Melbourne	Laverton	Sale	Bendigo	Mildura	Mt Gambier	Victoria
This report	15.7	11.6	6.0	15.5	52.9	12.1	19
Lucas 2007	14.8	11.8	5.4	13.9	56.6	11.5	19
1997–2010	22.7	15.1	8.6	28.9	77.2	15.5	28
1997–2010 (%)	45	30	43	86	46	28	47
2020 low %	6–7	2–4	1–7	12–16	5–7	1–3	5–7
2020 high %	15–19	9–15	10–32	26–32	16–18	7–12	14–21
2050 low %	9–12	5–9	18–50	20–13	10–13	5–7	11–32
2050 high %	43–59	42–63	50–107	81–106	50–60	22–34	48–72
Catastrophic							
2050 highest	0.4	0.4	0.2	0.1	1.2	0.2	0.4

Clark et al. (2021a) used the updated VicClim4 data set of fire weather and associated variables, including 32 atmospheric layers as the base climate and dynamically downscaled GCM data using coarse- and fine-scale synoptic reanalysis. The data downscaled were Tmax, RH, P and horizontal 10 m wind speeds for years 1973–2016 from the ACCESS 1.0 climate model. They assessed bias using the daily 99th percentile FFDI from VicClim4 for the 44-year timeseries. These tend to be underestimated and range up to -12 units but may be proportionally similar in coastal areas. The major contributing variables to the underestimates were windspeed on the plains, RH in hinterlands increasing to the NE, Tmax on coastal plains and DF across the Great Dividing Ranges from west to east. However, they assessed it as a considerable improvement on existing techniques (Clark et al., 2021a).

Clark et al. (2021b) applied the same technique to downscale 12 models, projecting future changes for the RCP4.5 and RCP8.5 emissions pathways. These represent the stabilisation of emissions by the end of the 21st century and an extreme pathway where emissions continue to increase (Moss et al., 2010). For the existing 44-year climatology, most models underestimated FFDI, while producing the overall pattern fairly well. Bias assessments calculated by placing individual variables into the climatology show that the greatest contributing factor varies from model to model (Clark et al., 2021b).

Changes for each pathway were assessed for 2045–2060 and 2085–2100 (Clark et al., 2021b). Results are shown in map form for annual maximum FFDI and for five selected stations for RCP8.5. The ranges of change for MaxFFDI are greatest in the NW of the state and range up to 15 points in the NW for RCP4.5 2045–2060 to 20 for RCP8.5 2045–2060. The latter exceeds RCP4.5 for 2085–2100 and the increase is greater than 15 points for over half the state in RCP8.5 2085–2100. These projections are more than double the baseline average in the NW with even greater relative increases in the cooler regions (Clark et al., 2021b). We analysed MaxFFDI in the Victorian baseline data for our project and did not detect any regime-like change, so cannot compare these with our results, with respect to possible regime shifts.

Stations where changes in days VHI+ are shown for the baseline and changes for RCP8.5 2045–2060 and 2085–2100 in Clark et al. (2021b) are compared with regime changes for the baseline stations in Table 10.

Constructing and assessing fire climate regimes

Consistent with Figures 15a and 16a, these show current change rivalling those projected for mid-century. Even with state-of-the-art downscaling techniques, climate models tend to underestimate future changes when compared with the recent regime shift.

Table 10: Changes in days VHi+ (FFDI >25) for the baseline data in this study compared with the downscaled results average from twelve climate models for RCP8.5 2045–2060 and 2085–2100 (Clark et al., 2021b). Note the baseline figures for the five lower stations are estimated from a chart, but the per cent changes were provided.

	Melbourne	Laverton	Sale	Orbost	Omeo	Bendigo	Mildura	Nhill	Mt Gambier	State Average
1972–2001	14	11	5	2	2	13	47	32	11	15
2002–2009	26	18	10	4	5	34	89	60	17	29
% change	81%	65%	78%	87%	154%	171%	88%	85%	50%	88%

	Melbourne	Mortlake	Bairnsdale	Wangaratta	Walpeup
1973–2016	12.5	12	3.5	17	58
RCP8.5 2045–2060	70%	40%	120%	59%	34%
RCP8.8 2085–2100	117%	71%	216%	103%	65%

Eastern Australia

Clarke et al. (2011) analysed future fire weather using FFDI calculated directly from the output of four climate models for the whole of eastern Australia. They partitioned regions according to rainfall patterns coinciding with fire regimes into summer tropical, summer, uniform and winter, north to south along eastern Australia. The resulting pattern of change is consistent with the pattern of shifts summarised here. The largest changes were projected for the winter-dominated region in the south by about 25%, reducing further north where only small changes were projected, dominated by decreases to 2050, then a return to current status by 2100 in the summer tropical region. These patterns included seasonal duration and extremes (FFDI >40). By 2100, all three models were projecting an earlier fire season and more extremes (Clarke et al., 2011). Two of the models projected increases in humidity everywhere and the larger increases were where FFDI decreased. Decline and increase patterns occurred where temperature increases overcame humidity increases and drought factor decreased.

Tasmania

Fox-Hughes et al. (2014) assessed future Σ FFDI for Tasmania by dynamically downscaling output from six climate models using CSIRO's Conformal Cubic Atmospheric Model. They calculated FFDI on a 10km grid and compared these with station data, concluding that the current climatology was reproduced reasonably well. They produced projections for six regions, starting from 1961 to 2090 assuming a linear trend, calculating a low, mid and high trend based on the model ensemble. Their baseline period was 1961–80, for an Σ FFDI of 1,206 across the six regions (not the whole of the state), whereas the base regime for HQD Σ FFDI 1957–58 to 1998–99 was 1,403 (and 1,316 for the 1961–80 period). Mean Σ FFDI 1981–2010 from CCIA 2015 was 1,395 for Hobart and 1,494 for Launceston, showing that the HQD Σ FFDI is more representative of Tasmania's higher fire danger regions.

The current regime for HQD Σ FFDI for Tasmania spans 1999–2000 to 2019–20, a 36% increase over the previous regime (1,316 to 1,792). Table 11 shows the relative increases from Fox-Hughes et al.'s (2019) projections, extrapolated from the baseline to the current regime of 1999–2019, and to 2090. The largest proportional change to the current regime is 9.7% to 14.8%, up to about one-third of the observed change. The mid to high trend to 2090 is of a similar magnitude to the estimated shift in 1999–2000 for the lower fire danger regions but the higher fire danger regions only project half the current regime change. This suggests that climate models may be underestimating future changes in Tasmania more than in other regions.

Fox-Hughes et al. (2014) also calculated the 99th percentile of FFDI, which is closest to the HQD days Hi+ category in the east of Tasmania (Fox-Hughes, 2008). Days Hi+ register a shift in 1997–98 from 15 to 25 days per year. Although an estimate for the whole of Tasmania, this average is close to changes for the higher risk regions. Estimated increases in the 99th percentile over the course of the 21st century is up to 5 days per year (Fox-Hughes et al., 2014). The largest observed changes and those modelled are in spring, spreading into summer over time (Fox-Hughes et al., 2014). This shows a large difference between observations and projections.

Table 11: Calculations of relative change in Σ FFDI from data in Fox-Hughes et al. (2014), showing the range of change from the baseline of 1961–80 to the current regime of 1999–2019 and the trend amount reached in 2090.

	Western	North-east	Central Plateau	East Coast	Upper Derwent	Midlands
Baseline (1961–80)	345	932	883	1521	1741	1817
1961–80 to 1999–2019						
Low	9.7%	4.3%	8.6%	3.2%	3.6%	4.4%
Mid	12.1%	5.9%	10.6%	4.6%	5.1%	5.8%
High	14.8%	7.4%	12.8%	6.0%	6.6%	7.3%
1961–80 to 2090						
Low	30%	13%	26%	10%	11%	14%
Mid	37%	18%	33%	14%	16%	18%
High	45%	23%	39%	18%	20%	22%

Events at the more severe end of the scale were investigated by Grose et al. (2014) using dynamical downscaling. These events reach into the range of days Sev+. They found the downscaling reproduced events better than the coarser climate models, but led to less change than the host models. The extreme fire weather average 0.7 to 0.8 days per year in the baseline and 0.6 to 1.1 days per year towards the end of the century. Based on the relative change for Σ FFDI to the current regime of 28% and even more for days Hi+ and VHi+, this seems quite low.

New South Wales

Clarke and Evans (2019) conducted a high-resolution downscaled study based on Clarke et al. (2016) but downscaled to a 10 km grid. Their baseline was model years 1990–2009 and the change period 2060–2079. The state average change was -162 to 842 in Σ FFDI. We lack a direct comparison but if we adopt the HQD Σ FFDI baseline, the current regime 2002–2019 estimates an increase of 358, 43% of the upper limit of 842. For days Sev+, the range is -1.7 to 4.5 and the current regime estimates an increase of 1.1, 23% of the upper limit. If the current regime change is attributed to external forcing, then the lower part of the projected range (-162 to 358) can be retired.

National

Clarke et al. (2016) investigated changes in fire weather and fuel load using the NSW and ACT regional climate modelling project that downscales GCMs into a set of regional climate models, selecting those that perform best (Evans et al., 2014). They compared model years 1990–2008 and 2060–2078 for temperate (57–550 Σ FFDI)-, grassland (-186–1372 Σ FFDI) and subtropical regions (-186–1372 Σ FFDI). It is difficult to interpret their results directly, but if we take SE Australia as representative of the temperate area, then the change of the current regime from the baseline is +317 or 58% of the worst case by 2069, reinforcing the previous point.

Summary

By comparing the different projections of future FFDI for Australia with observed fire regime changes, we can see how projections have evolved. The method for developing projections has changed little between the earliest release (Hennessy et al., 2005) and the later methods (CSIRO & Bureau of Meteorology, 2015; Timbal

Constructing and assessing fire climate regimes

et al., 2016) even though climate models and the understanding of impacts drivers has improved substantially. The most common method is to add the change measured between the model baseline and future period to the observed baseline.

The current strategy for assessing the impacts of climate change on fire risk is to develop regional climate models and combine them with more sophisticated experiments for conducting event attribution and the like. Selected results have been published for Tasmania (Fox-Hughes et al., 2014), New South Wales (Clarke & Evans, 2019) and Victoria (Clark et al., 2021a, 2021b) and are in progress in those states and other regions.

In a comparison with the NSW fires, Sanderson and Fisher (2020) assessed four current earth system models in the CMIP6 archive that had combined climate, vegetation growth and fuel condition to simulate wildfire. The scale of the recent fires was unmatched in simulations of current or future conditions, for NSW, Victoria, Queensland or Australia as a whole (Sanderson & Fisher, 2020). According to Sanderson and Fisher (2020), the models have to get a lot of processes right before they can estimate future fires well enough to contribute to management. This accentuates the need to have simple and robust tools for planning now, given that the regime shifts documented here have been in place for almost two decades but are not being explicitly managed as such.

If climate models systematically underestimate future fire risk, improvements in terms of finer resolution and more detailed simulations of land-surface – atmosphere interactions may not achieve the desired results. Models also underestimate other variables on the hydroclimate-pyroclimate spectrum, such as extreme rainfall. We interpret that as being due to their inability to capture features such as the tropical Pacific heat engine, which in turn limits their ability to simulate changes in tropical expansion (Jones & Ricketts, 2021a). The solution is likely to come from improving the large-scale thermodynamic response in climate models rather than small-scale processes.

Most of Australia has experienced regime changes in pyroclimate causing abrupt changes in fire risk that to date have not been fully recognised. Benchmarking these changes provides a better understanding of where we may be situated with respect to past and present baselines and potential future change.

5. Attributing recent fire climate regime changes in Australia. Part I Dynamics

Introduction

This chapter looks at changes to fire climate regimes through a dynamic lens; next chapter looks through a thermodynamic lens. The main approach used here combines an inverse linear method with change-point analysis for attributing anthropogenic influences on fire regime shifts, adapted from methods previously developed for temperature. We then investigate what role dynamics may have played in contributing to those shifts. In particular, the southern hemisphere subtropical ridge position and intensity (STRP, STRI) to see what influence tropical expansion and intensification have on changing fire risk. Previous work has determined that factors affecting variability, such as the El Niño–Southern Oscillation, Indian Ocean Dipole and Southern Annular Mode influence FFDI variability but not overall change (Harris & Lucas, 2019).

Exploring individual contributions to regime change

If robust links between regime changes in input variables and FFDI can be established, and those input variables have been formally attributed, a case for a causal link between anthropogenic forcing and fire regime change can be made. From Chapter 3, even though earlier shifts in temperature and rainfall occur, shifts in fire regimes were delayed until the late 1990s in Victoria and Tasmania, 2001–02 in SW WA and 2002–03 in most other states, except Queensland in 2012–13. WA and NT showed no shifts using the HQD model but FFDI in NW WA may have shifted in 2001–02 and central Australia in 1979–80, but these are based on averages from relatively short time series (1971–72 to 2016–17) from the HL2019 data set.

After omitting all the variables that showed limited or no relationship between regime changes and FFDI (e.g., C3pm, Tmax90, P), those that contain inhomogeneities (V) or few shifts at all (DF, KBDI), RH and TmaxFS remain as the main candidates for being the drivers of regime shifts.

Maximum temperature

Comparing Tmax (annual) and TmaxFS, in all cases but two, Tmax shifted first; the two exceptions being NT and SW WA where they shifted together (Table 12). For Vic, NSW, SA and Sea, TmaxFS shifted in 2002–03, Tas in 1965–66 and 2006–07, NT in 1979–80, SW WA in 1993–94 and Qld in 1979–80 and 2011–12. Comparisons between fire year and fire season Tmax show that in most cases, annual and winter season Tmax coincided with downward shifts in RH, RH preceding in NSW. Queensland shows no coordinated response between stations.

Table 12: Timing of shifts between RH from LH2019 (1972–73 to 2016–17) and Tmax and TmaxFS from the BoM high quality data set (1910–11 to 2019–20).

Region	RH (LH2019)		Tmax (HQD)		TmaxFS (HQD)	
	Date	P value	Date	P value	Date	P value
Vic	1996–97	<0.01	1997	<0.01	2002–03	<0.01
NSW	2001–02	<0.01	2001	<0.01	2002–03	<0.01
SA	1996–97	<0.01	2001	<0.01	2002–03	<0.01
Tas	1996–97	<0.01	1999	<0.01	1965–66, 2006–07	<0.01
SE Aust	1996–97	<0.01	1997	<0.01	2002–03	<0.01
SW WA	1993–94	<0.01	1994	<0.01	1993–94	<0.01
Qld	nr	nr	2001, 2013	<0.01	1979–80, 2011–12	<0.05, <0.01
WA	2001–02	<0.01	2001	<0.01	2002–03	<0.01
NT	1979–80	<0.05	1979, 2013	<0.01, <0.05	1979–80	<0.01

Shifts in TmaxFS followed Tmax by a few years in southern and eastern regions. These were successive years of relatively dry La Niña events following the global regime shift in 1997–98. Three of four summers were

cool, with P close to the long-term mean. The 2012–13 peak is associated with the return of high FFDI conditions after the wet years suppressed Tmax in 2010–2012. Annual Tmax also shifted warmer in the eastern states in 2013, and may have contributed to sustained high FFDI levels since that time.

Wind speed

In Equation 4, V has counterbalancing effect on spatial scales. Higher windspeed is associated with lower average FFD indices, mostly due to coastal–inland variations where coastal locations are windier but FFDI is suppressed. Considering interannual variability in the LH2019 record, V generally has positive correlations with FFDI across the 39 stations. Dividing the timeseries into three periods 1972–1990 (varied measurement), 1991–2002 (inhomogeneities and instrument changeover) and 2002–2016 (stable measurement), the resulting correlations vary widely and are negative for some periods and a few stations.

Records from Victoria are an exception, where windspeed data 1972–73 to 2009–10 was homogenised to calculate the FFDI values used as the baseline for this study. We extended that record to match the timing of LH2019 by adding 1971–72 to 2016–17, building a hybrid time series. The resulting shift in Σ FFDI in 1996–97 is 716. Using stepwise regression, the corresponding shifts from RH of -3.2 and Tmax of 0.8 °C from Equation 4 convert into an estimated shift of 691. For days Sev+, the results are 1.9 and 1.7, respectively. These results correspond within error margins. The shifts in FFDI are therefore a plausible response to changes in Tmax and RH. Contributions from V appear to be limited.

The relationship between wind speed and FFDI is therefore complex, with the spatial relationship for mean V being negatively correlated with mean FFDI, annual V mostly having a positive relationship with annual FFDI, and event-based FFDI having a very strong relationship with windspeed, especially for extreme values. Understanding these relationships better, therefore needs higher quality inputs. A detailed 1-hour climatology for Victoria 1972–2017 developed as part of the VicClim data sets (Brown et al., 2016; Harris, Mills, et al., 2019) was recently analysed by Mills et al. (2020), who find that the data set reproduces automatic weather station records fairly well, and reveals complex regional relationships between extreme wind and FFDI that can contribute to fire risk modelling. However, they do not investigate changes over time (Mills et al., 2020).

The difficulties in extracting a reliable record from historical wind speed observations are detailed by Jakob (2010). Troccoli et al. (2012) investigated changes in wind speed over Australia, analysing measurements and 2 m and 10 m height, and subjecting records to rigorous quality control. Wind speeds from 1975–2006 show a slight decrease at the 2 m height, also noted by McVicar et al. (2008), and an increase at 10 m height. Because the two show similar seasonal patterns of change, Troccoli et al. (2012) concluded that the 2 m readings are being affected by surface modification. Data from seven 10 m stations from 1948–2006 showed little change, so they concluded there were no evident long-term effects in circulation although they were present over shorter time scales (Troccoli et al., 2012). Recent adjustments to Australian 2 m wind data shows an overall decline over time in daily peak wind gusts and reductions in trends in both directions (Azorin-Molina et al., 2019).

With the absence of any strong patterns in V from the LH2016 data set after the mid-1990s, wind speed appears to have negligible effect on the FFDI response. In Chapter 3, we did find a shift in windspeed in central-western NSW in 2001 calculated from LH2019 data coincided with a shift in FFDI and an earlier inhomogeneity in 1995. This earlier shift had little effect on $M\Sigma$ FFDI calculated from that data. We therefore conclude that changes in mean windspeed are not strong drivers of fire regime change. Further work is needed to understand the relationship between changes to extreme winds and extreme fire conditions.

Relative humidity

RH from the LH2019 dataset, shifted simultaneously with TmaxFS in SWWA (1993–94) and NT (1979–80), but in other regions, preceded TmaxFS (shifting 2001–02 in NSW and WA and 1996–97 elsewhere). The latter timing coincides with the shift to dry atmospheric conditions at the beginning of the Millennium drought in SE Australia as documented by the Bureau of Meteorology (2006). National average annual RH from the LH2019 dataset shifted by -2.4 in 2001–02 at $p < 0.01$, similar timing to NSW and WA.

The source of most atmospheric moisture and rainfall over land is water vapour from the ocean (Gimeno et al., 2010; Van der Ent et al., 2010). Moisture is evaporated and transported by advection from ocean to land. When the oceans warm, specific humidity increases, over time following the Clausius-Clapeyron relationship (Dai, 2006; O’Gorman & Muller, 2010). The direction of any change in relative humidity over the land surface will therefore depend on the relationship between specific humidity and temperature. If temperature over the land and ocean shift upwards, temperature over the land surface is amplified by the drier surface and if specific humidity does not increase to compensate, RH will decrease.

Data from the HadISDH – gridded global land surface humidity dataset 1973–2020 shows that RH over southern hemisphere (SH) land has recently declined (Willett et al., 2014). It shifted by -1.1 in 2002 ($p < 0.01$), Dec 2001 using monthly data. Regimes for calendar-year average RH from the LH2019 data over Australia and HadISDH data for southern hemisphere land is shown in Figure 17. The correlation between the two is 0.74, 0.66 with shifts removed (both $p < 0.01$). In Figure 17, the Australian data is represented as a standard anomaly rather than units of RH. At the global scale, RH shifted up in 1990 and downwards in 2002, both at $p < 0.01$, followed by another downward shift in 2007 at $p < 0.05$. The timing of the global shift in HadISDH RH was Feb 2002. The upwards shift in 1989 is due to warming and wetting over the northern hemisphere and the downward shift in 2007 was influenced by NH land.

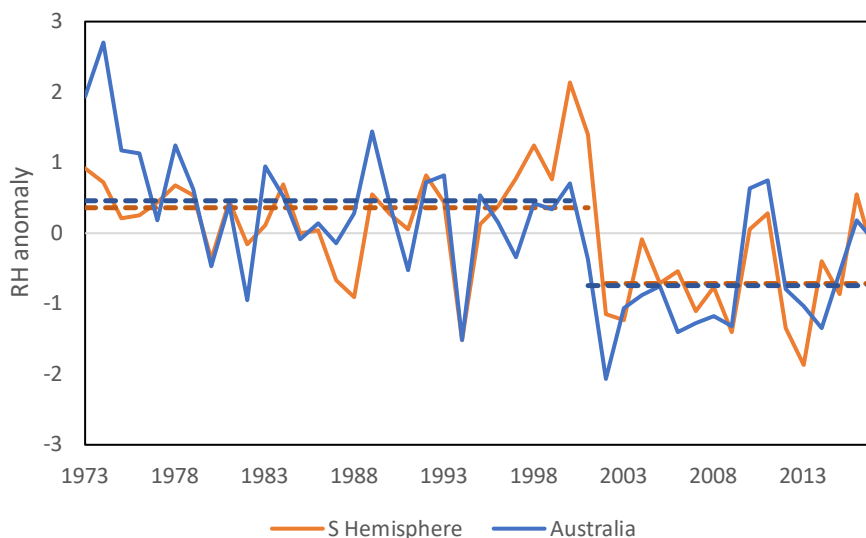


Figure 17. Mean daily average anomalies for RH from the Southern Hemisphere (HadISDH) and Australia (LH2019), the latter as standard anomalies.

Gu and Adler (2013) analysed global precipitation and atmospheric water vapour 1979–2010, detecting a regime shift in 1998/99 involving temperature and water vapour that they linked to Pacific decadal variability. Global vapour pressure (1901–2018) over land from the CRU_ts4.03 data set (University of East Anglia Climatic Research Unit et al., 2020) shows upward shifts in 1930 ($p < 0.01$), 1979 ($p < 0.05$), 1987 ($p < 0.05$), 1998 ($p < 0.01$), and 2015 ($p < 0.1$). The dates 1979, 1998 and 2015 line up with known shifts in air temperature over land, 1987 registers in the NH and 1930 was a shift date for the HadCRUt data set until recent years (it now

separates into 1920–21 and 1936–37). We have not used RH from the same data set because its correlation with HadISDH 1973–2018 for the SH is poor (0.14), whereas for specific humidity, it is good (0.95).

While the four variables in Equation 3 collectively produce regime shifts, TmaxFS is the only one that can be directly connected with the timing of those shifts. As described above, TmaxFS either shifts with Tmax or in the few years following. Shifts in Tmax are reflect large-scale shifts in climate regimes at the regional and global scale mediated by the land surface. The partitioning between sensible and latent heat is stronger during the warmer months, so a reduction in RH will have a larger impact on TmaxFS than on cool season Tmax. If persistent reductions in RH lead to a reduction in soil moisture, especially if exacerbated by reduced rainfall, the dryness-heat feedback effect will be larger. The underlying shift in global temperature occurred in 1997 but was followed by three out of four La Niña events delaying shifts in RH and TmaxFS in some regions. This is reflected in the staggered results between 1996–97 and 2002–03. The following section looks at what role tropical expansion may have played in this timing.

The subtropical ridge and FFDI

The expansion of the Hadley Cell brings descending dry air further into the midlatitudes, especially in summer and autumn (Lucas et al., 2014; Post et al., 2014). Subtropical Ridge Position (STRP) has been linked to changing global mean surface temperature (Timbal & Drosowsky, 2013) but its intensity (STRI) has not (Nguyen et al., 2015). Although the STR has not been strongly linked to FFDI, its influence on temperature, rainfall and drought has been, especially in SE Australia. As these factors sit within a physical continuum describing climate interactions with the land surface, the STR and other drivers of climate variability may influence changes in FFDI (e.g., Harris & Lucas, 2019; Lewis et al., 2019). Here, the STR position and intensity are based on the method of Drosowsky (2005) and Timbal and Drosowsky (2013) where it is based on sea level pressure and latitude 145–150 °E, updated by Pepler et al. (2018).

Larsen and Nicholls (2009); Timbal and Drosowsky (2013) linked the strength of the STR to drought conditions over southern Australia, showing that its intensity is more influential on rainfall than its position, and that this influence is increasing. The strongest relationship they found for SE Australia is between STRI and May–Oct P. The STR influenced the WWII drought in 1935–45 (Timbal & Drosowsky, 2013), timing that roughly coincides with an upward shift in Australian sea surface temperatures in 1936–37, which affected oceans globally (Jones & Ricketts, 2017). This was the driest 9-year period in SEA and Victoria in the instrumental record until 2000–2009. A subsequent regime shift to a negative PDO in 1947 is linked to increased rainfall in eastern Australia (Tozer et al., 2016; Warner, 1999). This is consistent with warm, dry conditions from 1936–37 ending with a shift to wetter conditions from 1947. Cooler Tmax occurring in NSW from that time can be explained through increased rainfall (Nicholls et al., 2004). In contrast to this, the shift in Tmax in SEA from 1997 has been attributed to external forcing because a shift $p < 0.01$ remains after the rainfall influence is removed (Jones, 2012).

The WWII Drought and earlier Federation Drought show different spatial patterns to the later drought (Post et al., 2014). The statistical link between the STR and the WWII drought is half that of the Millennium drought (up to 31% vs 62%) (Timbal & Drosowsky, 2013). Post et al. (2014) calculated a 12% reduction in mean annual rainfall 1997–2009 for mainland SEA, relieved by the wet (and low FFDI) years of 2010–2012 with a probable continuance of dry winter-spring conditions afterwards. Note also, that the PDO/IPO shifted negative in 2014, which would be expected to enhance rainfall in eastern Australia based on past patterns (Kiem & Franks, 2004; Power et al., 1999; Vance et al., 2015). Instead, drying has occurred.

More recently STRP, especially in the cooler months, has been linked to seasonal patterns of change in Australian temperatures (Crimp et al., 2018; Pepler et al., 2018), notably to the suppression of minimum temperatures in the southeast. Using the bivariate test on STR pressure data 1880–2019 updated by Pepler et al. (2018), STRI shifted in 1936 and 1933 for the calendar and fire years, respectively, for the whole time

series. When the series either side of those dates are tested, a stable result of 1918 and 1992 for the calendar year and 1923 and 1993 for the fire year emerges (all $p < 0.01$). Repeating the analysis with Rodionov's regime shift test v6-2 (Rodionov, 2015) detected 1936 and 1993 hPa for calendar years and 1933 and 1992 hPa for fire years.

Large changes in variability in the early record indicates the earlier dates may be affected by data quality. Dividing the record into summer and winter shows that the winter half of the year (1936 and 1993, $p < 0.01$) dominates the changes. The earlier shift in the STRI measures the inception of the WWII drought and warming of the Pacific Ocean from previously cooler temperatures. STRP shows little change in either shift or trend, with a positive shift in winter in 1936 ($p < 0.05$) being the only result of note. Overall, the subtropical ridge over Australia, shows limited regime-like behaviour in position, and 1936 and 1993 for intensity.

The STRI is greater in winter than summer by about 5 hPa and has moved further south in winter. STRP is further south in summer by about 5° and has moved further south than in winter in recent years. Tmax, P and Σ FFDI were correlated with STRI and STRP over the course of the year for selected periods between 1957–58 to 2019–20 for all regions. The STR indices, Tmax and P span the calendar year and for Σ FFDI the fire year, a lag of six months. STRI has a stronger influence than STRP, but both are similar, in that these effects vary by latitude. The more tropical regions are defined by negative correlations in the warmer, wet season and the more mid-latitude regions by positive correlations in the cooler, wet season. Regions in between have less pronounced seasonal variations.

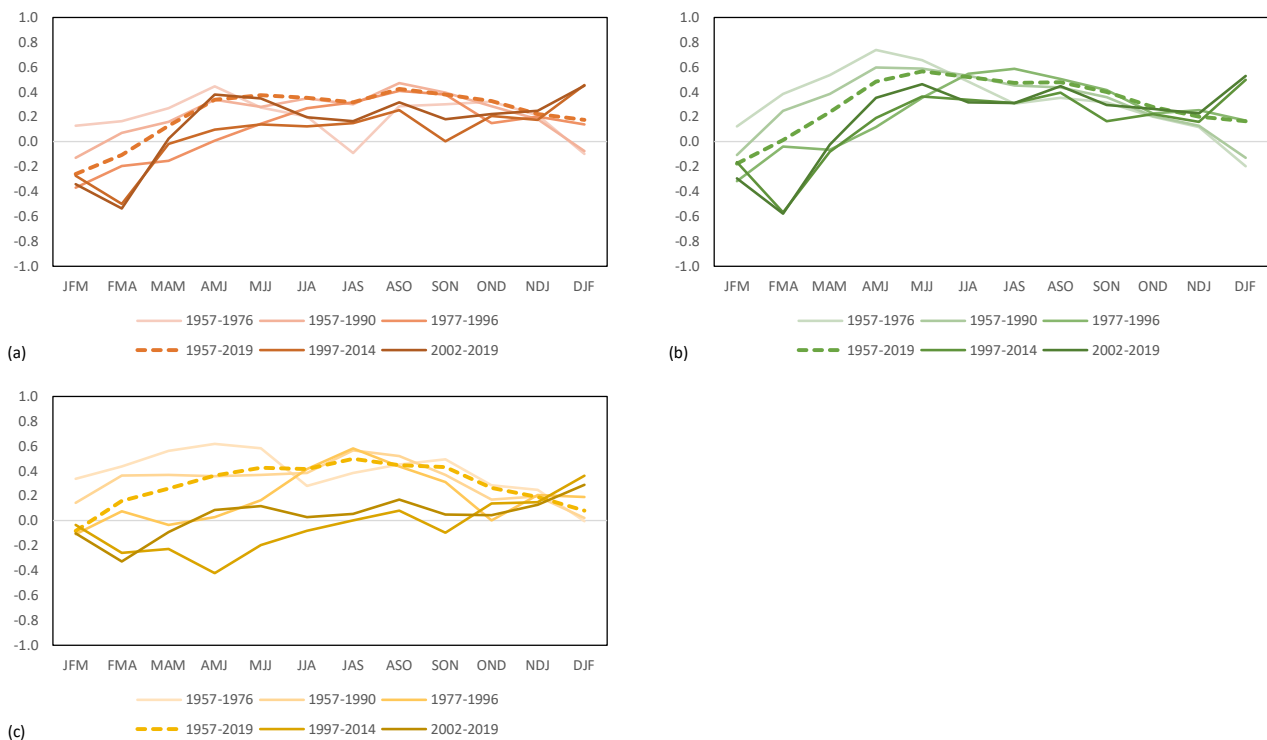


Figure 18: Running 3-month correlations for STRI with (a) Σ FFDI, (b) P reversed, (c) Tmax for selected periods where 1957–1976 marks a wet period, 1957–1990 STRI is stationary, 1977–96 positive PDO, 1957–2019 the whole period, 1977–2014 negative PDO and 2002–2019 the current FFDI regime.

Figure 18 shows running correlations with STRI for Victoria, the highest of all the regions analysed. Probabilities are not shown in the charts because of the different period lengths used, but for the latter two 18-year periods, are 0.44 and 0.56 for $p < 0.05$ and $p < 0.01$, respectively, and are 0.24 and 0.32 for 1957–2019. Figure 18a shows that positive correlations with FFDI with Tmax occur over the winter half of the year, while the late summer correlations move negative. P reversed and Tmax (Figure 18b and c) show similar patterns and both reach $p < 0.05$ levels over that period before 1996, and over the whole record, but not afterwards.

The highest correlations show the influence of the preceding rainy season on fire danger. Correlations between Σ FFDI and Tmax become negative over time and with P slightly more positive. This is almost totally a cool season rainfall effect, described by the close correspondence between Σ FFDI in Figure 18a and P reversed and 18b. The largest change over time is that Tmax becomes negative and P positive in early autumn. Combined, the tend to neutralise the influence of STRI on FFDI during the winter period. For Victoria, the relationship of these three variables with STRP is similar, and strongest for P and Tmax in late winter-spring before 1996.

Relationships with STRP by state over time shows variations that can be linked by timing to phases of the PDO/IPO, which regulates the size of the Hadley Cell. More northern states show even stronger relationships with the PDO/IPO, with STRI and Queensland Σ FFDI and P undergoing a series of reversals in correlation coordinated with PDO phase changes and/or warming. For Σ FFDI, the first in response to regional warming (1969 +ve), the next two timed with PDO phase changes and regional warming (1997 -ve, 2014 +ve; all $p < 0.05$). P is almost the mirror image of this (1969 -ve, 1997 +ve, 2012 -ve, all $p < 0.05$). With STRP, Σ FFDI undergoes one reversal (1997 -ve, 2002 +ve) and P remains stable.

Running correlations between STRI, STRP and Σ FFDI in Figure 19 are positive in higher latitude states and become neutral-negative closer to the tropics. The departures in Figure 19a around 1990 are due to reversals associated with phase changes in the PDO, not to regime change in Σ FFDI. Rainfall (not shown) is almost the mirror image of this as in Figure 18b (which is shown reversed). There is little evidence of changing relationships due to regime change other than phase changes in the PDO.

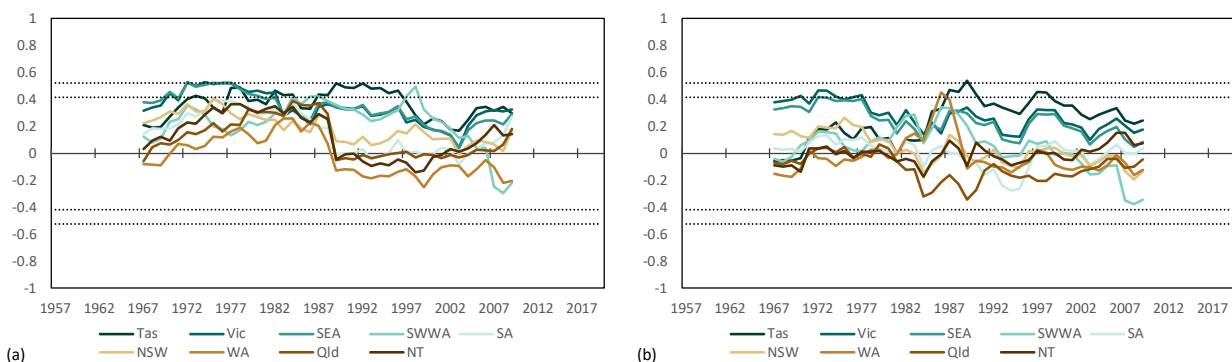


Figure 19: Running 21-year correlations between Σ FFDI and (a) STRI and (b) STRP for states and regions between 1957–2019 with $p < 0.05$ and $p < 0.01$ limits.

The results show that the relationship between P and FFDI is governed by rainfall during the cooler months preconditioning the severity of the following fire season. However, in Victoria the lag effect of the preceding calendar year P is becoming less important, and fire year P with no lag effect is becoming more important, showing the influence of drier and hotter conditions. In a moist climate, higher fire danger is caused by the landscape drying out, whereas in a drier climate, prevailing hot and dry conditions raise fire danger because the buffering effect of the landscape is reduced. In the tropics, the negative association between STRI in the warmer months are associated with higher rainfall increasing fuel loads. Negative correlations between FFDI and STRI further south during the warmer months hint that this effect may be becoming more widespread. In tropical regions, the relationship between interannual variability and the STR intensity and position are influenced by phases of the PDO more strongly. These analyses show that changes in the relationships between the measures of STRI and STRP with FFDI may have influenced interannual variability over time, but do not appear to have influenced the changes in mean.

Linear inverse analysis

Linear inverse analysis tests shifts in pairs of dependent and co-dependent variables, to see whether shifts are internally generated or externally forced (Jones, 2012). Examples of co-dependent pairs are Tmax and P,

and Tmin and Tmax. Internal climate variability will see a change in one member being reflected in the other. For example, if P changes, Tmax will respond accordingly, rising if P falls and falling if P rises. For example, decadal regime change from a drought- to a flood-dominated climate in eastern Australia in 1947–48, produced a sympathetic shift in Tmax in some areas of NSW (Nicholls et al., 2004). External forcing will change Tmax independently of P. If P changes as well, then paired analyses can be used to identify changes that are internally consistent and those in opposition.

The anthropogenic component of change is considered to be the residual after removing the influence of the reference variable; i.e., removing the influence of P from Tmax. If a time series becomes nonstationary due to regime change, the residual will contain a shift due to forcing. However, using simple techniques of separating pairs statistically will not work if both shift due to the same cause, or if, like FFDI, a variable is influenced by multiple factors. Lacking a reliable high-quality record for atmospheric moisture, here we were restricted to using Tmax and P.

The bivariate test used to detect shifts employs reference and test data sets. For general changes, where the data are serially independent, we use a randomly sampled reference data set and run multiple trials to overcome sampling uncertainty. With paired data, the driving variable acts as the reference, allowing only a single test. If a paired shift occurs that is additive, the test will not register a shift; i.e., if both variables shift together with no residual effect, a shift will not register in the test variable. However, if there is a nonlinear response, such as an additional feedback and/or amplified response, then a shift may be registered independently to the reference.

The tests triangulate between P, Tmax and Σ FFDI. If Tmax shifts with reference to P, warming has been externally forced. If either P or Tmax shift and the other does not respond according to the dependent relationship, then both have changed. Where both increase with respect to Σ FFDI, which remains unchanged, the Tmax relationship will produce a negative response; i.e., Σ FFDI should increase in response to Tmax, but is suppressed by higher P. If Σ FFDI/Tmax does not register and Σ FFDI is known to shift, then Tmax is part of that shift (Table 13).

Table 13: Guide to paired results in Table 13.

Pair (test/ref)	Explanation
HQD Σ FFDI	Date of shift
Σ FFDI/Tmax	If above date is not selected, they change in in step. If negative, Tmax increases relative to Σ FFDI
Σ FFDI/TmaxFS	If above date is not selected, they change in step. If negative, TmaxFS increases relative to Σ FFDI
Σ FFDI/P	If above date is not selected, they change in step. If positive, Σ FFDI increases relative to P
Tmax/P	If $p < 0.01$ and close to above date, Tmax is driving shift in Σ FFDI
Tmax FS/P	If $p < 0.01$ and close to above date, TmaxFS is driving shift in Σ FFDI
P/Tmax	If positive, P goes up with Tmax

The results are detailed in Table 14. Tas, Vic, SEA, SWWA, NSW and SA show no break between Σ FFDI/Tmax or Σ FFDI/Tmax FS at the time of the regime change in Σ FFDI, even though they both shifted when tested individually. The shift to warmer and wetter conditions in northern Australia in the early 1970s shows up in the northern states, extending down to NSW and SA as shown by the negative response to Σ FFDI/Tmax.

WA registered a shift in P in 1995 at $p < 0.01$ relative to Tmax, mainly in the warmer months. Further work is needed to determine the specific regions in WA. Warming in TmaxFS is delayed at the state scale until 2002–03, but was detected for SW WA in 1993–94. However, Σ FFDI/Tmax or Σ FFDI/Tmax FS did not detect a shift relative to 2000–01, indicating that Tmax, FFDI and P shifted in unison, the shift in P being cryptic.

Table 14: Test statistic (Ti0), year of change, size of change, p value and summary notes for Australian states and regions where pairs are test/reference. Variables are Σ FFDI calculated from high quality data, average daily maximum temperature for the fire year (Tmax) and fire season (Tmax FS), and annual rainfall for the fire year (P).

Region	Ti0	Year	Change	P value	Notes
Tasmania					
HQD Σ FFDI	9.1	1998	392	p<0.05	Σ FFDI shifted up in 1998 in concert with Tmax and Tmax FS. Σ FFDI shifts relative to P in 2006 and Tmax FS to P in 2009. This is a delayed response from the earlier shifts and is due to Tmax being sustained at higher temperatures, even in the wet year of 2010–11.
Σ FFDI/Tmax	5.7	1968	-276	ns	
Σ FFDI/Tmax FS	2.9	1967	-203	ns	
Σ FFDI/P	14.3	2006	337	p<0.01	
Tmax/P	19.1	1998	0.5	p<0.01	
Tmax FS/P	14.6	2009	0.8	p<0.01	
P/Tmax	5.2	1967	132	ns	
Victoria					
HQD Σ FFDI	17.4	1996	734	p<0.01	Blended Σ FFDI shifted up in 1996 in concert with Tmax, Tmax FS and P. Σ FFDI shifted relative to P in 2006 and Tmax FS to P in 2009. This is an occluded increase in warm season Tmax and P, where the increase in P fully compensates for that in Tmax.
Σ FFDI/Tmax	7.1	2009	-429	ns	
Σ FFDI/Tmax FS	6.2	2009	-402	ns	
Σ FFDI/P	20.8	2006	411	p<0.01	
Tmax/P	24.3	2006	0.8	p<0.01	
Tmax FS/P	21.4	2009	1.2	p<0.01	
P/Tmax	9.6	2009	102	p<0.05	
SEA					
HQD Σ FFDI	13.8	2002	623	p<0.01	Σ FFDI shifted up in 2002, mostly influenced by Tmax FS, but involving Tmax and P. Σ FFDI shifts relative to P in 2006 and Tmax FS to P in 2005. There is an occluded increase in Tmax and P in 2009 that has not altered Σ FFDI. Tmax FS is the strongest driver of Σ FFDI.
Σ FFDI/Tmax	8.5	2009	-422	p<0.1	
Σ FFDI/Tmax FS	7.3	2009	-382	ns	
Σ FFDI/P	23.8	2006	429	p<0.01	
Tmax/P	28.5	2000	0.8	p<0.01	
Tmax FS/P	24.1	2006	1.1	p<0.01	
P/Tmax	12.4	2009	108	P<0.01	
SWWA					
HQD Σ FFDI	9.7	2000	365	p<0.05	The lack of a response of Tmax and TmaxFS to Σ FFDI suggests they moved perfectly in step in 2000–01. TmaxFS responded to P from 2009, and previously in 1960 (p<0.05), but did not respond greatly in 1993–94. This suggests a cryptic increase P, which did shift over greater WA in 1995.
Σ FFDI/Tmax	6.3	1957	-870	ns	
Σ FFDI/Tmax FS	4.5	1957	-739	ns	
Σ FFDI/P	5.1	2001	112	ns	
Tmax/P	21.8	1992	0.7	p<0.01	
Tmax FS/P	15.0	2009	0.9	p<0.01	
P/Tmax	4.9	1968	-58	ns	
SA					
HQD Σ FFDI	10.4	2002	529	p<0.05	Σ FFDI shifted up in 2002 in concert with Tmax and TmaxFS. Σ FFDI/Tmax responded negatively in 1972 due to an increase in both P and Tmax in 1972 to warmer, wetter conditions
Σ FFDI/Tmax	18.9	1972	-495	p<0.01	
Σ FFDI/Tmax FS	9.4	1972	-330	P<0.1	
Σ FFDI/P	26.9	2002	433	p<0.01	
Tmax/P	32.6	2000	1.1	p<0.01	
Tmax FS/P	30.0	2002	1.3	p<0.01	
P/Tmax	17.2	1972	92	P<0.01	
NSW					
HQD Σ FFDI	10.7	2002	637	p<0.05	Similar to SA, the results line up for a shift in Σ FFDI in 2002, where both Tmax and TmaxFS shift in unison. The 1972 occluded increase in Tmax and P, which occurred across northern Australia, can also be detected.
Σ FFDI/Tmax	14.0	1972	-398	p<0.01	
Σ FFDI/Tmax FS	7.1	1972	-279	ns	
Σ FFDI/P	22.2	2002	420	p<0.01	
Tmax/P	31.7	2000	1.0	p<0.01	
Tmax FS/P	23.7	2002	1.3	p<0.01	
P/Tmax	10.0	2004	112	P<0.05	
WA					
HQD Σ FFDI	3.9	1973	138	ns	WA is so large that a coherent result did not emerge, but the results offer a solution for SWWA. FFDI/Tmax declining in 1994–96 is due to an increase in P that partially compensated for the increase in Tmax (P/Tmax of 153 mm in 1994), whereas the shift in TmaxFS was delayed.
Σ FFDI/Tmax	33.2	1995	-792	p<0.01	
Σ FFDI/Tmax FS	27.2	1996	-587	p<0.01	
Σ FFDI/P	13.1	2002	184	p<0.01	
Tmax/P	38.0	1994	1.0	p<0.01	
Tmax FS/P	28.9	2002	1.1	p<0.01	
P/Tmax	33.4	1994	153	P<0.01	
Qld					
HQD Σ FFDI	8.6	2012	626	p<0.1	Queensland shows all the signs of a shift in 2002, but there is an occluded shift in 1997, where Tmax and P both increased relative to each other, similar to that in the early 1970s (FFDI/Tmax shifts -ve in 1997 at p<0.05). This delayed the shift in Σ FFDI until 2012. From 2012–2019, Qld has been >1.2 °C warmer than similar past dry periods.
Σ FFDI/Tmax	18.5	1972	-472	p<0.01	
Σ FFDI/Tmax FS	10.7	1970	-340	p<0.05	
Σ FFDI/P	22.4	2001	318	p<0.01	
Tmax/P	30.4	1997	0.8	p<0.01	
Tmax FS/P	22.5	2002	0.9	p<0.01	
P/Tmax	18.5	1997	176	p<0.01	

Constructing and assessing fire climate regimes

Region	T ₁₀	Year	Change	P value	Notes
NT					
HQD Σ FFDI	5.0	2016	710	ns	Northern Australia had an increase in P in the early 1970s at $p < 0.01$, which meant that Σ FFDI decreased relative to T _{max} . The increase in T _{max} in 1979 had little effect on NT average Σ FFDI. There may be different regimes between the coast and the interior. The drier, warmer dry season needs a closer look.
Σ FFDI/T _{max}	26.4	1971	-656	$p < 0.01$	
Σ FFDI/T _{max} FS	22.2	1967	-577	$p < 0.01$	
Σ FFDI/P	22.7	2002	358	$p < 0.01$	
T _{max} /P	26.8	1979	0.8	$p < 0.01$	
T _{max} FS/P	25.5	1979	0.9	$p < 0.01$	
P/T _{max}	25.5	1971	224	$P < 0.01$	

Queensland shows a shift in T_{max}FS relative to P in 2002, but an occluded increase in P and T_{max} in 1997 may have masked this. The increase in Σ FFDI from 2012–13 in Queensland may reflect more generally warmer and drier conditions down the east coast. NT shows the clear shift in P in the early 1970s, which may have masked any changes with warming in 1979. It is possible that the monsoonal part of NT and the more arid areas of central Australia have different responses and need to be analysed separately.

If we consider these results with those for RH summarised in Figure 17, changes in T_{max} and P alone cannot produce a regime shift in FFDI. A reduction in atmospheric moisture and complementary increased in T_{max}FS is required.

According to Cai and Cowan (2013), tropical dry air moving poleward contributed to a decline in autumn rainfall from the early 1990s, but at other times, warmer air has been accompanied by increased vapour pressure. This may not be visible in rainfall records because of their high variability. For example, in SEA, P increased relative to T_{max} in 2009 ($p < 0.05$). Totals change little, but the shift is detectable in the paired test. This intensification may have been due to warmer SSTs off NW Australia in 2009 reaching southern Australian in 2010. Such changes can be cryptic or occluded; they have little visible impact but alter the relationship between variables. The results suggest that fire climates are buffered against change, not responding until climate is nonstationary and variables such as T_{max}, RH and P have responded.

Dynamic influences on FFDI

Attribution studies commonly address the role of dynamic processes, such as circulation changes and modes of climate variability, in order to separate internal from external influences (Grose et al., 2017; Harris & Lucas, 2019; Post et al., 2014). Climate model studies investigate these processes in baseline and perturbed runs to determine whether changes lie beyond the range of natural variability, or are a feature of externally-forced climate (Grose et al., 2014; Hasson et al., 2009).

The subtropical ridge features strongly in rainfall attribution studies in SE Australia (Cai et al., 2011; Murphy & Timbal, 2008; Post et al., 2014). With respect to climate modelling, any lack of capacity in positioning the STR appropriately will lead to errors (Maher & Sherwood, 2016; Pepler et al., 2018). Grose et al. (2015) found no relationship between past and future STR intensity or position in 36 climate models from the CMIP5 climate model archive. They also found with respect to May to October rainfall, declining trends simulated by models were less than observed, there was no relationship between mean, variability and trends of STR position and if trends in intensity were being underestimated, then trends in May–Oct P would also be underestimated if there was a relationship at all (Grose et al., 2015). Grose et al. (2015) estimated the rate of change in STRI April–October 1948–2002 to be 0.22 hPa per decade. With the updated time series (Pepler et al., 2018) the trend for May–Oct is 0.23 hPa per decade. However, this record is not trend-like. 1910–2019, a shift of 1.12 hPa occurs in 1993 ($p < 0.01$) and total internal trends are 0.15 hPa, while the simple trend is 1.47 hPa. The trend from 1993 following the shift has been slightly negative, so the simple trend and shifts plus internal trends give different totals.

Maher and Sherwood (2016) tested the ability of GCM 20th century simulations to reproduce rainfall variability and amount in regions across southern Australia covering SWWA to SE Queensland. They looked at drivers of variability and tropic edge metrics, concluding that models had skill at representing the broad patterns of moisture variability with respect to the position of the Hadley Cell and strength of the STR.

However, the models missed some connections between drivers of variability and over-emphasised others. Most importantly, they found that improving skill in driver covariability providing better spatial and temporal distribution of moisture did not translate into improved estimates of precipitation amount (Maher & Sherwood, 2016). We expect these findings would also apply to FFDI.

Our analysis shows that while STRI does show some regime-like behaviour, this has had little influence on fire climate regimes. Correlations between the STR indices and TmaxFS, P and FFDI indices reveal seasonal and interannual relationships but that these aspects of climate dynamics are not influencing change. From Figure 18, they show patterns becoming more tropical, with cool season correlations decreasing and warm season correlations increasing. This sees an evolution from preconditioning, where the previous cool season influences fire season severity, to in-season effects. STRI and STRP have a dynamic effect by redistributing sensible and latent heat. They also influence feedbacks with the land surface but because the climate is in steady state regimes, these also are expressed as variability rather than change. The effects of other influences, such as the El Niño – Southern Oscillation, Indian Ocean Dipole, Southern Annular Mode and Pacific Decadal Oscillation/Interdecadal Pacific Oscillation, have also been ruled out (Harris & Lucas, 2019). The next chapter investigates thermodynamic drivers of change.

6. Attributing recent fire climate regime changes in Australia. Part II Thermodynamics

Introduction to thermodynamic forcing

Thermodynamic changes originate with changes in energy flows within the climate system and dynamic changes are associated with changes in circulation (Chadwick et al., 2016). Decadal shifts in climate regimes occur because the coupled shallow ocean-atmosphere operates as a storage and release system (Jones & Ricketts, 2017). Powerful negative feedbacks at the ocean surface act to keep the climate in steady state. The additional heat remaining in the atmosphere from greenhouse gas forcing not taken up by strong sinks such as melting snow and ice and the ground surface is absorbed by the shallow ocean. If the build-up near the surface exceeds the available potential energy need to transport heat to the poles, the system becomes unstable and shifts to a new steady state (Jones & Ricketts, 2017; Jones & Ricketts, 2021a, 2021b).

Thermodynamic forcing occurs when the dissipative processes in the climate system respond to internal energy imbalances by changing state to a higher (lower) level of available potential energy where it can maintain steady state. The magnitude of change is roughly 0.25 °C for a large global shift and less for regional shifts. The spatial variation of shift size for average temperature can exceed 0.5 °C over land and down to 0.10–0.15 °C over parts of the ocean.

These regime shifts occur first in the ocean (Reid, 2016; Reid & Beaugrand, 2012), being transmitted from the equator to higher latitudes. This is followed in the space of months by warming of the atmosphere, higher temperatures being sustained in regions where circulation patterns are in contact with warmer sea surface temperatures (Jones & Ricketts, 2021b). Analysis of the timing and distribution of these changes shows most were initiated in the Pacific Ocean heat engine, a dynamic self-regulating heat pump that collects heat via the eastern Pacific Ocean and dissipates it via the Western Pacific warm pool (Jones & Ricketts, 2021b). A heat pump is maintained by kinetic energy, in this case by the Coriolis effect, where it maintains a constant balance of 1.9 °C and plays a key role in modulating ENSO and the PDO. The cold to warm structure provides a regulating mechanism that allows both cooling and warming. The heat pump sits within a global dissipative heat engine involved in meridional heat transport from the equator to the poles. This heat engine is linked to a broader climate network made of oscillations and circulations such as the Pacific Decadal and Atlantic Multidecadal Oscillations and the Atlantic Meridional Overturning Circulation (Jones & Ricketts, 2021a, 2021b).

Variables known to be dominated by steplike change are those associated with ocean surface atmosphere interactions such as surface and air temperature, local sea level, air pressure and rainfall (Belolipetsky et al., 2015; Jones, 2012; Jones & Ricketts, 2021b; Reid & Beaugrand, 2012; Reid et al., 2016; Ricketts, 2019). Variables known not to be so influenced are those with large storage potential that accumulate or deplete gradually, such as ice masses and the deeper ocean (below 700 m).

When analysing how the climate changes, most studies go straight from forcing to dynamics, overlooking the nonlinear, dissipative processes that drive climate internally (c.f., Ozawa et al., 2003; Westhoff et al., 2019). The explanatory model we use to understand the broader process moving from forcing to warming is shown in Figure 20. Radiative forcing and the trapping of greenhouse gases cause the initial energy imbalance. Many studies go straight from the first chevron to measurement of change attributing any non-gradual behaviour in the subsequent process to noise.

In asking ‘what drives regime change in FFDI?’ we need to understand whether influences are directly causal or whether they are induced by a combination of influences that may not be directly related to an underlying regime shift (Beaugrand et al., 2019; Marlon et al., 2009; Pausas & Fernández-Muñoz, 2012). The latter describes how ecological regime shifts are generally considered – where the climate drivers are gradual but

the system response is not (Conversi et al., 2015; Harley & Paine, 2009; Overland et al., 2008). In terms of fire, this would be akin to gradual changes in climatic variables and land surface characteristics affecting fuel supply and condition that leads to a one-way shift in fire regime (e.g., Zinck et al., 2011). However, we have already identified shifts in T_{max}FS and RH as the likely catalysts in fire regime shifts, so in the following we investigate the possible large-scale drivers of those changes to see whether a direct influence can be attributed.

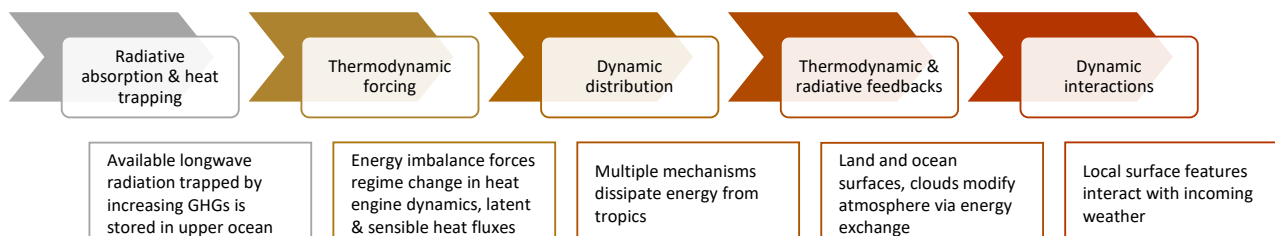


Figure 20: Schematic of the climate system as a nested system of processes describing the greenhouse effect and dissipation of energy through to measurement. Not shown are the multiple feedbacks that pass back up through this system (Jones & Ricketts, 2021a).

Thermodynamic drivers of fire climates

Timeline of historical regime changes

During the historical period, global climate has been in two modes: free and forced. In free mode the ocean-atmosphere is loosely coupled and decadal variability has the capacity to take climate on random walks over a ‘Brownian bridge’ where random departures away from steady state return and interannual variability is characterised by red noise. The transition between the two occurred between 1957 and 1972 (Jones & Ricketts, 2021b).

A widespread downward shift in sea surface temperatures occurred in the early 1900s, probability initiated from the mid-latitudes and spreading to the tropics. Land temperatures were largely unaffected (Jones & Ricketts, 2021b). Early 20th century warming in the Northern Hemisphere extratropical land was heavily influenced by solar forcing, which set an early peak around 1920 (Egorova et al., 2018; Hegerl et al., 2018; Wang et al., 2018). In the ocean, radiative forcing supported a partial recovery in temperature the 1920s and full recovery in 1936–37, when the ocean shifted back to pre-1900 levels. This commenced a period of little change that Broecker (2005) called the long pause.

In 1957, the ERSSTv4 ocean record switched from red to white noise, followed by GMST in 1969 and land in 1972. This marks the transition from a free to forced climate, where the ocean-atmosphere becomes more tightly coupled, teleconnections became more active including those between the low to the high latitudes and the northern and southern hemispheres. The increased heat being trapped collects in the tropics, becoming unstable when available potential energy to transport is exceeded and shifts to warmer conditions.

Early regime shifts affecting Australia occurred in 1957–58 influencing minimum temperature in the north, but the first major event was initiated in the Pacific warm pool in 1968, propagating to SST Australia-wide, affecting minimum temperatures coinciding with reduced winter P in SWWA. The 1972–73 ENSO provided the heat for a shift in T_{max} in southern Australia and an upward shift in wet season P in northern Australia. Some of these are featured in Table 13.

A major shift from a negative to positive PDO initiated in the eastern Pacific in 1976 (O’Kane et al., 2014), transferred to the western Pacific in 1978. The shift in eastern Pacific SST was 0.46 °C, in the western Pacific 0.18 °C and in GMST 0.19 °C. This led to shifts in T_{max} in the northern states mostly in 1979. The following

shifts in 1987–89 mainly influenced the northern hemisphere. This was accompanied by an increase in RH over NH land in the HadISDH data set.

The next shift was triggered by a phase change in the AMO in March 1995 and anomalous warming in the western Pacific Warm Pool in April 1995 also seen in the Coral Sea. This was followed by a positive shift in the ocean 30–60 °S in Feb 1996, moving onto land later in 1996 (Jones & Ricketts, 2021b). Shifts progressed through the southern and northern hemisphere with phase shift in the PDO to negative occurring in June 1998.

A minor series of shifts affected SST on the west and south coast influencing climate in SW WA in 2009–10. The most recent sequence was initiated in the warm pool in Dec 2012 and involved the eastern Pacific in 2014, propagating globally during 2014 and 2015, mainly affecting the NH. The PDO switched to positive in mid-2014 (Jones & Ricketts, 2021b).

Thermodynamic processes influencing moisture transport

The two key drivers of regime shifts in FFDI have been identified as and 3 pm relative humidity (RH) and fire season maximum temperature (TmaxFS), so we look at thermodynamic processes influencing moisture transport affecting RH.

Ninety percent of the moisture originating from the ocean rains out over the ocean, and ten percent falls on land (Gimeno et al., 2010). Two thirds of that is then recycled over land (Gimeno et al., 2010; Gimeno et al., 2012). Continental precipitation can be mapped according to its oceanic and recycled continental sources (Gimeno et al., 2012). Many continental regions with seasonally alternating hot, dry and wet climates are in zones where rainfall is mainly of oceanic origin. This includes regions of Mediterranean climate, tropical wet and dry season climates and some alpine and boreal climates. As an island continent with a dry interior, most of Australia depends on moisture of tropical origin. Any large-scale changes to moisture availability from the oceans will therefore affect both hydroclimate and pyroclimate.

Chadwick et al. (2016) used a simple model to scale specific humidity over land with that over the ocean, finding it reproduces land patterns fairly well. The results support the hypothesis that RH over land can decrease if the land warms by more than the ocean. Byrne and O’Gorman (2018) used a similar approach, where the transport of most static energy from the ocean to the land produces a fractional response that decreases RH over drier landmasses. According to Chadwick et al. (2016), the adjustment timescale of moisture over land in response to transport from the oceans is much faster than the warming timescale of the surface oceans under climate change. However, in doing so they assume that ocean warming is gradual, whereas it warms through regime shifts (Jones & Ricketts, 2021b; Reid, 2016; Reid & Beaugrand, 2012). Any shifts in surface ocean temperature and moisture availability will therefore result in immediate adjustments over land.

Both studies analysed their results as trends. Byrne and O’Gorman (2018) showed that for temperature and specific and relative humidity 40 °S to 40 °N (their Fig. 1) their model predicted the observed trend for all three over land. Their results captured the variability and shift for specific humidity but not fully for relative humidity. This may partly be due to the different sources of land and ocean data. Their land data was derived from an earlier version of HadISDH and the ocean data from the ERA-interim reanalysis. The time series of static energy and specific humidity over ocean and land (their Fig. 2), are clearly regime-like, as in Figure 17. RH is more prone to error than either.

Globally, increases in vapour pressure in 1930, 1979, 1987, 1998 and 2015 from the CRU_ts4.03 dataset (Harris et al., 2020) were consistent with shifts in warming. Drawing on the models proposed by Chadwick et al. (2016) and Byrne and O’Gorman (2018), we infer that before 1998, moisture either increased or maintained relative humidity over Australia with a few exceptions (e.g., SW WA, central northern Australia).

Large-scale negative shifts in the SH and globally over land in 2002 showed that the vapour pressure increase in 1998 was insufficient to match the increase in temperature, and following the series of La Niña events through to 2001, RH shifted downwards. At regional scales, these changes were staggered. The 1996–97 warming in the SH mid-latitude ocean coincided with temperature and RH changes in the southern states, whereas those further north were delayed to 2002–03. The shifts in temperature coincided with abrupt shifts further south of the Hadley Cell edge in eight reanalyses documented by Nguyen et al. (2013). Although the PDO switched into its positive phase in 2014, and SH land dewpoint temperatures have increased (0.24 °C in 2014, $p < 0.05$), T_{av} has increased globally by more (0.32 °C in 2013, $p < 0.01$) and RH is unchanged, in 2019 being at its lowest level since the beginning of the HadISDH record (Willett et al., 2014) in 1973.

Figure 21 shows 5° x 5° grid-based trends for two periods 1973–1999 and 2000–2019, almost picking up the 2002 break (Willett et al., 2014; data to 2020). Globally, RH shifted downwards in 2002 and the NH in 2005. Over 1973–1999, some areas show a drying trend, including Australia, marking a decline from the wet years of the early 1970s, whereas most areas had positive trends. NH land shifted in 1990 to moister conditions closely following the 1988–89 temperature shift across Eurasia. In the second period, large areas show a drying trend, including Australia. Show for comparison in Figure 21 is a density map of all fires, wild and controlled 1996–2007 from Moritz et al. (2012). This distribution is consistent with the areas of reduced humidity and also coincides with regions where most rainfall is ocean-sourced (see Gimeno et al., 2013). These regions have also experienced reduced rainfall and increased drought associated with the widening of the tropics (Lucas et al., 2014).

The hemisphere-wide reduction of RH over land of -1.1 in 2002 and -2.4 across Australia in 2001 (Figure 17), confirms that despite warmer conditions increasing the amount of moisture in the atmosphere overall, the relative amount over land has decreased. These decreases have occurred as regime shifts associated with shifts in specific humidity and temperature. When global fire season length Jolly et al. (2015) is compared with compared with the Australian median daily average FFDI from Lucas and Harris (2019), both time series shifted in 2002 (Figure 22). The global fire season length is a mean anomaly constructed from the number of days when fire danger was above its median value from three analysis data sets for three fire danger variables, covering the US, Canada and Australian FFDI for 1979–2013 Jolly et al. (2015). Although it shares some data with Lucas and Harris (2019), Jolly et al. (2015) found a relationship for all continents except Australia. Correlation between the two time series is 0.58 ($p < 0.01$) and with regimes removed, considering interannual variability only, it is 0.35 ($p = 0.03$).

Constructing and assessing fire climate regimes

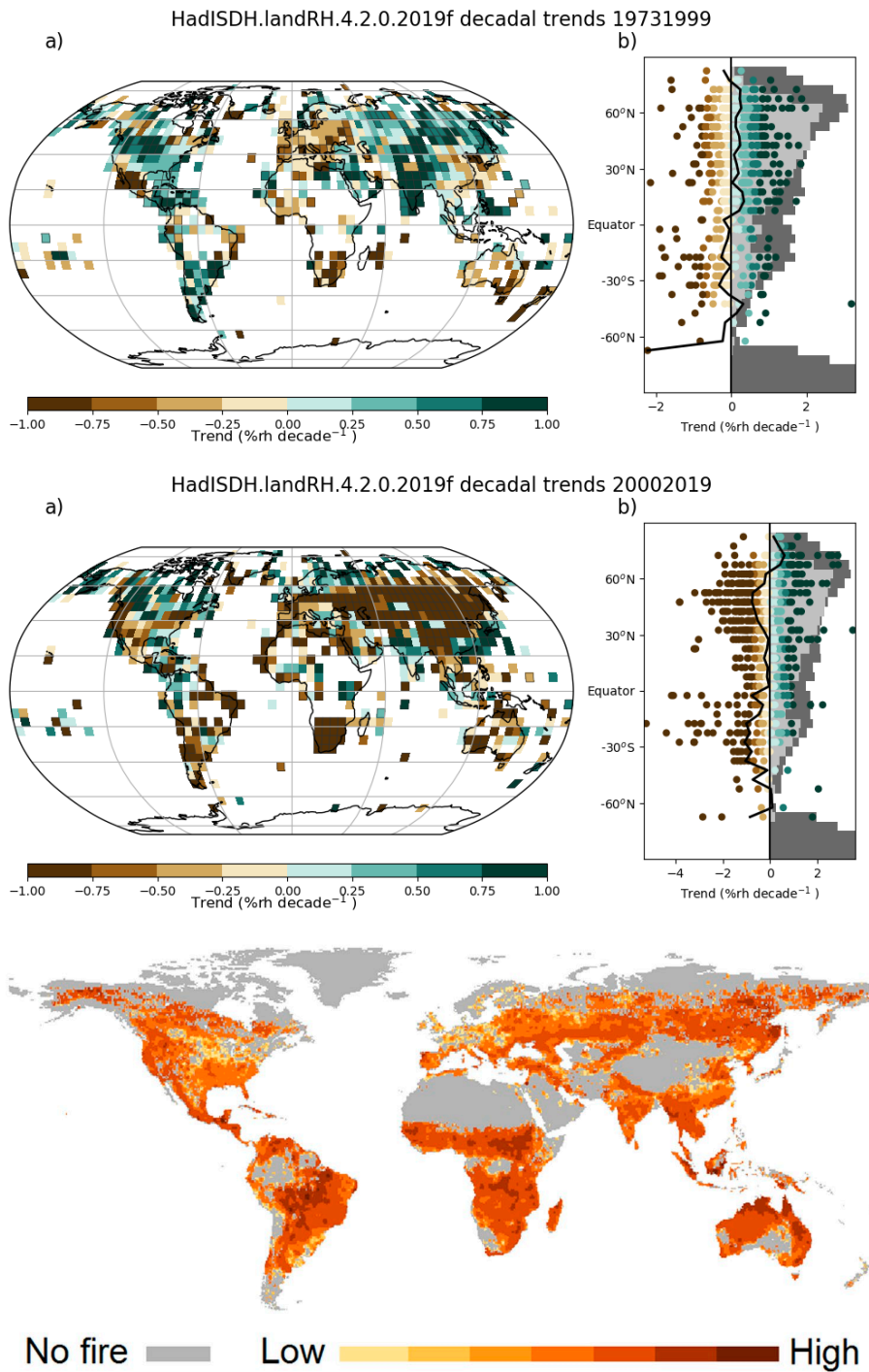


Figure 21: Trends for land RH from the HadISTH dataset (Willett et al., 2014) showing decadal trends 1973–1999 (top) and 2000–2019 (centre) on a 5° by 5° grid (a) with latitudinal spread of results (b), where dark grey shows proportion of land and light grey land with observational coverage (source K. Willett). Also shown (bottom) are number of fires counted from satellite images 1996–2007 on a 50 km grid (Moritz et al., 2012).

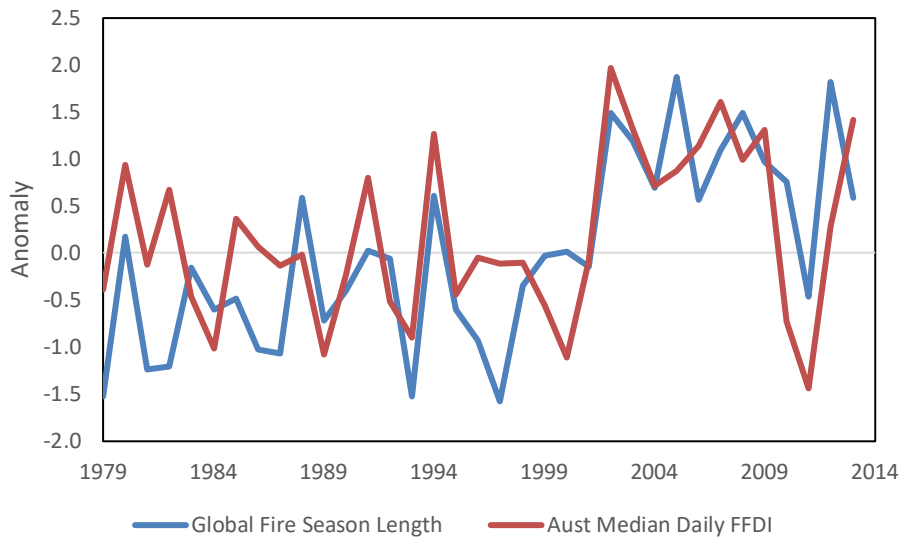


Figure 22: Global fire season length, the number of days when fire danger was above its median value (Jolly et al., 2015) compared with the Australian median daily average FFDI (Lucas & Harris, 2019).

Is tropical expansion regime-like?

In the previous chapter, STRP and STRI were calculated from the subtropical ridge situated in eastern Australia. Here we explore whether tropical expansion is regime-like at larger scales, affecting moisture transport. Tropical expansion is difficult to measure, with a variety of metrics that do not necessarily agree with each other, and different measurement systems such as observations, reanalyses and forced and unforced climate models (Davis et al., 2018; Grise et al., 2019). The underestimation of tropical expansion in climate models complicates this (Lucas et al., 2014; Nguyen et al., 2015). This makes it difficult to determine how the tropics are changing, and if any nonlinear responses are identified, such changes are routinely attributed to decadal variability.

In a synthesis paper, Grise et al. (2019) concluded that the more recent reanalyses are closer to the model estimates. They used two metrics to conclude that the rate of change in width of 0.2° – 0.4° per decade since 1979 is within the bounds of climate models for roughly the same period. Atmospheric models forced by observed SSTs expand at roughly twice the rate of the coupled models, attributed to the SSTs having the expansion of the PDO negative phase change directly represented, whereas coupled models are considered to represent such influences randomly (Allen & Amaya, 2018; Grise et al., 2019). Grise et al. (2019) allocated forced change to a trend and nonlinearity to variability so their reconciliation was achieved by removing the nonlinear effect.

Similarly, Amaya et al. (2018) used empirical orthogonal function analysis on a 20-member climate model ensemble forced by historical emissions to identify a secular trend that they attributed to greenhouse gases and stratospheric ozone. Internal variability from unforced simulations correlated highly with the Niña 3.4 region. This region sits within the central-eastern Pacific region, we have identified as a key driver of regime shifts (Jones & Ricketts, 2021a, 2021b). Combining the two in a multivariate regression with Hadley Cell edge indices showed both were involved in the modelled expansion (Amaya et al., 2018).

Allen and Amaya (2018) compared coupled and atmospheric versions of the CAM5 climate model 1979–2014, where the coupled model (with RCP8.5 2006–14, 35 members) produced NH widening of $0.03 \pm 0.04^{\circ}$ per decade and the atmospheric version forced by SST (10 members), $0.18 \pm 0.04^{\circ}$ per decade. They measured the latitude of the 500 hPa zero point in meridional circulation, which moves poleward with an increase in the amount of atmospheric heat transfer. They then forced the atmospheric model with a trend in SST, finding that the tropical widening averaged 0.02° in the NH and -0.03° in the SH. Their conclusion was that the recent

widening was dominated by climate variability, especially the phase change to a negative PDO (Allen & Amaya, 2018; Amaya et al., 2018). Atmospheric models forced by observed SST produce a nonlinear response whereas those forced by trends do not. Pacemaker experiments in coupled models forced by the eastern tropical Pacific, such as Kosaka and Xie (2016) produce regime shifts that closely correspond with observed shifts (Jones & Ricketts, 2021b).

Nguyen et al. (2013) assessed stream function measuring the edge of the Hadley Cell from eight climate reanalyses. They showed a pronounced shift in the late 1990s for the cell edge in both hemispheres, and one present but less clear for intensity. Observed SH STRI 1880–2008 from Nguyen et al. (2015) shows a shift in 1998 of 0.5 hPa. The ICOADS 2° enhanced record of ocean sea level pressure 1948–2019 for 30–35°S contains two shifts: 0.55 hPa in May–Oct in 1977 and 0.83 hPa in Nov–Apr in 1998, both at $p < 0.01$. The annual record 0.68 hPa in 1998 is 100% shifts with no trend, showing stable conditions between shifts. Both dates coincide with shifts in the PDO and both intensify, consistent with shifts in temperature, rather than following positive and negative phases in the PDO.

As the SH STR is dominated by the Asia-Pacific branch (Nguyen et al., 2018) any large-scale step-like behaviour is likely to affect the Australian region. In tracing the tropical edge, Nguyen et al. (2018) related its expansionary aspect in the Asia-Pacific region to a La Niña pattern in the tropical Pacific, consistent with a negative PDO. Nguyen et al. (2015) concluded that if the negative phase of the PDO/IPO during 1998–2014 was driving the recent tropical expansion, the austral component of the Hadley Cell would have expanded and the African and American centres contracted. However, all have expanded. If the shift in 1997–98 was solely due to climate variability, then an equatorward movement of the tropical edge would be expected after the PDO shifted positive in 2014, but most indices have remained stable.

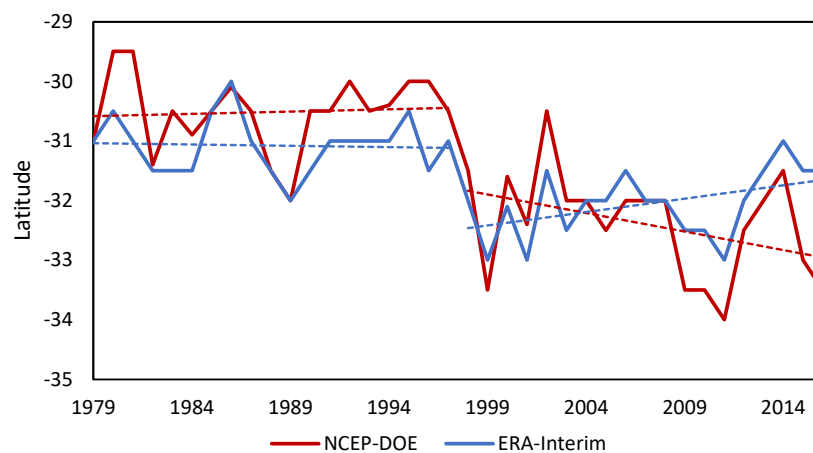


Figure 23: Latitude of the southern hemisphere Hadley Cell from the CEP-DOE v2 and ERA-Interim reanalysis datasets for the period 1979–2016, calculated by Moon and Ha (2020). Dashed lines show internal trends before and after the regime shift detected in 1998.

Moon and Ha (2020) calculated the latitude of the southern hemisphere Hadley Cell edge from the NCEP-DOE v2 and ERA-Interim reanalyses dataset for the period 1979–2016. Both shifted south in 1998 by 1.9° and 1°, respectively ($p < 0.01$; Figure 23). They concluded that greatest influence on the Hadley Cell edge is subtropical tropopause height (Moon & Ha, 2020). Greater height combined with a more poleward edge shows the increased transport of heat from the tropics, which reflects leads to greater meridional transport of heat.

Chapter 5 shows that the position and intensity of the STR over Australia does not drive fire regime changes but reflects how those changes are evolving, so its influence is largely dynamic. Here, tropical expansion can be linked by timing to regime shifts in RH and FFDI. This is consistent with the model of oceanic moisture feeding onto land where deficits are accentuated by accelerated warming and land surface feedbacks,

combining the respiratory effects of vegetation to elevated CO₂ and soil moisture deficits accumulating from reduced RH. In parts of southern Australia, this has also been accelerated by reductions in winter-spring rainfall. These responses are thermodynamic.

This has implications for the understanding of both dynamic and thermodynamic patterns. Nguyen et al. (2018) nominated the Asia-Pacific region as the most influential region for tropical expansion. This is where the Pacific Ocean heat engine is situated. Regime shifts in specific humidity are a thermodynamic response to forcing as this increases the transport of latent heat towards the poles. Downward shifts in RH occur when temperature increases fail to maintain the relative content of moisture in the atmosphere, leading to regime shifts in fire climates. With respect to dynamics, once in place, a specific regime sets up boundary conditions that constrain circulation patterns. This will affect things such as seasonal influences on FFDI and the frequency of synoptic patterns.

Thermodynamic drivers of regime change

Shifts in RH and T_{maxFS} and interactions between the two are the major ingredients of regime shifts in fire climates. Thermodynamically-forced regime shifts of global scale are the likely cause of the most recent regime shifts in Australia. When records from the US and Canada are included (Jolly et al., 2015; Figure 22), these changes appear global in extent. However, this would have to be confirmed for other regions in Europe, Asia, South America and Africa. For Australia, this does not preclude smaller regional shifts occurring at other times, as is the case for other climate regime shifts.

Historically, fire climate regimes have been fairly stable. Analysing data from 1957–58 we found little evidence of regime shifts until the late 1990s, except for a possible shift in inland northern Australia in the late 1970s. The major sequence commenced in the late 1990s in SE Australia, centred on Victoria at around 37° S, before registering further north in SWWA 2000–02, NSW and SA 2002–03 and Queensland 2012–13, and south in Tasmania between 1999 and 2006.

Most shifts in RH over Australia have followed the upward shift in sea surface temperatures in the Australian region ranging from 1995 in the Coral Sea, 1997 in the Southern Region and 1998 in the northern Tropics, Tasman Sea and nationally, the timing of the latter in December 1997. The exceptions are SW WA (1994–95) and central Australia (1979–80), where there T_{max} also shifted simultaneously. Nationally, from the Lucas and Harris (2019) data, RH shifted downward by 2.4 points in 2001–02 and SH land from the HadISDH data set by 1.1 points in 2002. Zonal SST 0 °S to 24 °S and 24 °S to 44 °S from the GISS surface temperature data set, derived from ERSST v4 (Huang et al., 2015; Liu et al., 2015), also both shifted in 1997. These cover the major source regions for moisture over Australia (see Gimeno et al., 2013).

Since the global 1996–98 shift, most movements in T_{maxFS} can be associated with a subsequent shift in FFDI (with some uncertainty about dates in Tas). All such shifts coincided with a severe fire season triggered by an El Niño event, except for perhaps SWWA in 2000–01. The 1996–97 El Niño event was followed by an extended La Niña event in 1998–2001, introducing cooler conditions. A brief break meant the summer of 2000–01 was reasonably warm, but three of the four fire seasons to 2002–03 were relatively cool. This complex series of events is associated with a regime shift to warmer conditions in 1997, followed by a shift to negative PDO in mid-1998, during a La Niña event. These cooler and moister conditions counteracted the regime change until conditions eased in 2002–03 and the shifts in RH and T_{maxFS} emerge as statistically robust. That fire season also marked the first in the sequence of major fires that have marked this sequence, the latest being 2019–20. The 1997 shift in T_{max} was most prominent in the cool season, whereas the shift in warm season T_{max} was delayed until the negative feedback between reduced moisture on the land surface resulting in higher warm season temperatures that have persisted.

Constructing and assessing fire climate regimes

Conventionally, attribution is undertaken on the basis that forced change is gradual, internal variability is not and attribution between change and variability is carried out on that basis. Here, we argue that the heat storage and release system in the coupled ocean-atmosphere is regulated by the Pacific Ocean heat engine and broader climate network. Energy imbalances due to heat accumulating in the tropics results in a regime shift involving both latent and sensible heat. The relationship between the two has a subsequent influence on the evolution of fire climate regimes.

The PDO and ENSO are key components of the heat engine. During the negative phase of the PDO (La Niña-like), the eastern Pacific is cooler and wider and meridional transport is increased. More heat moves laterally and into the deeper ocean and less into the warm pool. During the positive phase (El Niño-like) the heat engine is narrower, meridional transport is reduced, the warm pool receives more heat and convection is increased (Allen & Amaya, 2018; Zhang et al., 2009). These influence the position of the Hadley Cell, cell edge and STR, which affect circulation. For example, the reversals in correlation between ΣFDI and P with STRI in Queensland, occurring in 1969, 1997 and 2014 noted in the previous chapter. Phase shifts become more definite over time and the last cycle was shortened (Jones & Ricketts, 2019), which may be a response to forcing (e.g., Bonfils & Santer, 2011; Dong et al., 2014).

7. Summary

This report describes the construction, assessment and attribution of fire climate (pyroclimate) regimes for Australia. A fire climate (pyroclimate) is defined as the mean and distribution of climatic conditions contributing to the annual level of forest fire danger, independent of fuel loads and ignition. This is measured using different metrics of McArthur's Forest Fire Danger Index.

Recent work shows that instead of climate responding to external forcing via a gradual change in mean with variability superimposed, it passes through a series of steady states, much like a staircase. A climate regime is defined here as a steady state representation of one or more climate variables. Climate regimes can also be defined dynamically through circulatory or synoptic characteristics often associated with oscillatory modes of climate variability (e.g., Overland et al., 2008), whereas those discussed in this report are thermodynamic, relating to steady states in the dissipation of heat from the equator to the poles. A shift occurs when a critical imbalance between the heat needing to be dissipated exceeds the capacity of the current regime to dissipate that heat, either positive or negative. Regimes can be regional to global in extent and represent the interplay between internal and external forcing.

Earlier work showed that FFDI in Victoria had undergone a regime change in the late 1990s (Jones et al., 2013). In the wake of the 2019–20 Black Summer we sought to construct a robust representation of FFDI using readily obtainable climatic data capable of identifying regime changes in fire climates for the whole of Australia. The guiding rule was that data had to be publicly available and of high quality, ruling out windspeed and atmospheric moisture. The aim was not to replace the use of FFDI or other indices over seasonal and shorter timescales but to complement the current models and strategic planning representing land-surface, management, fuel growth and fuel conditions. Currently, there is a limited capacity to estimate the influence of externally-forced climate change on fire risk and a lack of awareness as to how fast those risks can change.

Using climate data from the Australian Bureau of Meteorology climate tracker we constructed a multivariate linear regression for FFDI in Victoria based on the annual average rainfall anomaly, TmaxFS, area exceeding the 90th percentile of Tmax and 3 pm cloud amount (Equation 3). This was developed from a baseline of Victorian average FFDI from nine stations 1972–73 to 2009–10 adjusted for inhomogeneities. Indices assessed were annual Σ FFDI and days above high, very high and severe fire danger.

The primary model was expanded to 1957–58 to 2019–2020 for Victoria and applied to the other states and regions. Regions that performed well (r^2 for Σ FFDI >0.8 , r^2 for days Sev+ >0.65) were Victoria, SE Australia, New South Wales, Queensland and Northern Territory. Moderate performers were South Australia and Tasmania and poor performers were Western Australia and SW WA. Performance depends on the representativeness of station coverage across a region and the presence of inhomogeneities within the station-based FFDI data, mainly in wind and RH.

The earliest confirmed regime change detected in FFDI was 1996–97 in Victoria for most indices through to 2002–03 for days Sev+, staggered dates in Tasmania from 1997–98 to 2006–07, 2000–01 in SW Western Australia, 2002–03 in SE Australia, New South Wales, South Australia and 2012–13 in Queensland. No shifts were found for the whole of WA or the Northern Territory, but there is evidence of a change in NW Western Australia in 2002–03 and possibly central Australia in 1978–79. When compared with future projections of change for Σ FFDI, Tasmania and SE Australia have already exceeded 2030 projections, Queensland is equal, NSW and SW WA just below and SA about one-third way up a large range of change. The results are similar for days Sev+ except for Tasmania, where the model does not provide a result.

We investigated a variety of variables known to affect fire weather to identify those involved in fire regime shifts. Although Σ FFDI can be estimated from total annual P and average Tmax, the involvement of all four

variables in Equation 3 is needed to produce the full regime shift for all indices. After eliminating those variables with no consistent involvement in the majority of shifts, only TmaxFS and RH remained.

RH from the LH2019 dataset showed shifts in averaged station data in SE Australia in 1996–97, and New South Wales and South Australia in 2001–02. Exceptions were SW Western Australia in 1993–94, where summer rainfall appears to have played a role and Northern Territory in 1978–79. However, inhomogeneities in this data has affected some regions, so these are not conclusive. A shift in national average RH in 2001–02 and SH land in 2002–03 confirm the recent shifts as being large-scale. Both southern hemisphere and global average RH from HadISDH shifted downwards in January 2002. Annual average Tmax first responded to the global shift in southern Australia in 1996–97 but TmaxFS was delayed in most regions until 2002–03, probably due to three of the four intervening years being La Niña events. Linear inverse analysis of co-dependent pairs showed that earlier shifts in Tmax had limited influence on FFDI whereas shifts in RH either with, or slightly preceding shifts in TmaxFS, were the minimum required to produce a regime shift.

A second model estimating mean FFDI at a specific location was constructed, based on fire year maximum temperature, 3 pm relative humidity and 3 pm windspeed. This was calculated from 35 stations common to Climate Change in Australia (CSIRO & Bureau of Meteorology, 2015) and Harris and Lucas (2019). Outliers in the model showed that the results could be highly location-specific, especially in windy and moist coastal environments.

Dynamic and thermodynamic influences were investigated via the relationships between rainfall, temperature, FFDI and the subtropical ridge and intensity, and Hadley Cell edge measurements. The subtropical ridge over Australia (Pepler et al., 2018; Timbal & Drosowsky, 2013) was implicated because the earliest shifts were at the latitude where the STR is most intense, propagating north, suggesting a degree of intensification and/or redistribution of the dry tropics. Neither the position or intensity have a driving role in regime shifts, but have a redistributive effect shown by changing seasonal patterns before and after regime shifts. This is consistent with findings for other modes of variability such as ENSO and the Southern Annular Mode (Harris & Lucas, 2019).

The thermodynamic aspect is revealed by the shifts in FFDI, TmaxFS and RH at hemispheric and global scales. A fire climate regime is maintained by a steady-state balance between latent and sensible heat, usually in the presence of high variability. Median Australian FFDI and global fire season length both shifted in 2002 as did global RH over land. This sequence began with a global regime shift in temperature in 1997 and specific humidity in 1998. Following an extended La Niña-dominated period to the end of 2001, a regime shift in RH over global land registered, earlier in some regions. Feedback effects over land led to shifts in TmaxFS, resulting in widespread shifts in fire climate regimes over Australia and other parts of the world. The size of the change needed to induce a fire regime shift is yet to be determined but the average change over Australia around the year 2000 for Tmax was 0.7 °C and RH decreased by -2.4 points.

There is also some evidence that widening of the tropical zone has been part of these shifts, resulting in the expansion of the Hadley Cell and the movement of dry air further poleward (Fu, 2015; Lau & Kim, 2015; Nguyen et al., 2013). Hotter and drier conditions expanding from the downward arm of the Hadley Circulation would help to explain why midlatitude locations such as Victoria shifted before those further north.

Pyroclimates and hydroclimates occupy two parts of a continuum. These are reflected in terrestrial climate zones such as the Köppen climate classifications (Peel et al., 2007), which range from rainforest to deserts and from hot to cold. The hydroclimate involves the climate↔water cycle including the transport of atmospheric moisture. Pyroclimates are biased towards the hot, dry end of hydroclimates but not at the highly arid extreme, because sufficient rainfall is needed to promote the growth of fuel.

Fire regimes in SE Australia have been just above or close to the upper limit of their 2030 maximum projections for two decades, three decades before these changes were anticipated. This has resulted in the paradox of current conditions exceeding future projections even when they are being constructed (e.g., CSIRO & Bureau of Meteorology, 2015). Projections of future fire weather from climate models are routinely being underestimated. This is usually considered to be due to shortcomings in land-surface and land cover relationships combining with insufficient model resolution. However, we relate this to the ability of models to project changes in the hydroclimate, reflected in their capacity to reproduce the historical performance of the Pacific Ocean heat engine and tropical expansion. Atmospheric models forced by SST reproduce historical shifts with reasonable accuracy (Jones & Ricketts, 2021a) and more rapid expansion of the tropics (Allen & Amaya, 2018), so whether they reproduce the recent fire regime shifts is of interest, even if earlier experiments are missing key land surface processes (Douville et al., 2020).

FFDI is a physically realistic and robust measure of pyroclimate. The most important variables are RH and T_{maxFS}. similar to how P and E_p can be used to estimate catchment scale hydrological response. Further work could look at producing response surfaces based on reproducing coarse scale fire risk using historical data. However, at finer landscape scale and sub-annual timescales, it has a number of limitations. For example, in measuring drought with respect to soil moisture and fuel condition (Finkele et al., 2006; Holgate et al., 2017) and at high values of FFDI where highly nonlinear responses such as pyroconvection can occur (McRae & Sharples, 2014; Sharples et al., 2016). However, it can act as a broad-scale indicator for such events (Dowdy & Pepler, 2018; Sharples et al., 2016).

Conclusions

This project has constructed fire climates for Australia, analysing when regime changes have occurred, locating them within the context of past change and future projections. Linking regime shifts in Australia with those more broadly, suggests that fire regime shifts are thermodynamically driven, being initiated in the Pacific Ocean heat engine and propagating globally.

An additional motivation was to place the 2019–20 fire season into a longer-term perspective. Working from anomalies at the state scale, New South Wales experienced a regime shift in the 2002–03 fire season from the previous regime 1957–58 to 2001–02, where for days Sev+ we estimate as a 28% increase. The three years to 2020 were 26% above the 2002–03 regime average and the driest and hottest on record. For the other states affected by these fires, South Australia exceeded the new regime average by one standard deviation in all measures; Victoria and Tasmania were just below their worst period of 2006–07 to 2008–09; Queensland as a state suffered its worst such period during 2002–03 to 2004–05; SW WA experienced its worst period 2008–10. The results for Queensland suggest that if not for the wet period around 2010, its fire regime may have also shifted in 2002–03.

The standard method of calculating anthropogenically forced change as a trend and nonlinear change as variability does not identify regimes, leading to current and future fire risk being underestimated. By linking regime changes in FFDI to thermodynamic drivers in a changing climate, we have revealed systematic shifts in fire climates, both in Australia and globally, which can be linked to large-scale climate regime changes originating in the tropics. By further developing fire climates that are easily updateable and better represent change over annual and longer timescales, we hope to provide a simple tool for strategic planning, complementing more applied management tools and indices that can be used for short-term planning and response. A better understanding of how thermodynamic drivers in observations and models would also contribute to the lack of progress in the climate modelling of fire risk. Since the early studies of Beer et al. (1988); Beer and Williams (1995) the modelling of FFDI under climate change has undergone considerable technical improvement but confidence in its application remains limited. This work has the potential to change that.

Appendix 1. Model and data sources

Data for calculating annual data for FFDI climatologies was sourced from the Bureau of Meteorology high quality datasets (Jones et al., 2009) via the climate tracker (<http://www.bom.gov.au/climate/change/index.shtml#tabs=Tracker&tracker=timeseries>). Quarterly data for 39 stations providing quarterly data from 1971–72 to 2016–17 incorporating median Σ FFDI, the 97th percentile FFDI, drought factor, Keetch-Byron Drought Index, Tmax, P, RH and V (Lucas & Harris, 2019)(LH2019). Four indices were calculated: total daily average FFDI (Σ FFDI), days above high fire danger (Hi+), days above very high fire danger (VHi+) and days above severe fire danger (Sev+, covering severe, extreme and catastrophic states). The regression was constructed using data from Victoria and was calculated for all states, SE Australia and southwest Western Australia (SWWA).

The original data for Victorian stations 1972–73 was supplied by Chris Lucas, BoM and adjusted for windspeed inhomogeneities. Data archived by Lucas and Harris (2019) was analysed extensively and is gratefully acknowledged. Data was also extracted from CSIRO and Bureau of Meteorology (2015) and the accompanying technical reports.

Other data used were hemispheric and global averages from HadISH, the gridded global land surface humidity dataset 1973–2018 (Willett et al., 2014) and the CRUts4.03 monthly high-resolution gridded multivariate climate dataset (Harris et al., 2020).

Monthly STRP and STRI 1890–2019 calculated from station data in the band in the band 145°E – 150°E using the latitudes 10°S – 44°S, following the method of Timbal and Drosdowsky (2013) based on Drosdowsky (2005) and updated by Pepler et al. (2018). Also used was STRP and STRI from the southern hemisphere, derived by Nguyen et al. (2015) from the HadSLP2 dataset (Allan & Ansell, 2006). This is calculated via the absolute maximum zonal average mean sea level pressure (MSLP) and its position (Nguyen et al., 2015).

Shifts in mean used to diagnose regime shifts are based on Maronna-Yohai bivariate test, codified by Potter (1981) and Bücher and Dessens (1991) with minor corrections detailed in Jones and Ricketts (2021b), conducted manually. Also used is Rodionov's regime shift test 6-2 (Rodionov, 2015), as supplementary test for estimating changes in mean and for estimating abrupt shifts in correlation.

Figure 22 global fire season data from Jolly et al. (2015).

Figure 23 taken from Moon and Ha (2020) based on data from the National Centers for Environmental Prediction and Department of Energy (NCEP-DOE) reanalysis dataset v2 (Kanamitsu et al., 2002)

References

- Abram, N. J., Henley, B. J., Sen Gupta, A., Lippmann, T. J. R., Clarke, H., Dowdy, A. J., . . . Boer, M. M. (2021). Connections of climate change and variability to large and extreme forest fires in southeast Australia. *Communications Earth & Environment*, 2(1), 8. doi:10.1038/s43247-020-00065-8
- Allan, R. and Ansell, T. (2006). A new globally complete monthly historical gridded mean sea level pressure dataset (HadSLP2): 1850–2004. *Journal of Climate*, 19(22), 5816-5842.
- Allen, R. J. and Amaya, D. J. (2018). The importance of ENSO/PDO to recent tropical widening. *US CLIVAR Variations*, 16(2), 8.
- Amaya, D. J., Siler, N., Xie, S.-P. and Miller, A. J. (2018). The interplay of internal and forced modes of Hadley Cell expansion: lessons from the global warming hiatus. *Climate Dynamics*, 51(1-2), 305-319.
- Azorin-Molina, C., Guijarro, J. A., McVicar, T. R., Trewin, B. C., Frost, A. J. and Chen, D. (2019). An approach to homogenize daily peak wind gusts: An application to the Australian series. *International Journal of Climatology*, 39(4), 2260-2277.
- Beaugrand, G., Conversi, A., Atkinson, A., Cloern, J., Chiba, S., Fonda-Umani, S., . . . Edwards, M. (2019). Prediction of unprecedented biological shifts in the global ocean. *Nature Climate Change*, 9(3), 237-243. doi:<http://dx.doi.org/10.1038/s41558-019-0420-1>
- Beer, T., Gill, A. M. and Moore, P. (1988). Australian bushfire danger under changing climatic regimes. *Greenhouse, Planning for Climate Change*, 421-427.
- Beer, T. and Williams, A. (1995). Estimating Australian forest fire danger under conditions of doubled carbon dioxide concentrations. *Climatic Change*, 29(2), 169-188.
- Belolipetsky, P. V., Bartsev, S., Ivanova, Y. and Saltykov, M. (2015). Hidden staircase signal in recent climate dynamic. *Asia-Pacific Journal of Atmospheric Sciences*, 51(4), 323-330. doi:10.1007/s13143-015-0081-6
- Bonfils, C. and Santer, B. D. (2011). Investigating the possibility of a human component in various Pacific decadal oscillation indices. *Climate Dynamics*, 37(7-8), 1457-1468.
- Bradstock, R. A. (2010). A biogeographic model of fire regimes in Australia: current and future implications. *Global Ecology and Biogeography*, 19(2), 145-158. doi:10.1111/j.1466-8238.2009.00512.x
- Broecker, W. S. (2005). Global warming: Take action or wait? *Jokull*(55), 1-16.
- Brown, T., Mills, G., Harris, S., Podnar, D., Reinbold, H. and Fearon, M. (2016). A bias corrected WRF mesoscale fire weather dataset for Victoria, Australia 1972-2012. *JOURNAL OF SOUTHERN HEMISPHERE EARTH SYSTEMS SCIENCE*, 66(3), 281-313.
- Brutsaert, W. (1982). *Evaporation into the Atmosphere: Theory, History and Applications* (Vol. 1). Dordrecht Netherlands: Springer.
- Bryant, C. (2008). *Understanding bushfire: trends in deliberate vegetation fires in Australia*. Technical and Background Paper No. 27, Australian Institute of Criminology, Canberra,
- Bücher, A. and Dessens, J. (1991). Secular trend of surface temperature at an elevated observatory in the Pyrenees. *Journal of Climate*, 4, 859-868.
- Budyko, M. (1974). *Climate and Life*. New York: Academic Press.
- Bureau of Meteorology. (2006). *An exceptionally dry decade in parts of southern and eastern Australia: October 1996-September 2006*. Special Climate Statement, Bureau of Meteorology, Melbourne,
- Byrne, M. P. and O’Gorman, P. A. (2018). Trends in continental temperature and humidity directly linked to ocean warming. *Proceedings of the National Academy of Sciences*, 115(19), 4863-4868. doi:10.1073/pnas.1722312115
- Cai, W. and Cowan, T. (2013). Southeast Australia Autumn Rainfall Reduction: A Climate-Change-Induced Poleward Shift of Ocean–Atmosphere Circulation. *Journal of Climate*, 26(1), 189-205. doi:10.1175/jcli-d-12-00035.1
- Cai, W., Van Rensch, P., Cowan, T. and Hendon, H. H. (2011). Teleconnection pathways of ENSO and the IOD and the mechanisms for impacts on Australian rainfall. *Journal of Climate*, 24(15), 3910-3923.
- Chadwick, R., Good, P. and Willett, K. (2016). A simple moisture advection model of specific humidity change over land in response to SST warming. *Journal of Climate*, 29(21), 7613-7632.

- Clark, S., Mills, G., Brown, T., Harris, S. and Abatzoglou, J. T. (2021a). Downscaled GCM climate projections of fire weather over Victoria, Australia. Part 1*: evaluation of the MACA technique. *International Journal of Wildland Fire*.
- Clark, S., Mills, G., Brown, T., Harris, S. and Abatzoglou, J. T. (2021b). Downscaled GCM climate projections of fire weather over Victoria, Australia. Part 2*: a multi-model ensemble of 21st century trends. *International Journal of Wildland Fire*.
- Clarke, H. and Evans, J. P. (2019). Exploring the future change space for fire weather in southeast Australia. *Theoretical and Applied Climatology*, 136(1-2), 513-527.
- Clarke, H., Evans, J. P. and Pitman, A. J. (2013). Fire weather simulation skill by the Weather Research and Forecasting (WRF) model over south-east Australia from 1985 to 2009. *International Journal of Wildland Fire*, 22(6), 739-756.
- Clarke, H., Lucas, C. and Smith, P. (2013). Changes in Australian fire weather between 1973 and 2010. *International Journal of Climatology*, 33(4), 931-944.
- Clarke, H., Pitman, A. J., Kala, J., Carouge, C., Haverd, V. and Evans, J. P. (2016). An investigation of future fuel load and fire weather in Australia. *Climatic Change*, 139(3-4), 591-605.
- Clarke, H., Tran, B., Boer, M. M., Price, O., Kenny, B. and Bradstock, R. (2019). Climate change effects on the frequency, seasonality and interannual variability of suitable prescribed burning weather conditions in south-eastern Australia. *Agricultural and Forest Meteorology*, 271, 148-157.
- Clarke, H. G., Smith, P. L. and Pitman, A. J. (2011). Regional signatures of future fire weather over eastern Australia from global climate models. *International Journal of Wildland Fire*, 20(4), 550-562. doi:<https://doi.org/10.1071/WF10070>
- Conversi, A., Dakos, V., Gårdmark, A., Ling, S., Folke, C., Mumby, P. J., . . . Casini, M. (2015). A holistic view of marine regime shifts. *Philosophical Transactions of the Royal Society B: Biological Sciences*, 370(1659), 20130279.
- Crimp, S., Nicholls, N., Kokic, P., Risbey, J. S., Gobbett, D. and Howden, M. (2018). Synoptic to large-scale drivers of minimum temperature variability in Australia—long-term changes. *International Journal of Climatology*, 38, e237-e254.
- CSIRO and Bureau of Meteorology. (2015). *Climate Change in Australia. Information for Australia's Natural Resource Management Regions: Technical Report*. Australia: CSIRO and Bureau of Meteorology.
- Dai, A. (2006). Recent climatology, variability, and trends in global surface humidity. *Journal of Climate*, 19(15), 3589-3606.
- Davis, N. A., Davis, S. M. and Waugh, D. W. (2018). New insights into tropical belt metrics. *Variations*, 16, 1-7.
- Della-Marta, P. M., Collins, D. A. and Braganza, K. (2004). Updating Australia's high-quality annual temperature dataset. *Australian Meteorological Magazine*, 53, 75-93.
- Dong, L., Zhou, T. and Chen, X. (2014). Changes of Pacific decadal variability in the twentieth century driven by internal variability, greenhouse gases, and aerosols. *Geophysical Research Letters*, 41(23), 8570-8577.
- Douville, H., Decharme, B., Delire, C., Colin, J., Joetzjer, E., Roehrig, R., . . . Voltaire, A. (2020). Drivers of the enhanced decline of land near-surface relative humidity to abrupt 4xCO₂ in CNRM-CM6-1. *Climate Dynamics*, 55(5), 1613-1629. doi:10.1007/s00382-020-05351-x
- Dowdy, A. J. (2018). Climatological Variability of Fire Weather in Australia. *Journal of Applied Meteorology and Climatology*, 57(2), 221-234. doi:10.1175/jamc-d-17-0167.1
- Dowdy, A. J. and Pepler, A. (2018). Pyroconvection risk in Australia: Climatological changes in atmospheric stability and surface fire weather conditions. *Geophysical Research Letters*, 45(4), 2005-2013.
- Drosowsky, W. (2005). The latitude of the subtropical ridge over Eastern Australia: The L index revisited. *International Journal of Climatology*, 25(10), 1291-1299.
- Duff, T. J., Chong, D. M., Cirulis, B. A., Walsh, S. F., Penman, T. D. and Tolhurst, K. G. (2014). *Understanding risk: Representing fire danger using spatially explicit fire simulation ensembles*. Paper presented at the Coimbra 2014, Coimbra.
- Egorova, T., Rozanov, E., Arsenovic, P., Peter, T. and Schmutz, W. (2018). Contributions of natural and anthropogenic forcing agents to the early 20th century warming. *Frontiers in Earth Science*, 6, 206.

- Enright, N. J. and Fontaine, J. B. (2014). Climate Change and the Management of Fire-Prone Vegetation in Southwest and Southeast Australia. *Geographical Research*, 52(1), 34-44.
- Evans, J., Ji, F., Lee, C., Smith, P., Argüeso, D. and Fita, L. (2014). Design of a regional climate modelling projection ensemble experiment–NARCLIM. *Geoscientific Model Development*, 7(2), 621-629.
- Finkele, K., Mills, G. A., Beard, G. and Jones, D. A. (2006). National gridded drought factors and comparison of two soil moisture deficit formulations used in prediction of Forest Fire Danger Index in Australia. *Australian Meteorological Magazine*, 55(3), 183-197.
- Fox-Hughes, P. (2008). A fire danger climatology for Tasmania. *Australian Meteorological Magazine*, 57(2), 109-120.
- Fox-Hughes, P., Harris, R., Lee, G., Grose, M. and Bindoff, N. (2014). Future fire danger climatology for Tasmania, Australia, using a dynamically downscaled regional climate model. *International Journal of Wildland Fire*, 23(3), 309-321.
- Fu, R. (2015). Global warming-accelerated drying in the tropics. *Proceedings of the National Academy of Sciences*, 112(12), 3593-3594.
- Gimeno, L., Drumond, A., Nieto, R., Trigo, R. M. and Stohl, A. (2010). On the origin of continental precipitation. *Geophysical Research Letters*, 37(13). doi:10.1029/2010gl043712
- Gimeno, L., Nieto, R., Drumond, A., Castillo, R. and Trigo, R. (2013). Influence of the intensification of the major oceanic moisture sources on continental precipitation. *Geophysical Research Letters*, 40(7), 1443-1450.
- Gimeno, L., Stohl, A., Trigo, R. M., Dominguez, F., Yoshimura, K., Yu, L., . . . Nieto, R. (2012). Oceanic and terrestrial sources of continental precipitation. *Reviews of Geophysics*, 50(4).
- Granger, R. J. (1989). A complementary relationship approach for evaporation from nonsaturated surfaces. *Journal of Hydrology*, 111(1-4), 31-38.
- Grise, K. M., Davis, S. M., Simpson, I. R., Waugh, D. W., Fu, Q., Allen, R. J., . . . Maycock, A. C. (2019). Recent tropical expansion: natural variability or forced response? *Journal of Climate*, 32(5), 1551-1571.
- Grose, M., Timbal, B., Wilson, L., Bathols, J. and Kent, D. (2015). The subtropical ridge in CMIP5 models, and implications for projections of rainfall in southeast Australia. *Aust. Met. Oceanogr. J*, 65, 90-106.
- Grose, M. R., Fox-Hughes, P., Harris, R. M. B. and Bindoff, N. L. (2014). Changes to the drivers of fire weather with a warming climate – a case study of southeast Tasmania. *Climatic Change*, 124(1), 255-269. doi:10.1007/s10584-014-1070-y
- Grose, M. R., Risbey, J. S., Moise, A. F., Osbrough, S., Heady, C., Wilson, L. and Erwin, T. (2017). Constraints on southern Australian rainfall change based on atmospheric circulation in CMIP5 simulations. *Journal of Climate*, 30(1), 225-242.
- Gu, G. and Adler, R. F. (2013). Interdecadal variability/long-term changes in global precipitation patterns during the past three decades: global warming and/or pacific decadal variability? *Climate Dynamics*, 40(11), 3009-3022. doi:10.1007/s00382-012-1443-8
- Harley, C. D. and Paine, R. T. (2009). Contingencies and compounded rare perturbations dictate sudden distributional shifts during periods of gradual climate change. *Proceedings of the National Academy of Sciences*, 106(27), 11172-11176.
- Harris, I., Osborn, T. J., Jones, P. and Lister, D. (2020). Version 4 of the CRU TS monthly high-resolution gridded multivariate climate dataset. *Scientific Data*, 7(1), 109. doi:10.1038/s41597-020-0453-3
- Harris, S. and Lucas, C. (2019). Understanding the variability of Australian fire weather between 1973 and 2017. *PLoS One*, 14(9), e0222328.
- Harris, S., Mills, G. and Brown, T. (2019). *Victorian fire weather trends and variability*. Paper presented at the MODSIM2019, 23rd International Congress on Modelling and Simulation, 1–6 December 2019, Canberra, ACT. <https://modsim2019.exordo.com/programme/presentation/590>
- Harris, S., Nicholls, N., Tapper, N. and Mills, G. (2019). The sensitivity of fire activity to interannual climate variability in Victoria, Australia. *JOURNAL OF SOUTHERN HEMISPHERE EARTH SYSTEMS SCIENCE*, 69(1), 146-160.
- Hasson, A., Mills, G., Timbal, B. and Walsh, K. (2009). Assessing the impact of climate change on extreme fire weather events over southeastern Australia. *Climate Research*, 39(2), 159-172.

- Hegerl, G. C., Brönnimann, S., Schurer, A. and Cowan, T. (2018). The early 20th century warming: Anomalies, causes, and consequences. *Wiley Interdisciplinary Reviews: Climate Change*, 9(4), e522.
- Hendon, H. H., Lim, E.-P., Arblaster, J. M. and Anderson, D. L. T. (2014). Causes and predictability of the record wet east Australian spring 2010. *Climate Dynamics*, 42(5), 1155-1174. doi:10.1007/s00382-013-1700-5
- Hennessy, K., Lucas, C., Nicholls, N., Bathols, J., Suppiah, R. and Ricketts, J. (2005). *Climate change impacts on fire-weather in south-east Australia*, CSIRO and Bureau of Meteorology, Melbourne,
- Holgate, C. M., van Dijk, A. I., Cary, G. J. and Yebra, M. (2017). Using alternative soil moisture estimates in the McArthur Forest Fire Danger Index. *International Journal of Wildland Fire*, 26(9), 806-819.
- Hope, P., Black, M. T., Lim, E.-P., Dowdy, A., Wang, G., Fawcett, R. J. and Pepler, A. S. (2019). On Determining the Impact of Increasing Atmospheric CO₂ on the Record Fire Weather in Eastern Australia in February 2017 [in "Explaining Extremes of 2017 from a Climate Perspective"]. *Bulletin of the American Meteorological Society*, 100(1), S111-S117. doi:/10.1175/BAMS-D-18-0135.1
- Huang, B., Banzon, V. F., Freeman, E., Lawrimore, J., Liu, W., Peterson, T. C., . . . Zhang, H.-M. (2015). Extended Reconstructed Sea Surface Temperature Version 4 (ERSST.v4). Part I: Upgrades and Intercomparisons. *Journal of Climate*, 28(3), 911-930. doi:<https://doi.org/10.1175/jcli-d-14-00006.1>
- Hughes, L., Steffen, W., Mullins, G., Dean, A., Weisbrot, E. and Rice, M. (2020). *Summer of crisis*, No. 1922404004, Climate Council Canberra,
- Jakob, D. (2010). Challenges in developing a high-quality surface wind-speed data-set for Australia. *Australian Meteorological and Oceanographic Journal*, 60(4), 227-236.
- Jeffrey, S. J., Carter, J. O., Moodie, K. B. and Beswick, A. R. (2001). Using spatial interpolation to construct a comprehensive archive of Australian climate data. *Environmental modelling & software*, 16(4), 309-330.
- Jolly, W. M., Cochrane, M. A., Freeborn, P. H., Holden, Z. A., Brown, T. J., Williamson, G. J. and Bowman, D. M. J. S. (2015). Climate-induced variations in global wildfire danger from 1979 to 2013. *Nature Communications*, 6(1), 7537. doi:10.1038/ncomms8537
- Jones, D. A., Wang, W. and Fawcett, R. (2009). High-quality spatial climate data-sets for Australia. *Australian Meteorological and Oceanographic Journal*, 58, 233-248.
- Jones, R., Chiew, F., Boughton, W. and Zhang, L. (2006). Estimating the sensitivity of mean annual runoff to climate change using selected hydrological models. *Advances in Water Resources*, 29(10), 1419-1429.
- Jones, R. N. (2012). Detecting and attributing nonlinear anthropogenic regional warming in southeastern Australia. *Journal of Geophysical Research*, 117(D4), D04105. doi:<https://doi.org/10.1029/2011jd016328>
- Jones, R. N. and Ricketts, J. H. (2017). Reconciling the signal and noise of atmospheric warming on decadal timescales. *Earth System Dynamics*, 8(1), 177-210. doi:10.5194/esd-8-177-2017
- Jones, R. N. and Ricketts, J. H. (2019). The Pacific Ocean heat engine: global climate's regulator. *Earth System Dynamics Discussions*, 1-42. doi:<https://doi.org/10.5194/esd-2019-72>
- Jones, R. N. and Ricketts, J. H. (2021a). Climate as a complex, self-regulating system. *Earth Systems Dynamics Discussions*, 2021, 1-47. doi:10.5194/esd-2021-62
- Jones, R. N. and Ricketts, J. H. (2021b). The Pacific Ocean heat engine. *Earth Systems Dynamics Discussions*, 2021, 1-47. doi:10.5194/esd-2021-61
- Jones, R. N., Young, C. K., Handmer, J., Keating, A., Mekala, G. D. and Sheehan, P. (2013). *Valuing Adaptation under Rapid Change*. Gold Coast, Australia: National Climate Change Adaptation Research Facility.
- Jovanovic, B., Collins, D., Braganza, K., Jakob, D. and Jones, D. A. (2011). A high-quality monthly total cloud amount dataset for Australia. *Climatic Change*, 108(3), 485-517.
- Kanamitsu, M., Ebisuzaki, W., Woollen, J., Yang, S.-K., Hnilo, J., Fiorino, M. and Potter, G. (2002). NCEP-DOE AMIP-II reanalysis (R-2). *Bulletin of the American Meteorological Society*, 83(11), 1631-1644.
- Kiem, A. S. and Franks, S. W. (2004). Multi-decadal variability of drought risk, eastern Australia. *Hydrological Processes*, 18(11), 2039-2050. doi:10.1002/hyp.1460
- Kosaka, Y. and Xie, S.-P. (2016). The tropical Pacific as a key pacemaker of the variable rates of global warming. *Nature Geoscience*, 9(9), 669-673. doi:10.1038/ngeo2770

- Krebs, P., Pezzatti, G. B., Mazzoleni, S., Talbot, L. M. and Conedera, M. (2010). Fire regime: history and definition of a key concept in disturbance ecology. *Theory in Biosciences*, 129(1), 53-69.
- Larsen, S. H. and Nicholls, N. (2009). Southern Australian rainfall and the subtropical ridge: Variations, interrelationships, and trends. *Geophysical Research Letters*, 36(8), L08708. doi:10.1029/2009gl037786
- Lau, W. K. and Kim, K.-M. (2015). Robust Hadley circulation changes and increasing global dryness due to CO2 warming from CMIP5 model projections. *Proceedings of the National Academy of Sciences*, 112(12), 3630-3635.
- Lewis, S. C., Blake, S. A., Trewin, B., Black, M. T., Dowdy, A. J., Perkins-Kirkpatrick, S. E., . . . Sharples, J. J. (2019). Deconstructing factors contributing to the 2018 fire weather in Queensland, Australia. *Bulletin of the American Meteorological Society*(2019).
- Liu, W., Huang, B., Thorne, P. W., Banzon, V. F., Zhang, H.-M., Freeman, E., . . . Woodruff, S. D. (2015). Extended reconstructed sea surface temperature version 4 (ERSST. v4): Part II. Parametric and structural uncertainty estimations. *Journal of Climate*, 28(3), 931-951.
- Lucas, C. (2006). *A high-quality humidity dataset for Australia*. Paper presented at the 17th Australia New Zealand Climate Forum, Canberra, ACT.
- Lucas, C. (2009). On developing a historical fire weather data-set for Australia. *Australian Meteorological and Oceanographic Journal* 60, 1-14.
- Lucas, C. (2010). On developing a historical fire weather data-set for Australia. *Australian Meteorological and Oceanographic Journal*, 60(1), 1.
- Lucas, C. and Harris, S. (2019). *Seasonal McArthur Forest Fire Danger Index (FFDI) data for Australia: 1973-2017*. Retrieved from: <https://data.mendeley.com/datasets/xf5bv3hcvw/2>
- Lucas, C., Hennessy, K., Mills, G. and Bathols, J. (2007). *Bushfire weather in Southeast Australia: recent trends and projected climate change impacts*, Bushfire Cooperative Research Centre, Bureau of Meteorology, CSIRO, Melbourne,
- Lucas, C., Timbal, B. and Nguyen, H. (2014). The expanding tropics: a critical assessment of the observational and modeling studies. *Wiley Interdisciplinary Reviews: Climate Change*, 5(1), 89-112.
- Luke, R. H. and McArthur, A. G. (1978). *Bushfires in Australia*. Canberra: Australian Government Publishing Service.
- Maher, P. and Sherwood, S. C. (2016). Skill in simulating Australian precipitation at the tropical edge. *Journal of Climate*, 29(4), 1477-1496.
- Marlon, J. R., Bartlein, P. J., Walsh, M. K., Harrison, S. P., Brown, K. J., Edwards, M. E., . . . Briles, C. (2009). Wildfire responses to abrupt climate change in North America. *Proceedings of the National Academy of Sciences*, 106(8), 2519-2524.
- Maronna, R. and Yohai, V. J. (1978). A bivariate test for the detection of a systematic change in mean. *Journal of the American Statistical Association*, 73(363), 640-645.
- McArthur, A. G. (1967). Fire behaviour in eucalypt forests.
- McRae, R. and Sharples, J. (2014). Forecasting conditions conducive to blow-up fire events. *CAWCR Research Letters*, 11, 14-19.
- McVicar, T. R., Van Niel, T. G., Li, L. T., Roderick, M. L., Rayner, D. P., Ricciardulli, L. and Donohue, R. J. (2008). Wind speed climatology and trends for Australia, 1975–2006: Capturing the stilling phenomenon and comparison with near-surface reanalysis output. *Geophysical Research Letters*, 35(20).
- Miller, C., Holmes, J., Henderson, D., Ginger, J. and Morrison, M. (2013). The response of the Dines anemometer to gusts and comparisons with cup anemometers. *Journal of Atmospheric and Oceanic Technology*, 30(7), 1320-1336.
- Mills, G., Harris, S., Brown, T. and Chen, A. (2020). Climatology of wind changes and elevated fire danger over Victoria, Australia. *JOURNAL OF SOUTHERN HEMISPHERE EARTH SYSTEMS SCIENCE*, 70(1), 290-303.
- Moon, H. and Ha, K.-J. (2020). Distinguishing changes in the Hadley circulation edge. *Theoretical and Applied Climatology*, 139(3), 1007-1017. doi:10.1007/s00704-019-03017-1
- Moritz, M. A., Parisien, M.-A., Batllori, E., Krawchuk, M. A., Van Dorn, J., Ganz, D. J. and Hayhoe, K. (2012). Climate change and disruptions to global fire activity. *Ecosphere*, 3(6), art49. doi:10.1890/es11-00345.1

- Morton, F. I. (1983). Operational estimates of areal evapotranspiration and their significance to the science and practice of hydrology. *Journal of Hydrology*, 66(1), 1-76.
- Moss, R., Babiker, W., Brinkman, S., Calvo, E., Carter, T., Edmonds, J., . . . Hibbard, K. (2008). *Towards new scenarios for the analysis of emissions: Climate change, impacts and response strategies*: Intergovernmental Panel on Climate Change Secretariat (IPCC).
- Moss, R. H., Edmonds, J. A., Hibbard, K. A., Manning, M. R., Rose, S. K., van Vuuren, D. P., . . . Wilbanks, T. J. (2010). The next generation of scenarios for climate change research and assessment. *Nature*, 463(7282), 747-756.
- Murphy, B. F. and Timbal, B. (2008). A review of recent climate variability and climate change in southeastern Australia. *International Journal of Climatology*, 28(7), 859-879.
- Nguyen, H., Evans, A., Lucas, C., Smith, I. and Timbal, B. (2013). The Hadley circulation in reanalyses: Climatology, variability, and change. *Journal of Climate*, 26(10), 3357-3376.
- Nguyen, H., Hendon, H. H., Lim, E. P., Boschat, G., Maloney, E. and Timbal, B. (2018). Variability of the extent of the Hadley circulation in the southern hemisphere: a regional perspective. *Climate Dynamics*, 50(1), 129-142. doi:10.1007/s00382-017-3592-2
- Nguyen, H., Lucas, C., Evans, A., Timbal, B. and Hanson, L. (2015). Expansion of the Southern Hemisphere Hadley cell in response to greenhouse gas forcing. *Journal of Climate*, 28(20), 8067-8077.
- Nicholls, N., Dellamarta, P. and Collins, D. (2004). 20th century changes in temperature and rainfall in New South Wales. *Australian Meteorological Magazine*, 53, 263-268.
- Noble, I., Gill, A. and Bary, G. (1980). McArthur's fire-danger meters expressed as equations. *Australian journal of ecology*, 5(2), 201-203.
- O'Kane, T. J., Matear, R. J., Chamberlain, M. A. and Oke, P. R. (2014). ENSO regimes and the late 1970's climate shift: The role of synoptic weather and South Pacific ocean spiciness. *Journal of Computational Physics*, 271, 19-38.
- O'Gorman, P. A. and Muller, C. J. (2010). How closely do changes in surface and column water vapor follow Clausius–Clapeyron scaling in climate change simulations? *Environmental Research Letters*, 5(2), 025207. doi:10.1088/1748-9326/5/2/025207
- Overland, J., Rodionov, S., Minobe, S. and Bond, N. (2008). North Pacific regime shifts: Definitions, issues and recent transitions. *Progress in Oceanography*, 77, 92-102.
- Ozawa, H., Ohmura, A., Lorenz, R. D. and Pujol, T. (2003). The second law of thermodynamics and the global climate system: A review of the maximum entropy production principle. *Reviews of Geophysics*, 41(4), 1018. doi:<https://doi.org/10.1029/2002RG000113>
- Pausas, J. G. and Fernández-Muñoz, S. (2012). Fire regime changes in the Western Mediterranean Basin: from fuel-limited to drought-driven fire regime. *Climatic Change*, 110(1-2), 215-226.
- Peel, M. C., Finlayson, B. L. and McMahon, T. A. (2007). Updated world map of the Köppen-Geiger climate classification. *Hydrology and Earth System Sciences*, 11(5), 1633-1644.
- Pepler, A., Ashcroft, L. and Trewin, B. (2018). The relationship between the subtropical ridge and Australian temperatures. *JOURNAL OF SOUTHERN HEMISPHERE EARTH SYSTEMS SCIENCE*, 68, 201-214. doi:10.22499/3.6801.011
- Post, D. A., Timbal, B., Chiew, F. H. S., Hendon, H. H., Nguyen, H. and Moran, R. (2014). Decrease in southeastern Australian water availability linked to ongoing Hadley cell expansion. *Earth's Future*, 2(4), 231-238. doi:10.1002/2013ef000194
- Potter, K. (1981). Illustration of a new test for detecting a shift in mean in precipitation series. *Monthly Weather Review*, 109, 2040-2045.
- Power, S., Casey, T., Folland, C., Colman, A. and Mehta, V. (1999). Inter-decadal modulation of the impact of ENSO on Australia. *Climate Dynamics*, 15(5), 319-324. doi:<https://doi.org/10.1007/s003820050284>
- Reid, P. C. (2016). Ocean warming: setting the scene. In D. Laffoley and J. M. Baxter (Eds.), *Explaining ocean warming: causes, scale, effects and consequences*. Gland, Switzerland: IUCN.
- Reid, P. C. and Beaugrand, G. (2012). Global synchrony of an accelerating rise in sea surface temperature. *Journal of the Marine Biological Association of the United Kingdom*, 92(07), 1435-1450. doi:<https://doi.org/10.1017/S0025315412000549>

- Reid, P. C., Hari, R. E., Beaugrand, G., Livingstone, D. M., Marty, C., Straile, D., . . . Aono, Y. (2016). Global impacts of the 1980s regime shift. *Global Change Biology*, 22(2), 682-703. doi:<https://doi.org/10.1111/gcb.13106>
- Ricketts, J. H. (2019). *Understanding the Nature of Abrupt Decadal Shifts in a Changing Climate*. (Ph D), Victoria University, Melbourne.
- Rodionov, S. N. (2015). A sequential method of detecting abrupt changes in the correlation coefficient and its application to Bering Sea climate. *Climate*, 3(3), 474-491.
- Sanabria, L., Qin, X., Li, J., Cechet, R. and Lucas, C. (2013). Spatial interpolation of McArthur's forest fire danger index across Australia: observational study. *Environmental Modelling & Software*, 50, 37-50.
- Sanderson, B. M. and Fisher, R. A. (2020). A fiery wake-up call for climate science. *Nature Climate Change*, 10(3), 175-177. doi:10.1038/s41558-020-0707-2
- Sharples, J. J., Cary, G. J., Fox-Hughes, P., Mooney, S., Evans, J. P., Fletcher, M.-S., . . . Baker, P. (2016). Natural hazards in Australia: extreme bushfire. *Climatic Change*, 139(1), 85-99. doi:10.1007/s10584-016-1811-1
- Timbal, B. and Drosowsky, W. (2013). The relationship between the decline of Southeastern Australian rainfall and the strengthening of the subtropical ridge. *International Journal of Climatology*, 33(4), 1021-1034.
- Timbal, B., Ekström, M., Fiddes, S., Grose, M., Kirono, D. G., Lim, E.-P., . . . Wilson, L. (2016). *Climate change science and Victoria: Bureau of Meteorology*.
- Tozer, C. R., Vance, T. R., Roberts, J. L., Kiem, A. S., Curran, M. A. and Moy, A. D. (2016). An ice core derived 1013-year catchment-scale annual rainfall reconstruction in subtropical eastern Australia. *Hydrology and Earth System Sciences*, 20(5), 1703.
- Trewin, B. (2013). A daily homogenized temperature data set for Australia. *International Journal of Climatology*, 33(6), 1510-1529.
- Trewin, B. (2018). *The Australian Climate Observations Reference Network – Surface Air Temperature (ACORN-SAT) version 2*. Bureau Research Report – BRR032, No. 9781925315981, Bureau of Meteorology, Melbourne,
- Troccoli, A., Muller, K., Coppin, P., Davy, R., Russell, C. and Hirsch, A. L. (2012). Long-term wind speed trends over Australia. *Journal of Climate*, 25(1), 170-183.
- University of East Anglia Climatic Research Unit, Harris, I. C. and Jones, P. D. (2020). *CRU TS4.03: Climatic Research Unit (CRU) Time-Series (TS) version 4.03 of high-resolution gridded data of month-by-month variation in climate (Jan. 1901- Dec. 2018)*.
- Van der Ent, R. J., Savenije, H. H., Schaefli, B. and Steele-Dunne, S. C. (2010). Origin and fate of atmospheric moisture over continents. *Water Resources Research*, 46(9).
- Vance, T., Roberts, J., Plummer, C., Kiem, A. and Van Ommen, T. (2015). Interdecadal Pacific variability and eastern Australian megadroughts over the last millennium. *Geophysical Research Letters*, 42(1), 129-137.
- Wang, J., Xu, C., Hu, M., Li, Q., Yan, Z. and Jones, P. (2018). Global land surface air temperature dynamics since 1880. *International Journal of Climatology*, 38, e466-e474.
- Warner, R. (1999). Climatic geomorphology. *Geomorphology of the Hawkesbury-Nepean River System—a review of landforms, processes and management*. Hawkesbury-Nepean Catchment Management Trust, Windsor, 157-167.
- Westhoff, M., Kleidon, A., Schymanski, S., Dewals, B., Nijse, F., Renner, M., . . . Dolman, H. (2019). Thermodynamic optimality in Earth sciences. The missing constraints in modeling Earth system dynamics? *Earth System Dynamics Discussions*. doi:<https://doi.org/10.5194/esd-2019-6>
- Willett, K., Dunn, R., Thorne, P., Bell, S., De Podesta, M., Parker, D., . . . Williams Jr, C. (2014). HadISDH land surface multi-variable humidity and temperature record for climate monitoring. *Climate of the Past*, 10(6).
- Williams, R. J., Bradstock, R. A., Cary, G. J., Dovey, L., Enright, N. J., Gill, A. M., . . . Lucas, C. (2013). Current Fire Regimes, Impacts and the Likely Changes—VII: Australian Fire Regimes under Climate Change: Impacts, Risks and Mitigation. In J. G. Goldammer (Ed.), *Vegetation Fires and Global Change* (pp. 133-142). Eifelveg: Kessel Publishing House.

Constructing and assessing fire climate regimes

- Williamson, G. J., Prior, L. D., Jolly, W. M., Cochrane, M. A., Murphy, B. P. and Bowman, D. M. J. S. (2016). Measurement of inter- and intra-annual variability of landscape fire activity at a continental scale: the Australian case. *Environmental Research Letters*, 11(3), 035003.
- Yang, D., Sun, F., Liu, Z., Cong, Z. and Lei, Z. (2006). Interpreting the complementary relationship in non-humid environments based on the Budyko and Penman hypotheses. *Geophysical Research Letters*, 33(18).
- Zhang, L., Potter, N., Hickel, K., Zhang, Y. and Shao, Q. (2008). Water balance modeling over variable time scales based on the Budyko framework—Model development and testing. *Journal of Hydrology*, 360(1-4), 117-131.
- Zhang, W., Li, J. and Jin, F. F. (2009). Spatial and temporal features of ENSO meridional scales. *Geophysical Research Letters*, 36(15), L15605. doi:<https://doi.org/10.1029/2009GL038672>
- Zinck, R. D., Pascual, M. and Grimm, V. (2011). Understanding shifts in wildfire regimes as emergent threshold phenomena. *The American Naturalist*, 178(6), E149-E161.